2020

# Theoretical Analysis of the Conduction Properties of Self Assembled Molecular Tunnel Junctions

Cameron Nickle
*University of Central Florida*

# THEORETICAL ANALYSIS OF THE CONDUCTION PROPERTIES OF SELF-ASSEMBLED MOLECULAR TUNNEL JUNCTIONS

by

CAMERON NICKLE
B.S. University of South Carolina, 2014
M.S. University of Central Florida, 2016

A dissertation submitted in partial fulfillment of the requirements
for the degree of Doctor of Philosophy
in the Department of Physics
in the College of Sciences
at the University of Central Florida
Orlando, Florida

Fall Term
2020

Major Professor: Enrique Del Barco

# ABSTRACT

As the size scale of electrical devices approach the atomic scale. Moore's law is predicted to be over for semiconductor devices. Studies into the replacement of semiconductor technology with organic devices was first predicted by Avriam and Ratner[1] in 1974. Since then significant research into molecular based organic devices has been conducted. The work presented in this dissertation explores the theoretical frameworks used to model transport through molecular junctions. We present studies which seek to garner a better understanding of the charge transport through molecular junctions and how the conduction properties can be optimized. We show that a single atom can change a molecule from an insulator to a conductor. We also study the effects of sigma and pi bridges on molecular rectification. We will then show molecular devices that act as viable electrical static and dynamic switches. The studies presented here help to demonstrate the viability of organic devices in the forms of rectifiers and switches with applications ranging from the replacement of traditional semiconductor devices to neuromorphic computing.

Dedicated to my fiancé, Ashley, whose support was invaluable.

# ACKNOWLEDGMENTS

I would first like to thank my parents, grandparents, stepparents and future in-laws who supported me throughout my education even when they did not quite understand what I was doing. My grandmother always encouraged my curiosity as a kid, calling me a little scientist at a young age. My mother would spend countless hours going through flash cards with me. I remember spending hours in the car with my father while he taught me everything he knew. He and my stepfather always supported me at every step. Not to mention my, aunt, uncle and cousins who have encouraged and supported me throughout.

My path from graduating high school to obtaining my PhD has introduced me to several great people along the way. Starting with my first internship at NASA Langley Research Center under the mentorship of Dr. Richard L. Boitnott. Dr. Boitnott picked my application out of a pool and was the first person to give me a chance at research experience. That first internship added to my resume helped me to progress in my career and gave me experience that I still utilize today. Dr. Boitnott also provided me with advice and recommendation letters for years after (even some very last-minute recommendation letters that he was able to provide in a couple of hours).

I would also like to thank the professors from the University of South Carolina who helped me in my undergraduate journey. Dr. Yordanka Ilieva is a great mentor of mine. She was the professor of my first collegiate physics class and author of my first recommendation letter. She taught me programming which is a skill set that was critical in this thesis. She also gave me my first conference experience by helping me to present a poster at the APS Division of Nuclear Physics. When writing my personal statements for graduate school I realized that a full half of the experience I had was somehow related to the opportunities provided by Dr. Ilieva. Dr. Thomas Crawford was also a very influential professor to

me. He provided me with opportunities when I was desperate for them. Working with Dr. Crawford, Dr. Longfei Ye, and Tyler Tatum lead to a patent in my name and taught me many skills such as entrepreneurship and how to work in a laboratory setting.

I would also like to thank the UCF Physics department for helping me to achieve my goals. The staff in the department were always kind and helpful. Particularly since dealing with paperwork and deadlines were never my strong suit. Academically, Esperanza Soto always made sure that I had everything completed accurately and on time. Bobby Wong helped me to build every random gadget or piece part that I needed. Jessica Brooks and Leida Vera Nater were very helpful in making sure that we had all the tools and equipment we needed to succeed in our experiments. Everything else I needed was taken care of by Nikkita Campbell, Elizabeth Rivera and Shelley Glaspie, even when all I needed was a short distraction from the stressors of a Ph.D.

I would like to thank a few notable professors at UCF. Dr. Elena Flitsiyan who was always very kind and helpful. She was nicknamed 'Mother Physics' among the teaching assistants because of how much she cared and helped everyone. Dr. Eduardo Mucciolo was a phenomenal teacher. He was always very approachable and helpful to students. His style of teaching made complicated topics seem simple and I learned a lot from him. I took three classes taught by Dr. Robert Peale who was also a great teacher and mentor. He always made himself available to the students who could just walk into his office and ask him questions. He taught me a lot and helped me several times throughout my five years at UCF. I would also like thank Dr. Masahiro Ishigami. I likely spent several hours each week talking to Masa. I will miss our lunch time discussions.

Some of the most important people in my journey were my group mates. In the short time I had with Alvar, he taught me a lot about the project I was to take over. However, Marta was truly the person

who taught me the ins and outs. She patiently put up with all my dumb mistakes, shenanigans, and silly jokes. She somehow managed to shoulder the responsibility of all the junior graduate students' projects while finishing her own. We are all indebted to her. Priyanka did not so much put up with my shenanigans, but rather was a partner in crime. She was a great help and a great friend and will hopefully continue to be so for years to come. Seth and Sara had the monumental task of maintaining and repairing the cleanroom and its equipment. Without them, the numerous equipment delays and issues would have been even worse. The most junior member of the 'old crew', Gyan went from being my trainee to someone who has taught me a lot in turn. He is shaping up to be the new Marta for the next group of graduate students. Also, all the students who came later in my Ph.D. were a great help in continuing projects as I focused on other tasks. My undergraduate mentee Conner not only managed to take over fabrication of devices, but also managed to keep me on task and not get distracted by minor issues. Dr. Ran Liu really stepped up to the challenge during the pandemic, making great progress during a very challenging time. Francis helped to obtain some of the results presented here and I am confident he will take over this project and do great things with it. Finally, all the other group mates, office mates and friends who made life in the lab and office more enjoyable, Tommy, Tyrone, Justin, Rebecca, John, Chris, Jaesuk, Romena and so many others.

I also need to thank all our collaborators. Without them the projects presented in this work would not have happened. Notably, Dr. Christian A. Nijhuis' group provided much of the experimental data analyzed in this thesis. As well as provided, molecular samples to be studied experimentally by our group. Much of the DFT work was conducted Dr. Damien Thompson's group.

Finally, I would like to thank my adviser Dr. Enrique Del Barco. It is impossible to count the number of things I have learned from Enrique. He has helped us, and he has pushed us to achieve our

goals. Throughout my Ph.D. he was always dependable and available to his students. I respect him both as my mentor and as friend.

# TABLE OF CONTENTS

# LIST OF FIGURES

# LIST OF TABLES

# CHAPTER ONE: INTRODUCTION

## Background

The first solid-state transistor was invented at Bell labs in 1949[2] and by 1965 Moore was already predicting that the number of components "crammed" onto an integrated circuit would double every year (later revised to two years)[3]. Moore's law has governed the exponential progress of computing technologies for the last fifty-five years. However, if the current scale of miniaturization continues the semiconductor industry will soon be faced with creating electrical components on the size scale of single molecules. Many technology companies are predicting the end of Moore's law[4] and alternative solutions are needed.

Studies conducted as early as 1974 suggested that organic molecules could be a replacement for semiconductor technology[1]. Aviram and Ratner commented that biological systems use organic molecules to perform many of the same tasks that are performed by modern computers. These organic molecules tended to be more efficient at storing and transporting energy and electrons[1, 5]. Aviram and Ratner proposed that the starting point for organic electrical components should be molecules that act as rectifiers, devices which allow current to flow in one direction but not the other, with molecular memory and logic elements coming later[1, 5].

Aviram and Ratner proposed that a molecular rectifier would need an electron-rich (donor) and an electron-poor (acceptor) subunit. These would be analogous to the n-type and p-type regions found in semiconductor rectifiers. These donor and acceptor units would need to be isolated from one another to act as a rectifier. Aviram and Ratner proposed this could be accomplished by having a sigma-electron system (insulator) sandwiched between two pi-electron systems. In this vision, the donor or Highest

Occupied Molecular Orbital (HOMO) and acceptor or Lowest Unoccupied Molecular Orbital (LUMO) would be spatially separated by a σ bridge. This donor-insulator-acceptor (D-σ-A) mechanism dominated molecular electronic studies for decades. However, the first rectifier discovered didn't take the form predicted by Aviram and Ratner. Twenty-six years after Aviram and Ratner's paper D-π-A rectifiers were discovered[6-11]. Now, there are multiple known methods of obtaining molecular rectification, some of which will be touched on in this work.

## Rectification in Molecular Junctions

### Mechanisms of Rectification

At the time of Metzger's review paper[12] in 2003, three known methods of obtaining molecular rectification were identified. The first method identified by Metzger was what he deemed to be true unimolecular rectification. This is the mechanism first proposed by Aviram and Ratner and is caused by electron transfer between the donor and acceptor subunits whose probability asymmetries within the molecule produce rectification[6-11, 13-16]. The next method was denoted as 'S' rectifiers for 'Schottky' barriers. 'S' type rectifiers create dipoles at the metal-organic interfaces. A difference in the size of these dipoles at either end of the molecule results in rectification[17-21]. The final method of producing rectifiers comes from the placement of the conductive unit, deemed the 'chromophore'[13, 22-27]. Long alkyl chains branch out from the chromophore in each direction and bridge the gap between the chromophore and each electrode. Rectification occurs when the length of these two chains differ. Molecules that rectify in this way were called 'asymmetric molecules'[12].

Since Metzger's 2002 article other sources of rectification have been identified such as the use of dissimilar electrode materials[28] and conformational changes within the molecule that occur as a

result of an applied bias voltage[29]. In chapters four and five we will see examples of this type of rectification.

## Limits of Rectification

The quality of a rectifier is determined by comparing the amount of magnitude of the current which flows in one direction with the other direction. This is accomplished with a 'rectification ratio' defined below.

$$RR \equiv abs\left(\frac{I(V)}{I(-V)}\right) \qquad (1.1)$$

Here a ratio is taken between the magnitude of the current at positive bias with the magnitude of the current at negative bias. Inorganic devices found in modern technology can achieve RR values that are on the order of $10^6$[30]. Organic rectification ratios are typically rather small by comparison. Some of the largest rectification ratios in organic molecules have been found with asymmetric molecules[26, 27, 31] which have given ratios of up three orders of magnitude. As we discussed in the previous section, in asymmetric molecular junctions, the chromophobe is positioned a distance $L_R$ from the right electrode and $L_L$ from the left electrode. The asymmetry arises when $L_R \neq L_L$. This difference in lengths produces a difference in the capacitive couplings between the molecule and each electrode. This in turn creates an asymmetry in the voltage drops that occur at each end of the junction which leads to rectification. Figure 1 helps to illustrate this by showing a Ferrocene (Fc) subunit separated from two electrodes top (right) and bottom (left) by two long chains. For the left-most graphic the conductive unit or chromophobe is off-center, closer to the bottom electrode. This represents the case of $L_L < L_R$. In the middle graphic, the lengths of both tails are equal, placing the Fc unit directly in the center of the electrodes which would create a symmetric junction without rectification.

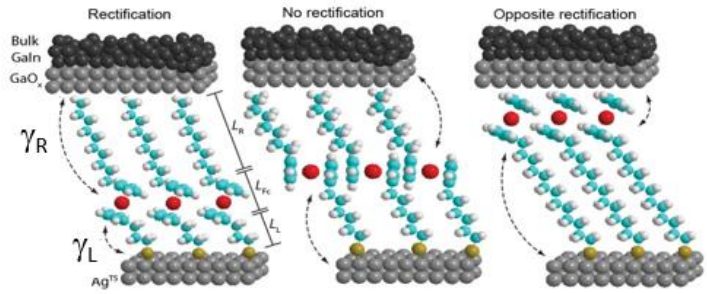


**Figure 1 This schematic shows a molecule in which the location of the active unit's position is placed in different locations within the junction resulting in Rectification in one direction, no rectification, and then finally rectification in the opposite direction. For the middle graphic, the distances between the active Fc unit and the electrodes are equal $L_R$=$L_L$. For the left graphic, $L_L$<$L_R$ and in the right graphic $L_L$>$L_R$. Reproduced from Ref [32].**

To classify the degree of asymmetry in a given molecule, a dimensionless asymmetry parameter, $\eta$, known as the voltage division parameter, is used which is defined below.

$$\eta = \frac{V_R}{V_R + V_L} \tag{1.2}$$

$\eta$ here is gives us as the ratio between the voltage drop across the right electrode and the total voltage drop across the junction. Depending on the degree of asymmetry in the molecule $\eta$ can take a range of values from 0 to 1. A value of 0.5 represents a fully symmetric molecule. As $\eta$ moves away from 0.5 in either direction the molecule progressively becomes more asymmetric. At extremes values of 0 or 1 the molecule can be fully pinned to the Fermi level of one of the electrodes[33, 34].

Further, one can write the energy level of the frontier orbital in terms of $\eta$ as $E_m = \mu_R(V) + \varepsilon + \eta V$. Here $\epsilon$ is the zero bias energy difference between the molecular orbital and the electrodes and $\mu_R(V)$ is the electrochemical potential of the right electrode. Notice here that as the voltage is swept, different values of $\eta$ will cause the frontier orbital to behave in different ways. For extreme values of $\eta$ the molecular orbital moves in step with the left/right electrode, following it as the voltage is increased

or decreased. However, for $\eta$ = 0.5, the energy of the level remains constant as the bias is increased. Since the level remains constant, the ability to conduct remains the same for both positive and negative biases and therefore no rectification occurs.

The record rectification ratios[26, 27, 31] mentioned before maybe the theoretical limits of what can be achieved with this form of molecular rectifier. A theoretical analysis shown by Garrigues et al [32] showed that for common junctions and an extreme rectification ratio ($\eta = 0{,}1$) the highest possible rectification achievable from a single level tunnel junction is three orders of magnitude. Garrigues[32] used the Landauer formalism, which is discussed in the next section, to create a single level tunneling model for molecular junctions. This model was then used to create the graphics in Figure 2 which show the current (a) and rectification ratio (b) as a function of the molecule-electrode coupling parameter $\gamma$. From this study it was determined that even fully asymmetric molecules have a maximum rectification ratio of three orders of magnitude when limited to considering reasonable values for $\gamma$. This work will be discussed in more detail in the section on Landauer theory.

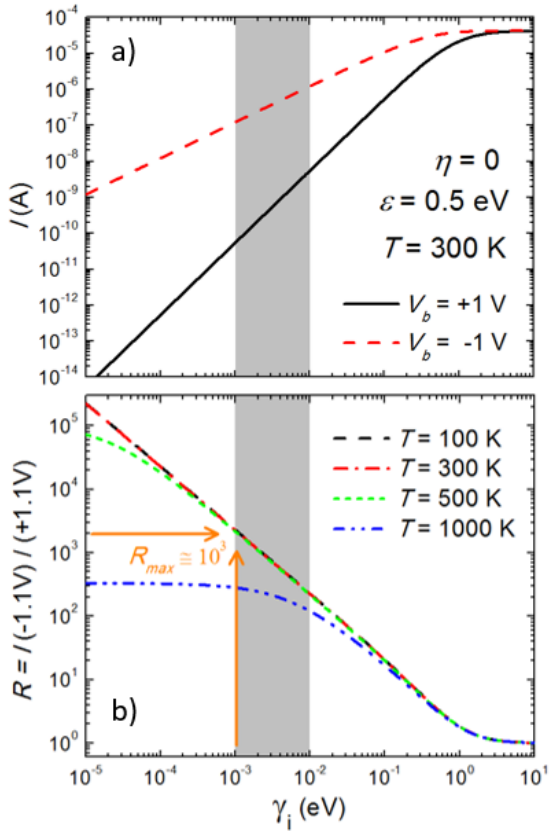


**Figure 2 Shows the electrical current a) using Landauer formalism and rectification ratio (RR) b) as a function of the electrode coupling parameter $\gamma_i$. These graphs show that for reasonable values of $\gamma_i$ the highest RR value that can be expected is about three orders of magnitude for a single level tunneling model. Reproduced from Ref [32]**

While there are some approaches to increasing the theoretical limit of asymmetric molecules, these are not expected to increase it substantially. For instance, a larger electrode Fermi level – molecular orbital gap, $\epsilon$, could lead to larger applied voltages and therefore increase the rectification ratios. However, ratios on the order of what is available in semiconductor devices are not. While chances of reaching larger RR values with a single level are slim, one could envision a molecule which utilizes more than one molecular orbital in conduction for reasonable voltages. The magnitude of rectification would be enhanced by a factor proportional to the number of levels involved. Two-level

molecular conduction and their corresponding RR values have already been observed in $S(CH_2)_{11}Fc_2$ molecules[26, 32, 35], and RR values of up to $10^5$ have been reported an $SC_{15}$Fc-C≡C-Fc molecular junction where the number of molecules responsible for conduction grows with applied bias[36]. However, again this presents limitations as the number of accessible molecular orbitals within a junction is limited. There is still hope for yet higher rectifications by utilizing conformational changes which will be discussed later. In general, the mechanisms that contribute the conduction through a molecule are still of particular interest[37-40].

## Beyond Rectification

As mentioned in pervious sections, interest in molecular electronics began by studying how molecular structures are used in biological systems. Continued research into this area hopes to use the lessons learned from biological processes[41-44] to solve problems like catalysis, energy conversion, neuromorphic computing, pattern recognition, self-learning devices, biohybrid devices and molecular switches[42, 45-57].

Electrically driven switches are a basic component used in modern computing. Creating switches from molecules could reduce the size, complexity, and power consumption of existing electrical devices. Molecular switches could also add functionality that can't be obtained through traditional semiconductor devices such as soft robotics and neuromorphic computing[54, 56, 57]. The dual functionality molecular devices we show in chapters four and five act in a way similar to 1D1R semiconductor memory devices without suffering the challenges seen in previous devices[58-62]. So far, many molecular switches have needed external stimuli such as magnetic fields or light to produce a stable switch[58, 61, 63-65]. However, needing an external light and magnetic field to switch the devices is not practical for computing purposes. The challenge in producing entirely electrical devices arises

from obtaining stable molecular states in high electric fields. Thermal relaxation can produce unstable on/off states that result in stochastic switching[59, 65] between the two states. However, molecular orbitals that are too stable states results in slow switching speeds. Studies of molecules in solution have shown stable on/off states through the formation/breaking of chemical bonds or changes in redox state[66-69]. However, these again are not practical in molecular junctions.

Another interesting aspect of biological systems is that they are dynamic. They are not in thermodynamic equilibrium and consequently they are dissipative and continuously consume energy[70, 71]. Nonequilibrium systems are adaptive and can self-heal, emulating microtubule growth[72], molecular pumps[73], or machines[74, 75]. Molecular switches that have been studied so far are static and can only switch between fixed values of on/off states[51-53]. For neuromorphic computing, dynamic switching is desirable so that it can evolve akin to biological systems. Dynamic switches must have at least two time constants to create complex dynamic behavior[70-72, 76]. Many biological systems couple a fast electron transfer process with a slow proton transfer step that stabilizes the switching process[77].

## Molecular Electron Transport Theory

### Conceptual Basis

Here we discuss a conceptual understanding of a molecular junction. Figure 3 shows a simplistic electrical schematic (a) and energy diagram (b) to give a conceptual understanding of a molecular junction. The schematic represents a three-terminal junction with a source, drain, and gate. The molecule is separated from the three terminals by a tunneling barrier. In Figure 3b) the discrete molecular energy levels are represented by N, N+1,… etc. For molecular junctions, the two orbitals closest to the Fermi levels of the electrodes contribute to the conduction across the junction. These two

levels are classified as the HOMO (N) and LUMO (N+1) levels. In Figure 3b) the electrodes are shown as black rectangles labeled L and R. These rectangles show the electrostatic potential across the junction as a bias (shown as eV here) is applied. Conduction across this example junction will only occur when a molecular energy level (here N+1) lies between the energy levels of the two electrodes. The gate is applied to move the energy levels of the molecule up and down with relation to the electrodes. Spectroscopy of the molecular energy levels can be achieved by sweeping the gate and bias voltages. However, renormalization effects caused by the junction can cause the energy levels observed in this way to vary from other measurements and calculations. This effect is known as gap reorganization and results in a compression of the HOMO and LUMO levels[16, 78-80]. A molecule with a 5 eV HOMO-LUMO gap in the gas phase could be 2-3 eV in a SAM junction and a few meV in a single molecule SET junction.

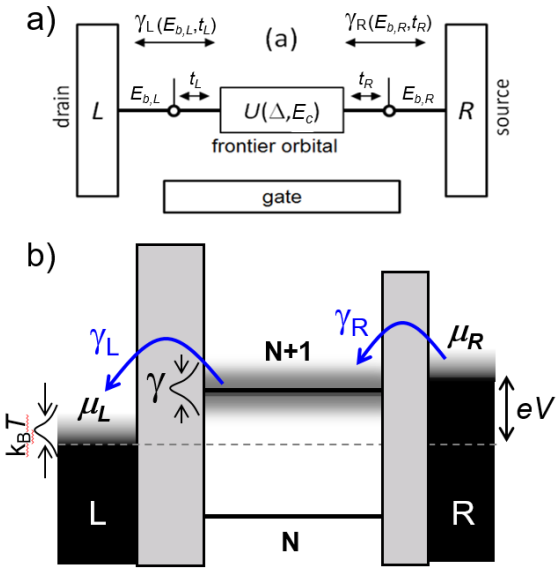


**Figure 3: Conceptual understanding of electron transport. a) shows an electrical schematic which shows the source, drain (L and R) on either side. B) Is an energy diagram that represents the energies involved in charge transport through the molecule. The left and right electrodes have chemical potentials $\mu_L$ and $\mu_R$. $\gamma_L$ and $\gamma_R$ are the partial level widths due to the coupling with the electrodes and $\gamma$ here represents the broadening of the molecular energy level. Source: Adapted from [32]**

## Theoretical Models

There are many theoretical models used to describe junctions in a variety of circumstances. Many of these models have already been well reviewed in previous works[16, 42, 81]. Here we focus on four models to describe a molecular junction. The first model describes a junction in which the molecular orbitals play no direct role in the conduction process. Simmons ignores the presence of a molecule altogether and assumes a junction that simply contains a modified vacuum between the electrodes. In this case, the molecule can still affect conduction across the junction by altering the permeability of free space between the electrodes, but the energy levels of the molecule are not considered. The next cases consider a junction of sequential tunneling. The electron travels from one electrode, into the molecule and then into the other electrode. These models can be differentiated by considering the amount of time the electron spends within the molecule. If the electron passes quickly through the molecule and maintains its energy and phase, then the tunneling is coherent. Coherent tunneling described by the Landauer model activationless and typically temperature independent (although a weak temperature dependence arises from the electronic thermal population in the leads). If the electron remains in the molecule long enough for the molecule to be coupled to the internal/external degrees of freedom, then it is called incoherent tunneling. This can further be differentiated by considering the intramolecular coupling within the molecule. Strong coupling is best described by Marcus theory which is typically temperature dependent. When the intramolecular coupling is small then temperature independent superexchange tunneling dominates[16, 82].

These models represent the extreme cases and there have been interesting studies that explore their boundaries. For instance, studies have shown coherent tunneling that transitioned into thermally

activated tunneling as a molecule's length increased[78, 83-85]. We have also seen activationless incoherent tunneling[86-88] and temperature dependent coherent tunneling[89].

## Simmons Model

Simmons' model describes a junction in which no molecular level participates in conduction. Simmons' model can be used to describe a junction with or without a molecule. However, the presence of a molecule can change the permeability of free space between the electrodes which is captured by Simmons' model. The model as described by Simmons[90-92] is reproduced in Equation (1.3).

$$\boldsymbol{J(V) = \frac{e}{4\pi^2\hbar d^2}\left\{\left(\Phi_B - \frac{eV}{2}\right)\exp\left[-\frac{2d}{\hbar}\sqrt{2m_e\left(\Phi_B - \frac{eV}{2}\right)}\right] + \left(\Phi_B + \frac{eV}{2}\right)\exp\left[-\frac{2d}{\hbar}\sqrt{2m_e\left(\Phi_B + \frac{eV}{2}\right)}\right]\right\}} \quad (1.3)$$

Here e is the elementary charge, $\hbar$ is the reduced Planck's constant, $\Phi_B$ is the height of the tunneling barrier and $m_e$ is the mass of the electron. Now as shown by Metzger[16] if we take the voltage (V) to be small compared to the barrier height ($\Phi_B \gg V$) then Equation (1.3) can be simplified[92-94] as reproduced in Equation (1.4).

$$\boldsymbol{J(V) = \frac{e^2V}{h^2d^2}\sqrt{2m_e\Phi_B}} \quad (1.4)$$

From the simplified Simmons model, we can see that the current is linearly dependent on voltage. Therefore, if the molecule in the junction is taking no part in the conduction, then the response should be ohmic for low voltages.

## Landauer Model

Landauer's theory comes about as a one dimension transmission problem[16] in which the electron transits coherently through the molecular junction. Both coherent tunneling and incoherent tunneling in which there is minimal energy loss can be described by the Landauer model. Strictly speaking, coherent tunneling occurs when an electron transits from one electrode into the molecule and then into the other electrode without altering its energy or its phase. This however rarely occurs in an experimental junction as there is usually some form of coupling with the molecule as the electron tunnels through. The Landauer model uses coupling parameters referred to as $\gamma$ to account for the energy loss due to coupling with the internal degrees of freedom such as vibrational modes. Typically, the energies of these other degrees of freedom are smaller or comparable to other effects such as thermal broadening due to coupling with the electrodes. Therefore, in a junction in which only a single level contributes to conduction (the majority of junctions), the vibrational modes can be incorporated into a temperature dependent level broadening [32], rendering the Landauer model applicable.

We can separate level broadening into two main groups. First, we consider the level broadening as a function of the electrodes. We define two coupling parameters $\gamma_L$ and $\gamma_R$ which represent the coupling to the left and right electrodes respectively with the tunneling rate being $\gamma = \gamma_L + \gamma_R$. The second main contribution is from the other degrees of freedom within the molecule which are described by $\gamma_0$. When the contributions from the second group ($\gamma_0$) are negligible and only a single level contributes to the tunneling then an expression similar to the Landauer-Buettiker formula[95] that has been used to describe the conduction through the junction in previous works[96, 97].

$$I = \frac{2q}{h}\int dE\left[f_L\left(\frac{E-\mu_L}{k_BT}\right) - f\left(\frac{E-\mu_R}{k_BT}\right)\right] Tr\left\{\frac{\gamma_L(E)\gamma_R(E)}{\gamma_L(E)+\gamma_R(E)}\, Im[G^r(E)]\right\} \tag{1.5}$$

Here $f_{L,R}(E)$ is the fermi distribution as described by Equation (1.6). The Fermi distribution describes the electron occupation levels in the electrodes and the thermal broadening of the electron. $\mu_L$ and $\mu_R$ are the chemical potentials of the left and right electrodes respectively, and $G^r$ is the molecule's Green's function. The Green's function considers the molecule's a self-energy term that includes the coupling to the leads and other degrees of freedom as an imaginary part. When a bias is applied across the junction two distinct Fermi distributions are used to describe each electrode.

$$f_{L,R}(E) = \frac{1}{e^{\frac{E-\mu_{L,R}}{k_B T}}+1} \tag{1.6}$$

Garrigues et al.[32] showed that if you solve the rate equations for each side of the junction and let the level broadening be very small, $\gamma \ll k_B T, |\epsilon|, |\mu_L - \mu_R|$ then current through the junction can be reduced to the following.

$$I = I_L = -I_R = \frac{2q}{h}\frac{\gamma_L \gamma_R}{\gamma_L + \gamma_R}[f_L(E) - f_R(E)] \tag{1.7}$$

The formalism here assumes incoherent tunneling through the complete loss of phase as the electron tunnels through the junction. This occurs due to elastic relaxation processes. A limitation of this approximation lies in the width of the level broadening. Increasing the coupling to the electrodes should not increase the current indefinitely. There exists a quantum mechanical limit to the resistance of the junction known as the Landauer limit[98].

If the small level broadening condition is relaxed, level broadening can be incorporated into the density of states density of states (DOS) function. This density of states takes the form of a normalized Lorentzian centered at an energy level $\epsilon$ given below.

$$D_\epsilon(E) = \frac{\frac{\gamma_L + \gamma_R}{2\pi}}{(E-\epsilon)^2 + \left(\frac{\gamma_L + \gamma_R}{2}\right)^2} \tag{1.8}$$

This leads to the following:

$$I = \frac{q}{h}\int_{-\infty}^{\infty} dE\ D_{\epsilon}(E)\Gamma[f_L(E) - f_R(E)] \tag{1.9}$$

Here $\Gamma = \frac{\gamma_L\gamma_R}{\gamma_L+\gamma_R}$ is the coupling parameter to the electrodes. Interestingly, this formalism was derived by assuming incoherence, but matches previous results which assumed coherence[95]. This is because when considering single level tunneling quantum interference plays no role in the conduction[99]. Equation (1.9) is also similar to the equation Landauer derived in which it was assumed that the entire system, leads, and molecule, were one dimensional. This leads to the conclusion that Equation (1.9) is a good approximation for the conduction through a molecular junction provided that the conduction through the junction is largely dependent on a single energy level and that any molecular couplings can be incorporated into the level width.

A large portion of molecular studies are conducted using Self-Assembled Molecular junctions (SAM). Equation (1.9) describes the current across a single molecule. However, SAM junctions are composed of many molecules, therefore the multiplier n is added to account for the additional current. Further, the molecules bridging the gap are not all placed identically into the junction which leads to dispersion in the system. This results in additional level broadening. A gaussian distribution is added to the model in order to account for this level broadening so that the $\gamma$ values can more accurately represent the coupling to the electrodes. This adjusted model is described below.

$$I = \frac{nq}{h}\int\int_{-\infty}^{\infty} dEdE' G_{\epsilon}\,(E)D_{E'}(E)\frac{\gamma_L\gamma_R}{\gamma_L+\gamma_R}[f_L(E) - f_R(E)] \tag{1.10}$$

$$D_{\epsilon}(E) = \frac{\frac{\gamma_L+\gamma_R}{2\pi}}{\left(E - \left(E' + \left(\eta - \frac{1}{2}\right)V\right)\right)^2 + \left(\frac{\gamma_L+\gamma_R}{2}\right)^2} \tag{1.11}$$

Here $\eta$ has been incorporated to account for asymmetry in the junction and $G_\epsilon\ (E)$ is the Gaussian distribution given by the following.

$$G_\epsilon\ (E) = \exp\left[\frac{(E-\epsilon)^2}{2\sigma^2}\right] \tag{1.12}$$

This model has been shown to effectively describe the conduction through single-molecule junctions[89, 100, 101], and has described molecular diodes in large-area junctions effectively in previous publications[22, 32, 42, 101, 102]. In preceding chapters, it will be used to describe molecular diode behavior as well as molecular switches in large-area junctions.

As we discussed in the previous section, In three terminal junctions a gate is applied to the molecule which will raise or lower the molecular energy levels. Therefore, we need to alter Equation (1.9) to account for the change in level position due to gating. Therefore, a parameter Vg is added to the density of states with a capacitive coupling parameter c. The density of states function for a three terminal device is given below.

$$D_\epsilon(E) = \frac{\frac{\gamma_L+\gamma_R}{2\pi}}{\left(E-\left(\left(\epsilon-cV_g\right)+\left(\eta-\frac{1}{2}\right)V\right)\right)^2+\left(\frac{\gamma_L+\gamma_R}{2}\right)^2} \tag{1.13}$$

Before moving on to Marcus theory, we'll study the temperature dependence of Equation (1.9). Something of particular interest is to find the high temperature asymptotic limit of Equation (1.9). The derivation of which was provided by Garrigues et al [32] and reproduced below.

$$I = \frac{2q}{\hbar}\frac{\gamma_L\gamma_R}{\gamma_L+\gamma_R}\left(\frac{qV}{k_BT}\right)e^{-\frac{E_m}{k_BT}} \tag{1.14}$$

Interestingly the temperature dependence in Equation (1.14) resembles that of Marcus' theory. Here a fully coherent tunneling model decays exponentially as a function of temperature much like Marcus theory. Here $E_m$ is like the activation energy seen in Marcus theory. However, $E_m$ here represents the energy level of the molecule and the Fermi level of the electrodes which would decrease as the voltage is increased. This is not necessarily true for the polaron-assisted conduction described by Marcus Theory. This shows that temperature dependence in a junction needs to be carefully considered to differentiate between coherent and incoherent transport.

**Marcus Model**

As mentioned previously, Marcus Theory[103-105] is typically used to describe incoherent electron transfer through a molecule. It is characterized by an activation energy that arises from a classical energy barrier. The incoherent, 'hopping' charge transport described by Marcus Theory works well to explain redox reactions where donor and acceptor molecules are surrounded by polar solvent molecules. These reactions are characterized by whether the reaction occurs in the molecules and even molecular ligands (inner shell reorganization) or in free solvent molecules (outer shell reorganization). For the former case, the solvent has little effect due to the strong coupling of the reactants. In the latter case, the polar solvent molecules rearrange the direction of the field created by the charges thereby creating a solvent polarization that determines the free energy of activation. In both cases nuclear renormalization shapes the Gibbs free energy associated with the transfer process.

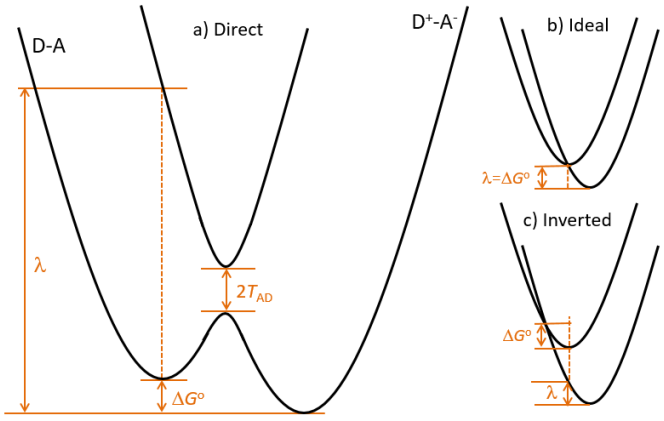


**Figure 4 Shows the commonly referred to Marcus parabolas which represent free energy diagrams of the neutral and charged states in three different charge transport regimes directed (a), ideal (b) and inverted (c). $\lambda$ here represents the reorganization energy, $T_{DA}$ is the electronic coupling energy and $\Delta G^0$ is the free energy during the transfer.**

Figure 4 shows the free energy parabolas of the Marcus Theory. Each panel a), b) and c) shows two parabolas that describe two states of the molecule. The first state is the neutral molecule where there has been no charge transfer from the donor to the acceptor site (D-A) The second parabola represents the charged state in which a transfer has occurred ($D^+$-$A^-$). The x-axis here is the 'reaction coordinate (rc)', this is not to be mistaken with distance. In each case, $\lambda$ represents the reorganization energy, and $\Delta G^0$ is the free energy during the transfer process. $T_{AD}$ represents the coupling between the donor and acceptor moieties. The strength of this coupling determines whether the transport will be adiabatic (strong coupling) or non-adiabatic (weak coupling). Marcus theory can be applied to adiabatic junctions when there is strong coupling between moieties. Weak coupling between reactions can be captured using superexchange models which will be discussed next. Figure 4a) shows the direct regime in which a finite activation energy is required for transfer. Figure 4b) shows a regime in which activationless transport is allowed from one moiety to the other. Figure 4c) describes the inverted Marcus regime in which the activation energy is again required. The inverted Marcus regime was

predicted by Marcus in 1956[103]. However, it was not observed until 1984[106] due to the reaction rate being diffusion limited[107]. Rigid bridge units between the donor and acceptor moieties fixed the distance between the two thereby allowing the inverted Marcus regime to be observed. In molecular junctions, this diffusion limit is already circumvented due to the molecule being anchored to the electrodes on either end[102]. We will explore this further in chapter six when we discuss a molecular junction pushed into the inverted Marcus regime.

As was mentioned before, when the intramolecular coupling parameter is large (adiabatic transfer) the electron transfer rate can be explained by Marcus theory given by Equation (1.16)[16]

$$k_{ET} = \left(\frac{2\pi}{\hbar}\right)|T_{DA}|^2 F_{DA} \tag{1.16}$$

Here $F_{DA}$ is the thermally averaged Franck-Condon rearrangement factor which in the classical limit becomes[103, 105]:

$$F_{DA} = \frac{1}{\sqrt{4\pi\lambda k_B T}} e^{-\frac{\left(\Delta G^0+\lambda\right)^2}{4k_B T}} \tag{1.17}$$

At high temperatures, the charge transfer is exponentially related to the temperature which results in an Arrhenius-like behavior.

$$J = J_0 e^{-E_a/k_B T} \tag{1.18}$$

Here $J_0$ is a prefactor that is dependent on the intramolecular coupling and $E_a$ is the activation energy, $k_B$ is the Boltzmann constant and $T$ is the temperature. An analysis of this the Arrhenius equation shows that an increase in the temperature results in J becoming larger until it approaches the prefactor $J_0$.

## Hopping Conduction via Superexchange

As Marcus theory describes hopping conduction for when the intramolecular coupling is strong, McConnell's superexchange model can be applied when the intramolecular coupling is weak. If the coupling is weak then nonresonant phase-coherent temperature-independent superexchange-modulated tunneling dominates[16, 82]. The superexchange model serves as a method of classifying molecules into insulators and conductors. As mentioned previously, Aviram and Ratner's first molecular rectifier depended on the σ bond (insulator) between the donor and acceptor sites. By contrast, $\pi$-bonds are typically referred to as molecular conductors. Classifying molecules into either conductor or insulator is done by considering how quickly the current decays as it crosses the junction[12, 16].

$$J(V) = J_0(V)e^{-\beta d} \tag{1.19}$$

Equation (1.19) describes McConnell's superexchange model where $J_0$ is a prefactor, d is the length of the molecule and $\beta$ is the decay coefficient. Analyzing Equation (1.19) one can quickly see that as $\beta d \to \infty$, then $J(V) \to 0$. Conceptually this makes sense as large molecules will have more current decay. Conversely, molecules with large $\beta$ values would also suffer from more decay thereby making them insulators. Molecules with conjugated π-bonds have small decay coefficient values on the order of (0.1-0.4 $Å^{-1}$) [16, 43, 84, 108, 109]. While this is a rule of thumb, many aspects contribute to a molecule's conductance[16, 42, 92] making molecular design difficult.

## Closing Remarks

As mentioned in previous sections molecular junctions can show essentially temperature-independent charge transport or substantially temperature-dependent charge transport. In the former case, the electron tunnels through the junction coherently and in the latter case the electron fully relaxes on the molecule which results in incoherent or 'hopping' charge transport. To accurately model

the conduction through a junction one first needs to identify the conduction process (coherent or incoherent). In large area junctions in which multiple molecules take part in conduction or in junctions where the constituent molecules are large, Marcus-like processes are more likely and tend to have large activation energies. Landauer-like conduction tends to occur in single-molecule junctions with small activation energies (arising from the thermal broadening of electronic occupation distribution in the leads). However, there have been examples of large activation energy Landauer-like conduction[110], low activation energy Marcus-like conduction[111] and Landauer temperature dependent behavior in single molecule tunnel junctions[89, 100, 112]. Further, in chapters five and six we discuss junctions that require a combination of both regimes to accurately model their behavior.

# CHAPTER TWO: TURNING INSULATING SATURATED WIRES INTO MOLECULAR CONDUCTORS VIA A SINGLE ATOM

In chapter one we discussed McConnell's Superexchange model which gives us a mechanism via equation (1.19) to classify molecules into either insulators and conductors. In this chapter we will use that formalism to show that changing a single atom at one end of the molecule can turn it from a conductor to an insulator. Here the molecules used are of the form $S(CH_2)_nX$ where X = H, F, Cl, Br, or I, with n = 10-18. Thereby showing that a molecule's $\beta$ is also dependent on the molecule-electrode coupling strength $\gamma$.

## Experimental Results

Fabrication, characterization, and experimental results were obtained by our collaborators in Singapore[113]. Figure 5 a) shows a schematic of the molecular junction. The molecule $S(CH_2)_nX$ is sandwiched in a self-assembled monolayer (SAM) junction between an Ag bottom electrode and a $GaO_x$/EGaIn top electrode, utilizing a well-established method[113-115] and were characterized using familiar methods as described in ref [113]. Figure 5 b) shows an energy diagram that shows how the energy difference between the electrodes and molecule changes as a function of X.

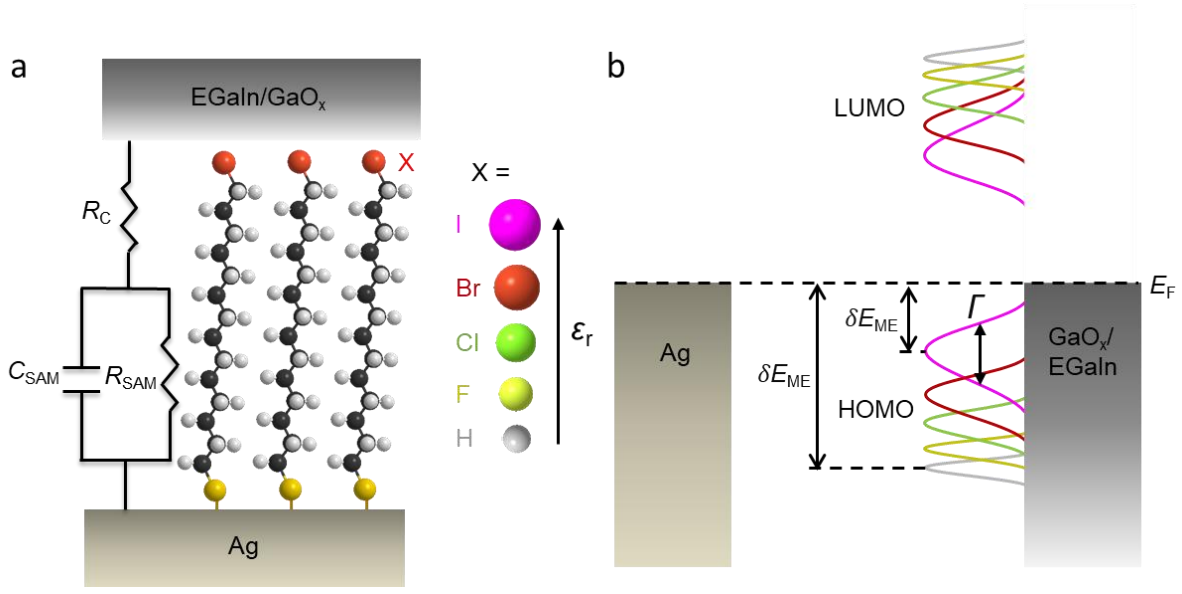


**Figure 5 (a) An illustration of an $S(CH_2)_nX$ molecule within an Ag- $GaO_x$/EGaIn. Alongside an equivalent circuit diagram. (b) Shows an energy diagram to illustrate how $\delta E_{ME}$ changes with X. Reproduced from ref [113].**

These junctions were studied through their J(V) profiles and impedance spectroscopy. The SAM junction can be treated as a capacitor (top and bottom electrodes) with a dielectric (self-assembled molecules). Therefore, one way of studying the molecular junctions is by studying the dielectric constant of the SAM junction via impedance spectroscopy[116]. For this work, statistically large numbers of J(V) curves were measured, and a Gaussian log-average was taken for each junction. Figure 6 shows a sample of the J(V) curves measured. Figure 6 a) and b) show J(V) curves for X=F and X=I plots respectively as a function of the length of the molecule. Changing the 'n' value changes the length of the molecule, thereby allowing a fit to the data using Equation (1.19). Figure 6c) shows this fit to the data for each X. From these fits $\beta$ was obtained for each molecular species and summarized in Table 1.

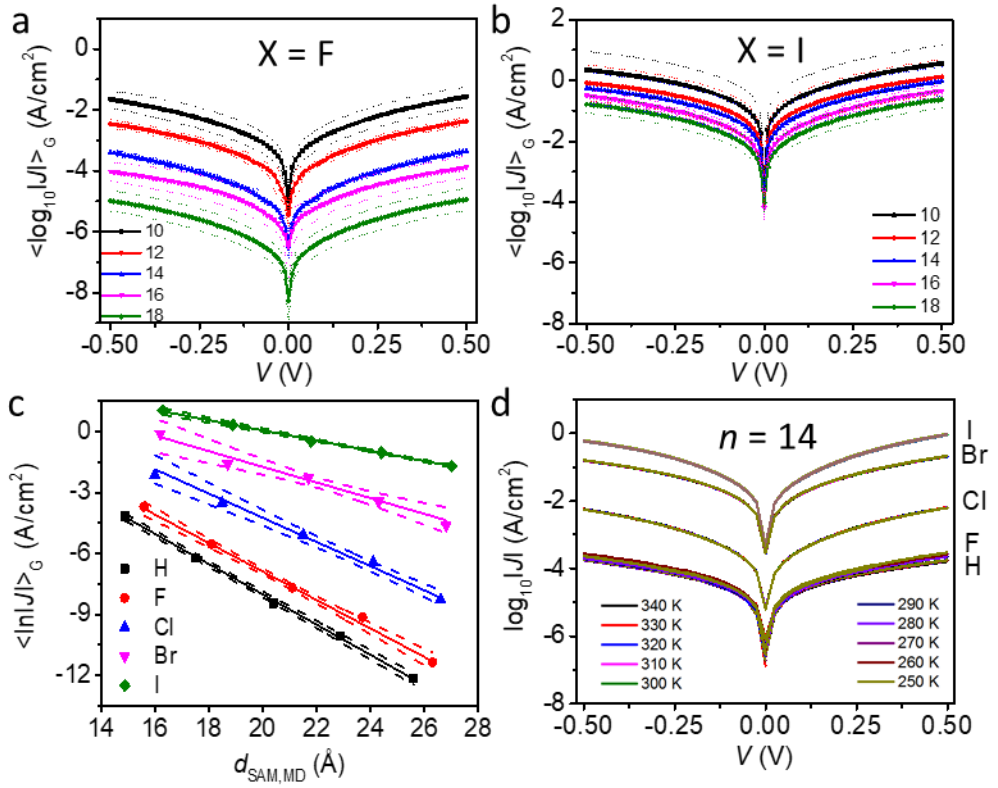


**Figure 6 a) Shows the gaussian log average current density as a function of voltage for the X=F molecule. Each curve describes a different value for n = 10,12,14,16,18. (b) Shows the gaussian log average current density as a function of voltage for the X=F molecule. Each curve describes a different value for n = 10,12,14,16,18. (c) Shows the change in current density as a function of the length of the molecule d. These are fit using Equation (1.19). (d) Shows current density plots as a function of temperature. Reproduced from ref [113]**

The dielectric constant was determined through impedance spectroscopy measurements. A previously reported method[116] was used to conduct these measurements and the data was fitted to the equivalent circuit shown in Figure 5a). Figure 7 summarizes the results of these fits. Figure 7a) shows a sharp decay in $R_C$ as the X atom changes from F to Cl to Br to I. However, the inset into Figure 7b) shows that $R_C$ is independent of n. The response of $R_C$ is larger than the odd-even effects that are expected[55] and suggested that $\gamma$ is changing substantially as a function of X. This could be explained by an increase in the van der Waals force between the molecule and top contact[115].

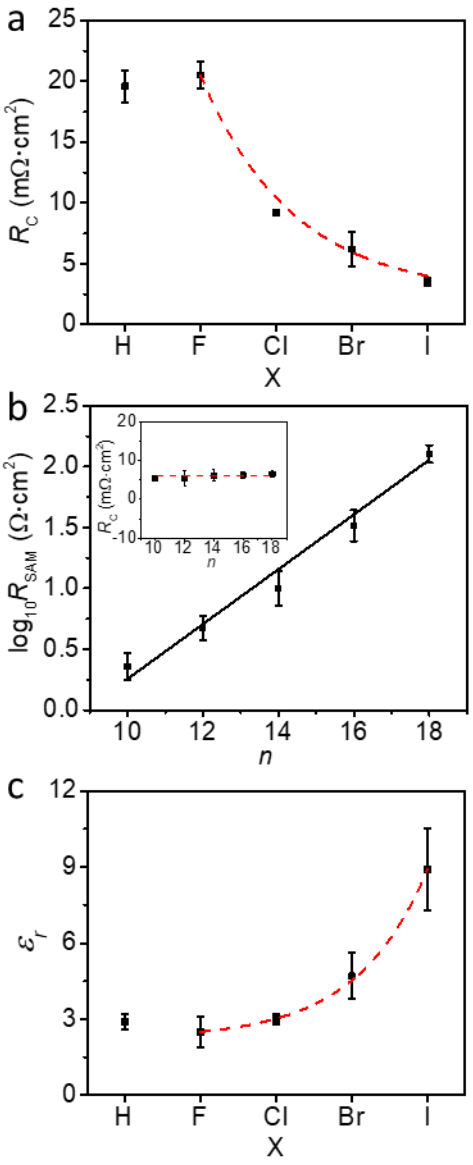


**Figure 7 (a) Shows $R_C$ (defined in Figure 5a) as a function X at 0 V. (b) Shows $R_{SAM}$ (defined in Figure 5a) and $R_C$ (inset) as a function of. n at 0 V with the black line being the fit to the curve. (c) Shows the dielectric constant as a function of X. Reproduced from [113].**

Figure 7b) shows an exponential relationship between $R_{SAM}$ and n. This is not surprising if we consider Equation (1.19) which gave us the relationship between the current density J(V) and d which is related to n. Using ohms law we can obtain the following equation for $R_{SAM}$.

$$R_{SAM}(V) = R_{SAM,0}(V)e^{\beta d} \tag{2.1}$$

Equation (2.1) and the data from Figure 7b) were used to confirm the results obtained from the J(V) measurements and summarized in Table 1. Finally, the relative permittivity was calculated using the equation for capacitance defined below.

$$C = \epsilon_0 \epsilon_r \frac{A}{d} \tag{2.2}$$

Where $\epsilon_0$ is the permittivity of free space, $\epsilon_r$ is the relative permittivity of the junction, A is the area of the capacitor or in this case, the area of the SAM junction, and d is the distance between the 'plates'. Here again, d is dependent on 'n' the number of linker units in the molecule and can be calculated from such. Figure 7c) shows this calculated $\epsilon_r$ as a function of X. It is clear from the figure that $\epsilon_r$ is climbing exponentially as a function of X while being independent of n (see supplemental information ref [113]).

## Density Functional Theory Calculations

Density Function Theory (DFT) analysis, conducted by our collaborator in Scotland, was used to gain further insight into the electronic structure of the molecular wires. First-principles calculations were conducted using the VASP code[56]. Determining the interface geometries of Ag-S$(CH_2)_{14}$X can be challenging due to the tilt angles of the SAM molecules being a soft degree of freedom. Changes in the molecular structure involve only minute changes in energy. This leads to very carefully applying the

minimization to optimize the surface geometry. The range for tilt angles for instance can range from 14.7 deg for X=H and 32.8 deg for X=C.

Figure 8 a) Shows that the potential energy at the tail end of the molecule is strongly affected by the atom at the X site. This results in a change of the Ag work function which is expected[115, 117-120]. Comparing the calculated work function with the experiment work functions shown in Figure 8 b), it can be seen that there is a strong agreement for X= H. However, for I, Br, Cl, and F, the DFT deviates from the experimental values substantially. This could be explained in one of two ways: (i) the assumption of perfect molecular order could be a factor in these calculations. As was discussed in chapter one, experimentally, there is no expectation that the molecules will all sit in the junction the same way with the same couplings to the electrodes, (ii) the previously mentioned problems with the tilting angle could also be a contributing factor here.

Figure 8 c) shows the density of states along the backbone of the molecule. One interesting feature which is shared by all varieties of X occurs at -1.5V and is marked by a (*) in the graphic. This can be explained by the hybridization of Ag-S. Further, the energy shifts that occur near 1-2 eV show a strong correlation with the X functionalization and show an increase in magnitude along the halogen series. Looking at Figure 8 d) helps to confirm that these energy shifts are due to changes occurring at the X-site.

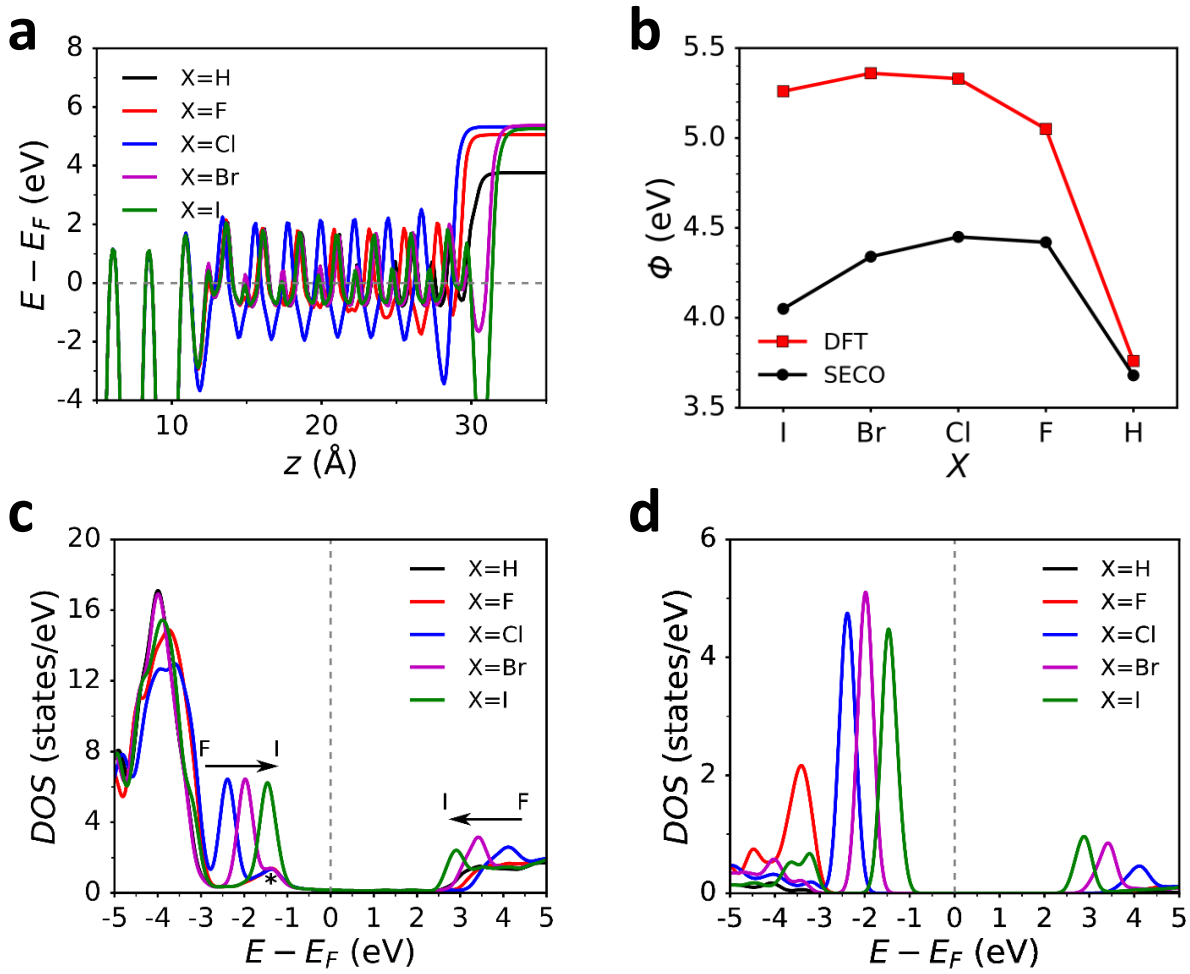


**Figure 8 a) Shows the DFT-calculated electrostatic potential of the Ag-S($CH_2$)$_{14}$X where X = H, F, Cl, Br, or I. These results were averaged over the plane and plotted along a line normal to the surface of the plane. (b) Shows the work function ($\Phi$) of the SAM junction for both the experimentally obtained values (black dots) and the values calculated from DFT(red squares). c) Shows the density of states along the backbone of the molecule. d) Shows the density of states projected onto the X site. Reproduced from ref [113]**

Finally, the relative permittivity was calculated with known methods[121, 122]. The calculations did not produce significant changes in $\varepsilon_r$ as a function of X. This understanding that $\varepsilon_r$ does not change with the functionalization of X agrees with previous findings[121, 123, 124]. However, this sharply disagrees with the experimental findings. The calculations only probe the organized SAM molecules

outside of the junction. The interaction between the electrodes and molecule could affect the dielectric behavior and therefore not be modeled by the DFT calculations. The experimental values for $R_C$ shown in Figure 7a) lend credibility to this thought. The substituents in high electric fields may be partially charged during the charge transport. Iodines in particular are known to be susceptible to this type of charging effect[125].

## Discussion and Theoretical Modeling

It has been previously noted[16, 42, 92] that the decay coefficient can be determined from the energy by $\beta = \sqrt{\delta E_{ME}}$ where $\delta E_{ME}$ refers to the energy difference between the Fermi level of the electrode and the energy level of the molecule (denoted as $\epsilon$ in chapter 1). Figure 9a) shows the relationship between the DFT calculated $\sqrt{\delta E_{ME}}$ and the experimentally determined $\beta$ a straight line is plotted in red to show the linear relationship. This agrees with commonly used coherent tunneling models[16, 42, 92] including the Simmons model which is discussed in chapter one. Simmons' model also incorporates the relative permittivity which it predicts will decrease with decreasing tunneling rates. This is effect is described by considering the image charging effects of the electrodes[91, 92]. However, again the trend seen in this work disagrees with Simmons' model and can't be explained by changes in the effective electron mass as this is already incorporated into Simmons' model[126].

**Table 1 Summary of all fitting parameters used to model with Landauer Model**

| X | $\gamma_L$ (eV) | $\gamma_R$ (eV) | $\Gamma$ (eV) | $\tau$ | ε | $\sigma$ | $n$ |
|---|---|---|---|---|---|---|---|
| H | 0.00493 | 3.25E-06 | 3.25E-06 | 0.688 | 0.469 | 0.191 | 50 |
| F | 0.00304 | 5.25E-06 | 5.24E-06 | 0.671 | 0.493 | 0.191 | 50 |
| Cl | 0.00115 | 3.56E-05 | 3.45E-05 | 0.599 | 0.484 | 0.191 | 50 |
| Br | 0.00121 | 3.10E-04 | 2.47E-04 | 0.523 | 0.474 | 0.191 | 50 |
| I | 0.00607 | 0.00201 | 1.51E-03 | 0.5 | 0.442 | 0.191 | 50 |

The Landauer model discussed in chapter one was used to fit the Gaussian log average data for each value of X. These fittings are shown in Figure 9b). The full set of parameters used are given in Table 1. However, two sets of parameters are shown in Figure 9c) and Figure 9d). These are the energy difference $\delta E_{ME}$ (referred to as $\epsilon$ in chapter one) and the coupling parameter $\Gamma$. Figure 9c) shows $\delta E_{ME}$ decreasing as we move through the halogen sequence. This trend agrees with the calculated values given by DFT (although Figure 9a) plots them in reverse order). However, the absolute values of the energies are not in agreement between DFT and the Landauer modeling. This is explained in chapter one as gap renormalization. Further, as the junctions never enter resonance the exact energies cannot be fully resolved. Therefore, the trend rather than the exact values should be considered.1. Figure 9d) shows the tunneling rate through the junction which increases exponentially as a function of X. This is expected due to the exponential increase of the current shown in Figure 9a). What is more interesting, with regards to $\Gamma$ is the relationship to the experimentally determined values for $R_C$. It has been suggested previously[127] that the coupling of the electrodes $\Gamma$ is related to $R_C$ by the relation $R_C \propto \Gamma^{-2}$. This relationship was plotted in figure Figure 9e) and shows a nice linear agreement. This suggests that changes in both $\delta E_{ME}$ and $\Gamma$ can lead to a decrease in β which agrees with results from other works[84, 110, 127-136]. The red line plotted in Figure 9e) represents a fit to the relationship between $\Gamma^{-2}$ and $R_C$. The slope of this line is 0.15 which is considerably lower than the expected value of 1. This is due to the large values of $\Gamma$ that were needed to fit the data. However, the Landauer formalism does not explicitly compensate for the changes in the dielectric constant that is observed experimentally. Therefore, the small slope could be explained by $\Gamma$ compensating for the change in the relative permittivity. As with the energy level, the trend in $\Gamma$ which agrees with the experimental results is more meaningful than the exact.

The last panel in Figure 9 shows a strong exponential relationship between $\beta$ and $\varepsilon_r$ with a slope of -0.82 (on a log-log scale). Belin and Ratner[137] suggested a relationship of $\beta \propto 1/\sqrt{\varepsilon_r}$ which would give a slope of -0.5. Their model suggests a thickness dependent barrier that arises from charge traps along the path of charge migration. Here the DFT calculations suggest a change in the barrier shape at the top electrode which may explain the differing values for the slope.

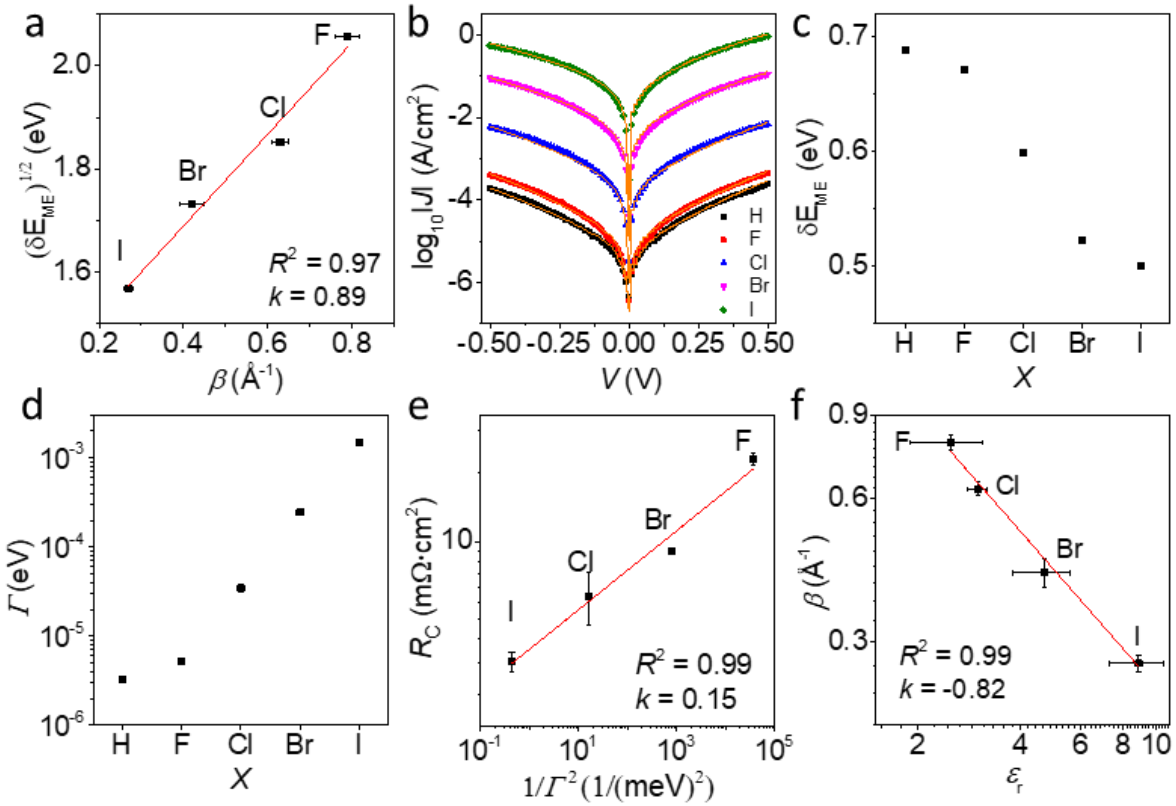


**Figure 9 a) Shows a plot of the DFT calculated $\sqrt{\delta E_{ME}}$ vs the experimentally determined β with a linear fit (red line). b) Shows the gaussian log average of the experimentally obtained data plotted alongside the fitted model (orange lines). c) and d) show two of the parameters used to fit the experimental J(V) data. e) Shows the experimentally obtained $R_c$ values plotted against $\Gamma^{-2}$ with a power law fit to the data plotted in red with slope 0.15. f) Shows the relationship between $\beta$ and $\epsilon_r$ with another power law fit plotted in red with slope -0.82. Reproduced from ref [113]**

**Table 2 Summary of parameters**

| X and *n* | $\Gamma_{SAM}$[a] | $d_{SAM,XPS}$ (nm) | $d_{SAM,MD}$ (nm) | $E_{mol,MD}$ (eV) | $\Phi_{SECO}$ (eV)[b] | $\Phi_{DFT}$ (eV) | $\beta$ (Å-1) | $\varepsilon_r$ | $\varepsilon_{DFT\text{-}VdW}$ |
|---|---|---|---|---|---|---|---|---|---|
| *n* = 14, X = H | 0.74 | 1.8 | 2.04±0.05 | 1.8±0.1 | 3.46 | 3,76 | 0.75±0.04 | 2.9±0.3 | 2.2 |
| *n* = 14, X = F | 1 | 2.1 | 2.11±0.03 | 2.0±0.1 | 4.42 | 5,05 | 0.70±0.02 | 2.5±0.6 | 2.2 |
| *n* = 14, X = Cl | 0.86 | 2.1 | 2.15±0.03 | 2.2±0.2 | 4.45 | 5.33 | 0.60±0.03 | 3.0±0.2 | 2.3 |
| *n* = 14, X = Br | 1.1 | 2 | 2.17±0.03 | 2.4±0.2 | 4.34 | 5.36 | 0.39±0.04 | 4.7±0.9 | 2.3 |
| *n* = 14, X = I | 1.2 | 2.1 | 2.18±0.03 | 2.2±0.1 | 4.05 | 5.26 | 0.25±0.01 | 8.9±1.6 | 2.4 |
| *n* = 10, X = Br | 1 | 1.5 | 1.62±0.04 | - | 4.28 | - | - | 4.4±0.4 | - |
| *n* = 18, X = Br | 1.1 | 2.9 | 2.68±0.03 | - | 3.96 | - | - | 4.6±0.2 | - |

## Conclusion

We have demonstrated that the substitution of a single atom can have a large effect on a molecule's conduction. This is reflected in changes to the molecules level alignment, coupling with the electrodes, and dielectric response. Changing the atom allowed us to tune the decay coefficient over a range of 0.25 Å$^{-1}$ to 0.75 Å$^{-1}$. DFT and Landauer modeling was used to describe the charge transport through the junction and identified three major contributions to the change in $\beta$: a change in the energy difference between the Fermi level and molecular energy level as seen by the $\delta E_{ME}$ values obtained from both DFT and Landauer modeling, the shape of the tunneling barrier at the SAM-electrode interface has shown by DFT, and the coupling between the molecule and electrode. Given that none of the models used could fully explain the experimental results, our findings point to their limitations. The Simmons model[126] predicts a behavior of $\varepsilon_r$ that would contradict our findings. Furthermore, Superexchange models[82, 138, 139] also fail to explain our findings, and the Landauer model, while able to fit the data

effectively, cannot explain the dielectric change see from the experimental results. The Landauer model produced extreme changes in the coupling with the electrodes which are unphysical. DFT was unable to explain the correlation found in the experiment between $\beta$ and $\epsilon_r$. This suggests that this correlation is due to interactions between the SAM and the junction. Berlin and Ratner's model[137] provided us an approximately close relationship between $\beta$ and $\epsilon_r$. However, the explanation given for this model relies on charge traps rather than electrostatic response. Therefore, while our work proposes an effective method of tuning the conductivity of the molecule, its nature is not fully accounted for by any theory examined here. This will hopefully stimulate further investigations into better understandings of the transport mechanisms in molecular junctions.

# CHAPTER THREE: RECTIFIERS WITH SIGMA AND PI BRIDGES

The properties of sigma and pi bridges were discussed in chapter one. Here a comparative study of them was conducted. As has been mentioned before, many factors may contribute to the measured rectification ratios found in experimental results[23, 140, 141]. Therefore, to minimize the number of extraneous factors that can contribute to the rectification ratios, similar molecules with similar fabrication techniques were used. The two molecular structures $Rh_2(O_2CCH_3)_4$ and $Rh_2(O_2CCF_3)_4$ were fabricated using a stepwise fabrication technique the details of which can be found in ref [142]. The difference between these two structures is the bridge between the donor and acceptor sites. In one molecule the ligand connecting the two is a saturated (σ) bridge (2H-s-2F) and the other is a conjugated (π) bridge (2H-c-2F). This leads to a single bond difference between the two molecules C-C vs C=C.

These two molecular structures were placed in asymmetrical Self-Assembled Monolayer (SAM) junctions and were modeled using the Landauer formalism referenced in Chapter One. The fabrication, characterization and experimental measurements were conducted by our collaborators in China[142] while the theoretical analysis conducted later was completed at the University of Central Florida (UCF). Figure 10 shows the IV curves for both the 2***H***-***s***-2***F*** (A) and 2***H***-***c***-2***F*** (B) species. From the data in each figure, there is a clear rectification in the 2***H***-***s***-2***F*** structure while there exists little to no rectification in the 2***H***-***c***-2***F*** species.

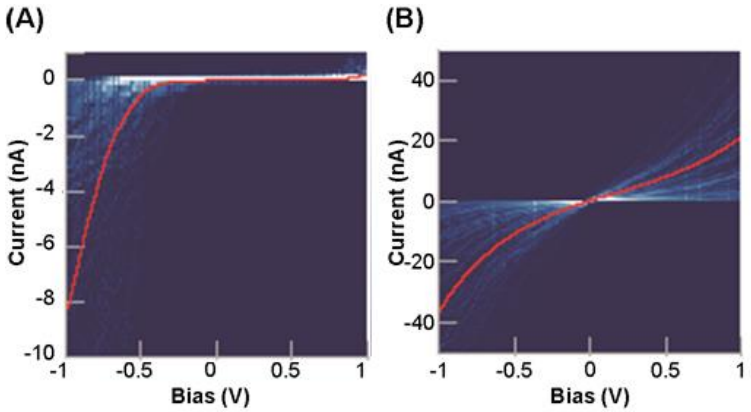


**Figure 10 Current and voltage plots for 2*Hs*2*F* (A), and 2*Hc*2*F* (B), respectively. The red line plotted on top of the data is the log average. Reproduced from [142].**

Current profiles were measured over 150 times and the rectification ratios were calculated for each run at ±1V. These rectification ratios were calculated using Equation (1.1). Figure 11 shows two histograms of the rectification ratios of the 2***H***-***s***-2***F*** (A) and 2***H***-***c***-2***F*** (B) molecules. Gaussian models were plotted over both histograms with positions 1.58 and 129 for the 2***H***-***s***-2***F*** and 2***H***-***c***-2***F*** molecules respectively.

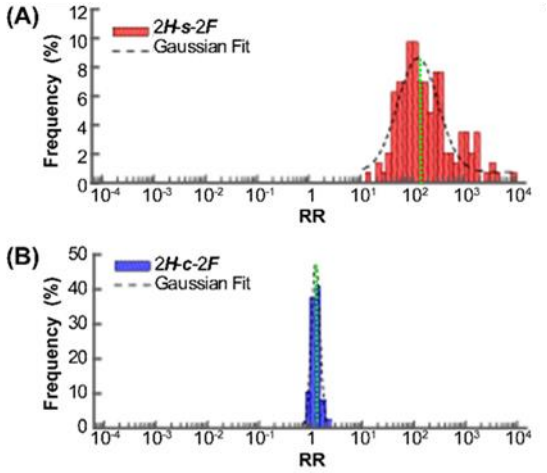


**Figure 11 Provided are histograms of the two molecular species 2*Hs*2*F* (A), and 2*Hc*2*F* (B). A gaussian was used to fit the histograms with the positions of the Gaussians being 1.58 and 129 for the 2*Hs*2*F and 2Hc2F* molecules respectively. Reproduced from [142].**

Further, the single level tunneling model described in Equation (1.10) was used to fit the log average of the experimental data. These fits are shown in Figure 12. As discussed previously, the single level tunneling model has limitations when applied to SAM junctions. Therefore, a gaussian was used to help explain the dispersion of molecules within the junction. All of the parameters used to fit the data are shown in Table 3.

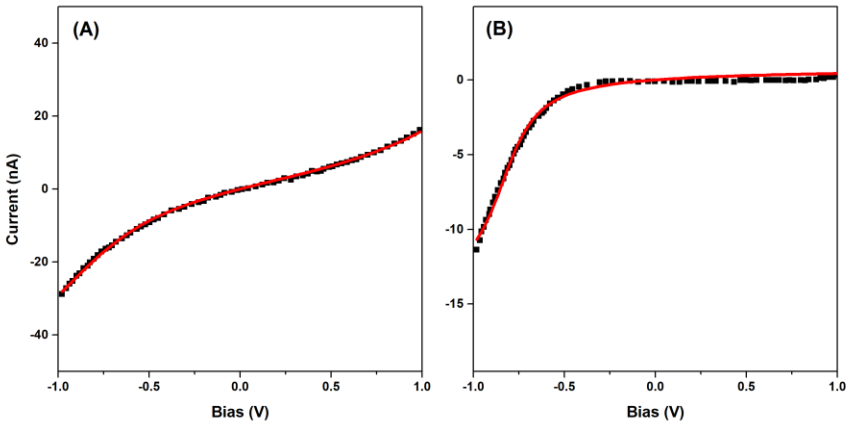


**Figure 12 Shows the experimetnal data (black) and the theoretical fit (red) for the 2H-c-2F (a) and 2H-s-2F (b) molecules.**

**Table 3 Fitting Parameters of the 2*H*-*c*-2*F* and 2*H*-*s*-2*F* molecules.**

| | 2***H***-c-2***F*** | 2***H***-s-2F |
|---|---|---|
| $\gamma_L\ (meV)$ | 32.0 | 0.06 |
| $\gamma_R$ (meV) | 8.50 | 6.33 |
| $\epsilon$ (eV) | 0.88 | 0.71 |
| $\eta$ | 0.59 | 0.74 |
| $\sigma$ (meV) | 8.78 | 178. |

The tunneling rates and level positions are shown in Table 3 all lie within the expected values for this kind of junction. However, the most important parameter to consider in this work is the asymmetry parameter. It is clear from the fitting results and the rectification ratios that the saturated molecule has an enhanced rectification over the conjugated molecule. This one bond difference between the two molecules shows that decoupling the donor and acceptor sites is crucial for molecular rectification.

# CHAPTER FOUR: ELECTRIC-FIELD-DRIVEN DUAL-FUNCTIONAL MOLECULAR SWITCHES IN TUNNEL JUNCTIONS

## Experimental Results

In chapter one we discussed molecular switches, their limitations, and applications. Here we will show a molecular switch that is reproducible and stable. Figure 13 shows a schematic of the SAM junction studied in this work. Figure 13 a) shows the SAM junction with the molecule $S(CH_2)_{11}MV^{2+}X^-_2$ sandwiched between the bottom Ag electrode and the top $GaO_x$/EGaIn electrode in a fashion similar to the other junctions studied in this thesis. The fabrication and experimental conduction measurements for this work were conducted by our collaborators in Singapore[29].

Methyl viologen, MV, has three oxidation states. The ground state is $MV^{2+}$, the neutral state takes the form $MV^0$[143],and the radical cation $MV^{\bullet+}$. $MV^{\bullet+}$ dimerizes to form a stable dimer complex $[MV^{\bullet+}]_2$. This is driven by π-π stacking and pairing of the electron spins of each $MV^{\bullet+}$[144]. Figure 13 a)-b) shows the process of dimerization and migration of the counterions.

Figure 13b) shows an inset that gives the equivalent circuit of the junction. This circuit resembles that of a 1D-1R RRAM or resistive random-access memory. Often a resistive switch and diode are paired together in series to reduce cross talk. This pairing of devices often comes with an increase in the design complexity, energy usage, and operating voltage[145]. However, as the inset in Figure 13b) suggests this molecule provides a dual functionality of a diode and a variable resistor effectively taking a complicated circuit and reducing it to a molecule of about 2 nm in length. This molecular molecule has a high rectification ratio of $2.5 \times 10^4$ which is aided by asymmetric placement of the $MV^{2+}$ unit.

Furthermore, the diode is in series with a switch or variable resistor with a high on/off ratio $\left(R_{\frac{1}{2}} = \frac{R_1}{R_2}\right)$ of 6.7 x $10^3$. This diode is made possible by the formation of the $[MV^{\bullet+}]_2$.

The SAM junctions were pre-organized and formed using known processes[144, 146]. The SAMs were then characterized using x-ray photoelectron spectroscopy and cyclic voltammograms. Figure 13c) shows the results of the voltammograms and the two successive reduction waves. The details of this characterization are provided in ref [29].

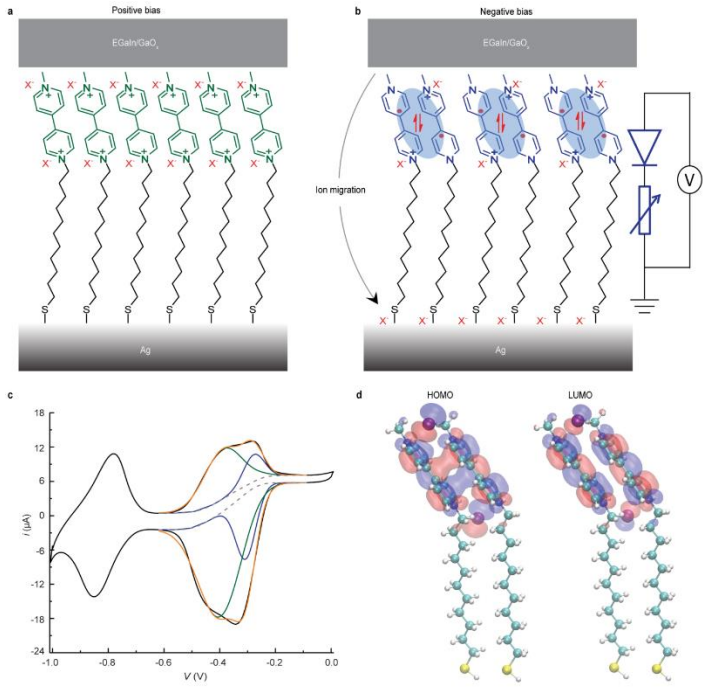


**Figure 13 a) Shows a schematic of the junction at positive bias. Here the $S(CH_2)_{11}MV^{2+}X^-_2$ (where $X^-$=$I^-$, $Br^-$, $Cl^-$, $F^-$, $ClO_4^-$ and $PF_6^-$) molecule is placed in between the Ag bottom electrode and $GaO_x$/EGaIn top electrode. b) Shows the same schematic at negative bias but the $MV^{2+}$ is reduced and $[MV^{\bullet+}]_2$ forms. The shaded blue region shows the dimer formation, and the arrow shows the direction of ion migration. Further, an equivalent circuit is shown. c) Shows a cyclic voltammogram (black line) of the $S(CH_2)_{11}MV^{2+}(Cl^-)_2$ molecule on Au in 0.1 M NaCl at a scan rate of 0.2 V/s with Ag/AgCl as a reference electrode. The first redox-wave is split into two components associated with a reduction of $MV^{2+}$to $MV^{\bullet+}$ (blue line) and $[MV^{\bullet+}]_2$ formation (green line); the orange line is the sum of blue and green lines. (d) Show the HOMO and LUMO levels of $[MV^{\bullet+}]_2\ I^-_2$ computed using Gaussian16 with dispersion-corrected B97D functional. Reproduced from ref [29].**

A statistically large sample of J(V) measurements was taken and is shown in Figure 14. Figure 14 panels a-d) show heat maps of the J(V) voltage sweeps for each variety of $X^-$. All varieties of the counterion show large hysteresis. Figure 14 panels e-h) show the on/off ratios for each $X^-$ variety. The largest recorded ratio was for the $X^-$=$I^-$ molecule at 6.7 x $10^3$. Figure 14i) shows a representative J(V) curve. The dotted lines define the variables $R_1$, $R_2$, and $I_{RR}$. Here, $I_{RR}$ is the rectification ratio defined in Equation (1.1). As is discussed in chapter 1, $I_{RR}$ ratios of three orders of magnitude are considered to be the theoretical limit for an asymmetric molecule. However, the molecules synthesized here undergo a conformational change which allows them to cheat the theoretical limit. The largest rectification was observed for $X^-$=$I^-$ at 2.5 x $10^4$.

Something else to note from Figure 14 are the voltages in which the junction switches from the low conduction state to the high conduction state. This is called the SET voltage or $V_{SET}$. We will show later that this voltage for $X^-$=$I^-$ is $V_{SET}$ = -0.90V. This voltage is comparatively low because in devices in which the diode and variable resistor are in series, two sequential voltage drops are leading to a large $V_{SET}$.

Figure 14j) shows a series of write-read-erase-read (WRER) cycles. These cycles were done to demonstrate the read and write ability of the junction. The cycles were conducted with an 11s cycling time and with a werite voltage of $V_W = -1.0V$, a read voltage of $V_R = -0.3V$ and an erase voltage of $V_E = 1.0V$. Figure 14k) shows the output of 80 the WREW cycles without loss of fidelity.

Furthermore, the junctions demonstrate excellent stability. The EGaIn top electrode stabilized microchannel were cycled ±1.5V for 2.0 x $10^6$ voltage sweeps without degradation. Figure 14l) shows voltage cycling for 1 hour with cone shaped EGlan tips. This particular junction was exposed to high electric fields and was operated continuously yet no degradation in the junction was observed. Voltage

cycling stability has been observed in previous works[36, 62, 147], however data retention with such large values for $R_{\frac{1}{2}}$ has not be observed.

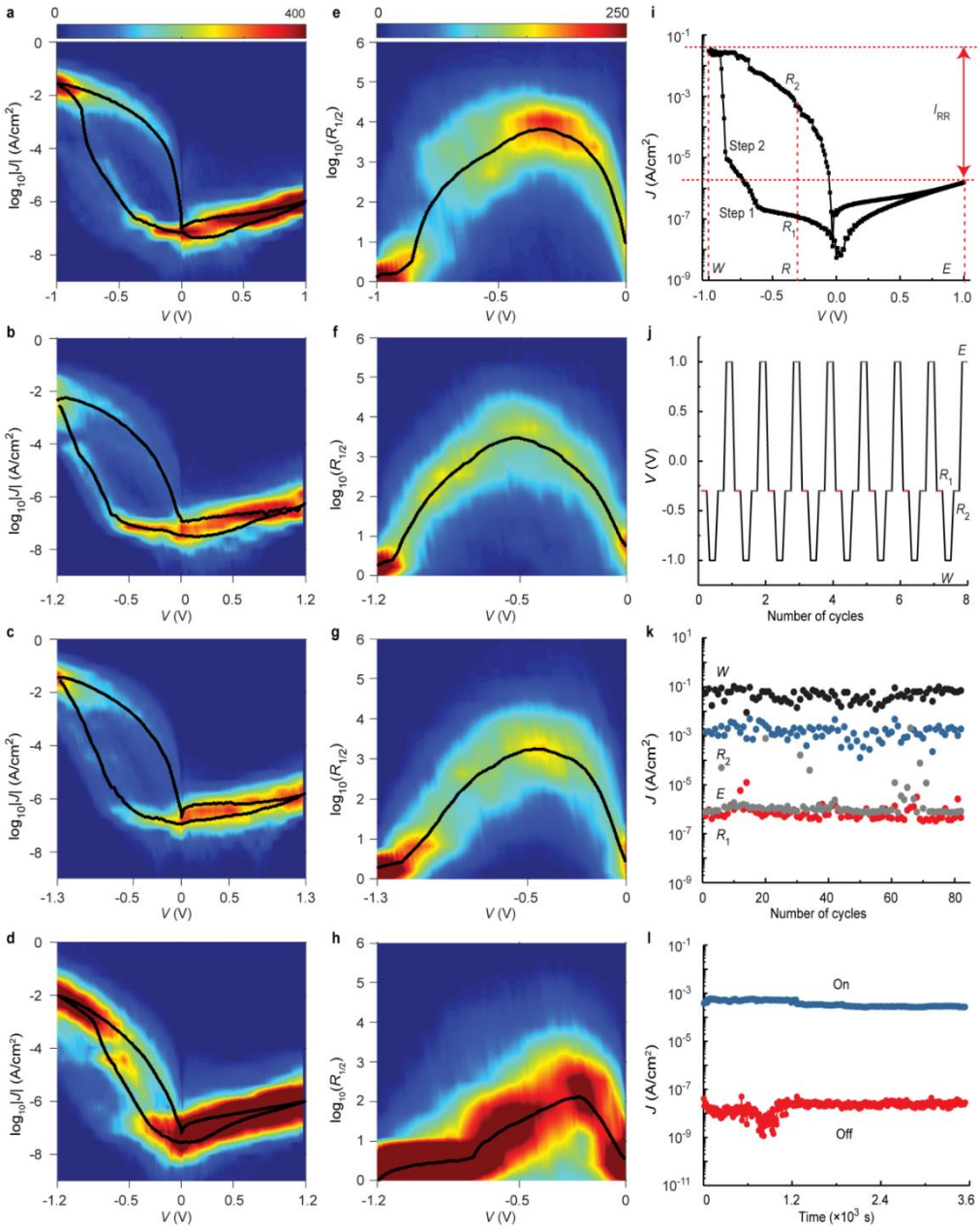


**Figure 14 Panels a-d) are heat maps showing all of the current sweeps conducted with the Ag-S(CH₂)₁₁MV²⁺X⁻₂//GaOₓ/EGaIn junctions. Panels e-h) show the heat maps for the log of the on/off ratio. Each row of panels correspond to a different counterion where X⁻= [I⁻,Br⁻,Cl⁻ and F⁻] for panels [a-e,b-f,c-g and d-h] respectively. The**

**solid black likes are gaussian log averages of the data. Panel i) shows a single representative voltage sweep for $X^-$ $=I^-$. j) Shows a read-write-read-erase pulse sequence with $V_W$=-1V, $V_E$=+1V,$V_R$=-0.3V. k) Shows the output current from this read-write-read-erase sequence. I) Gives the current retention in the on (blue) and off (red) states. Reproduced from ref [29].**

## DFT Calculations

Electronic structure calculations were conducted by our collaborators in Scotland to further understand the operating mechanism. The DFT modeling confirmed a two-step switching process in which charging of the junction was followed by dimerization and ion migration. Figure 15 shows the results of the DFT calculations. Figure 15c) and d) demonstrate the operating mechanism of the junctions. The asymmetry of the molecule means that the LUMO is coupled to the top electrode. Once the bias is high enough and the LUMO enters conduction, an electron is injected into the molecule resulting in the formation of $MV^{\bullet+}$. Dimerization then occurs and the migration of excess counterions to the bottom electrode. The HOMO-LUMO gap of $[MV^{\bullet+}]_2$ is smaller than that of $MV^{2+}$ therefore after the transition there is an immediate increase in conduction as the HOMO of $[MV^{\bullet+}]_2$ enters the conduction window. To further demonstrate the conduction mechanism the Landauer theory from chapter one was used to describe the J(V) curve shown in Figure 14i).

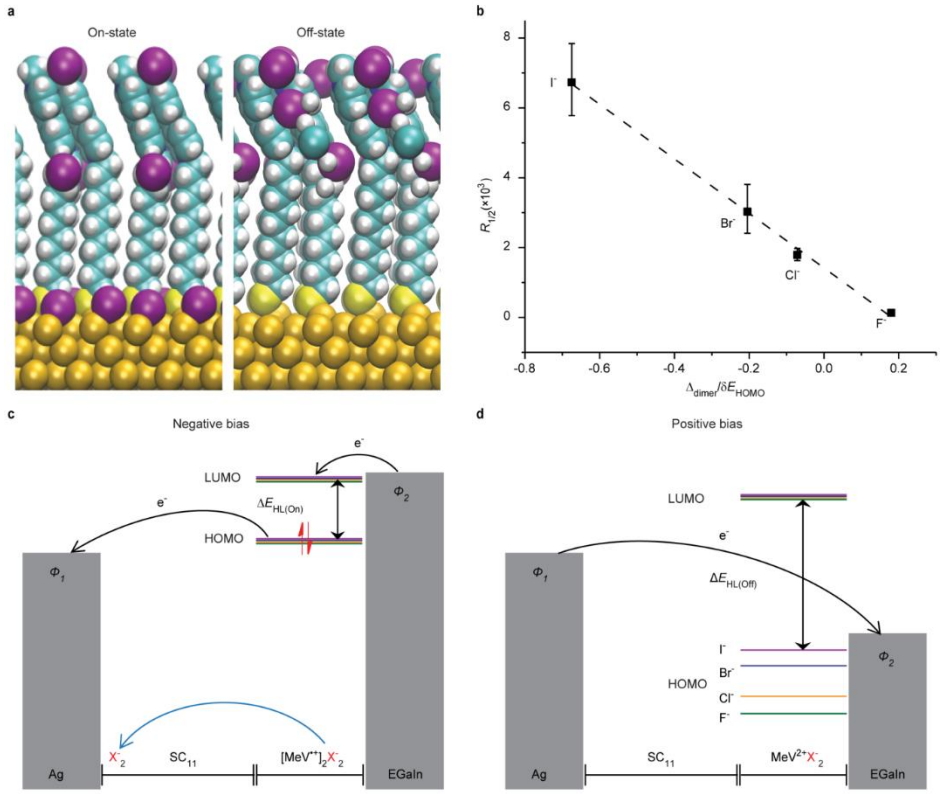


**Figure 15 a) DFT calculations for the on and off state on Au. b) Shows the experimentally obtained values for $R_{1/2}$ for each value of X as a function of $\Delta_{dimer}/\delta E_{HOMO}$. Where the error bars represent 95% confidence intervals. The dotted line is a linear fit to the data. c) and d) are energy level diagrams for the positive (1V) and negative(-1V) biases. Reproduced from ref [29].**

## Landauer Modeling

Experimental and DFT results show that the SAM junction is transitioning between the two conduction states $[MV^{\bullet+}]_2$ and $MV^{2+}$. Given that this is an ensemble of molecules we can assume that not all the molecules make the transition at the same time. Therefore, there exists some probability of being in the $[MV^{\bullet+}]_2$ or $MV^{2+}$ state which we denote as $P^{MV^{2+}}$ and $P^{[MV^{\bullet+}]_2}$. However, since the molecule can only be in one state or the other, we can confidently say that the probability of being in

the low conduction state $MV^{2+}$, can be written as $P^{MV^{2+}} = 1 - P^{[MV^{\bullet+}]_2}$. From this we can write an equation for the total current through the junction:

$$I^T = I^{MV^{2+}}\left(1 - P^{[MV^{\bullet+}]_2}\right) + I^{[MV^{\bullet+}]_2} P^{[MV^{\bullet+}]_2} \tag{4.1}$$

Where the two currents $I^{MV^{2+}}$ and $I^{[MV^{\bullet+}]_2}$ can be modeled using the single level tunneling model described by Equation (1.10). However, DFT calculations show that both the HOMO and LUMO levels enter resonance for the $[MV^{\bullet+}]_2$ form. Therefore, the current, $I_{[MV^{\bullet+}]_2}$ is dependent on the current contributions from each of the two levels, $I_{[MV^{\bullet+}]_2} = I_{h_1} + I_{h_2}$ where both $I_{h_1}$ and $I_{h_2}$ can each be described by Equation (1.10).

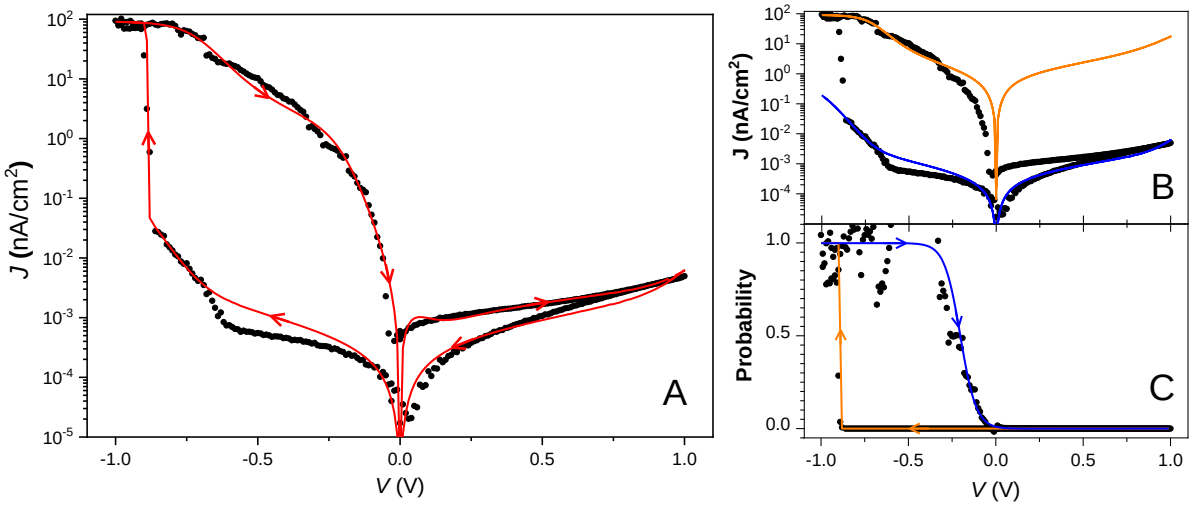


**Figure 16 A) Shows the experimental J(V) curve (black dots) and theoretical fitting using the Landauer formalism. B) Shows the two conduction states corresponding to the $[MV^{\bullet+}]_2$ (orange) and $MV^{2+}$ (blue) states. C) Uses the theoretical values from panel B and the experimental values for the current to extract the probability of being in the $MV^{2+}$ state. The solid Blue and Orange lines represent the function used to model the probability. Reproduced from ref [29]**

**Table 4 Summary of fitting parameters used to fit the data presented in Figure 16.**

| Parameter | $MV^{2+}$ | $[MV^{\bullet+}]_2$ |
|---|---|---|
| ε | 0.600 eV | 0.340 eV |
| γ | 0.003 meV | 0.414 meV |
| γ | 5.37 meV | 53.8 meV |
| η | 0.580 | 0.780 |
| σ | 0.0530 eV | 0.0140 eV |
| ε | -- | 0.560 eV |
| γ | -- | 0.334 meV |
| γ | -- | 35.1 meV |
| σ | -- | 0.007 meV |

All that is left is to determine a functional for $P^{[MV^{\bullet+}]_2}$. To accomplish this the two conduction states $[MV^{\bullet+}]_2$ and $MV^{2+}$ were fit and the results of this fitting are plotted in Figure 16b) where the experimental data (black dots) is plotted alongside the models $I^{MV^{2+}}$(blue) and $I^{[MV^{\bullet+}]_2}$(orange) models the parameters of which are described in Table 4. Since $I^{MV^{2+}}$ and $I^{[MV^{\bullet+}]_2}$ have already been determined via good fits to the data Equation 4.1 was solved for $P^{[MV^{\bullet+}]_2}$ giving the following:

$$P^{[MV^{\bullet+}]_2} = \frac{I^T - I^{MV^{2+}}}{I^{[MV^{\bullet+}]_2} + I^{MV^{2+}}} \tag{4.2}$$

Using the experimental data for $I^T$and the theoretical values for $I^{MV^{2+}}$ and $I^{[MV^{\bullet+}]_2}$ an estimated probability was calculated for each data point. These calculated probability values (black dots) are plotted in Figure 16c). From the data in Figure 16c) there is a sharp transition around -1V, and then perhaps a slower transition in the positive voltage range. Therefore, a step-like function with a variable width can describe the probability. A sigmoid function was chosen to describe the probability such that:

$$P^{[MV^{\bullet+}]_2} = \frac{1}{1+e^{\frac{V+V_{SET}}{W_{SET}}}} + f(V) \tag{4.3}$$

Where $V_{SET}$ was defined earlier as the voltage in which a transition occurs. For this junction there would be two such transitions and Equation (4.3) would be applied to each of them giving two transition voltages. Using Equations (4.1) and (4.3) the experimental J(V) data from the $X^-$=$I^-$ species was fit with the parameters in Table 4. The results of this fit are shown in a). The first transition ($MV^{2+}$→$[MV^{\bullet+}]_2$) is very sharp with a position $V_{SET} = -0.90\ V$ and width $w_{SET} = 0.001\ V$. The second transition ($MV^{2+}$→$[MV^{\bullet+}]_2$) is broader with a position at $V_{SET} = -0.16\ V$ and width $w_{SET} = 0.045\ V$. However, the sigmoid alone does not fully explain the small difference in conductance that occurs after zero bias. To model this, a linear function $f(V) = m(V - 1)$ where m = -7.1x$10^4$ $V^{-1}$ was added to Equation (4.3) to capture this. Both theoretical transitions are plotted in Figure 16c) with the data.

## Conclusion

In this chapter we demonstrated molecular switches with high resistive on/off and rectification ratios. The dual-functionality switches provide diode and memory functionality at low drive voltages and at molecular size scales. Further, studies are needed to fine tune the balance between stability and switchability. However, this system already demonstrates a highly stable and effective system. This was accomplished by optimizing the size of the counterion and the preorganization of the molecules. These findings can also be extended. The molecular device was stabilized by switching in two distinct steps that were associated with the charging and dimerization of the molecule. Although redox processes have been studied[148-150], the results here show that the switch can be stabilized by ion migration. Further, these junctions were modeled by adapting the Landauer formalism to effectively model the switching behavior.

# CHAPTER FIVE: DYNAMIC MOLECULAR SWITCHES

## Dynamic Molecular Switches

Typical molecular switches have fixed probabilities of transitioning from one state to the other. Figure 17 panels A-D show different switch varieties. The panels show the probability of being in the 'on state', $P_{on}$ as a function of an applied voltage. Figure 17A) Is an example of a static switch. As the voltage increases, the probability is turned on. As the voltage decreases, the probability is turn off and returns via the same path. Figure 17B) Shows a hysteretic switch like the one studied in Chapter Four. In this case, the switch is resistant to change. Therefore, there is a delay in switching which gives rise to the molecule 'remembering' which state is in. These two types of switches have been studied for a large variety of molecules[51-53]. Figure 17C) Shows an example of stochastic switching. Stochastic switching has been observed in molecular junctions before[59, 65], but it is hard in these cases to determine the source of the stochastic switching. In this chapter, we show a dynamic switch which is the molecular equivalent of a memristor. The proton-coupled electron transport (PCET), eliminates the stochastic behavior. In this case, the dynamic switch has a memory that is decoupled from the time scale of the voltage sweep. The molecule 'remembers' its previous switching history Figure 17D).

Figure 17E) shows the molecule considered in this study. The SAM has an Au bottom electrode and an EGaIn top electrode. The molecule has a 5,6,11,12,17,18 hexaaztrinaphthylene (HATNA) terminus. This molecule, $H_0$-HATNA, will undergo six successive steps (n=1-6) for dynamic covalent N-H bond formation[151, 152]. Here the 'on state' of the molecule occurs during the first few oxidation states (n=0-2). For the 'off-state' the molecule is progressively reduced (n=3-6). This progressive reduction occurs in the negative bias range. In the positive bias range, $H_6$-HATNA oxidizes back to HATNA.

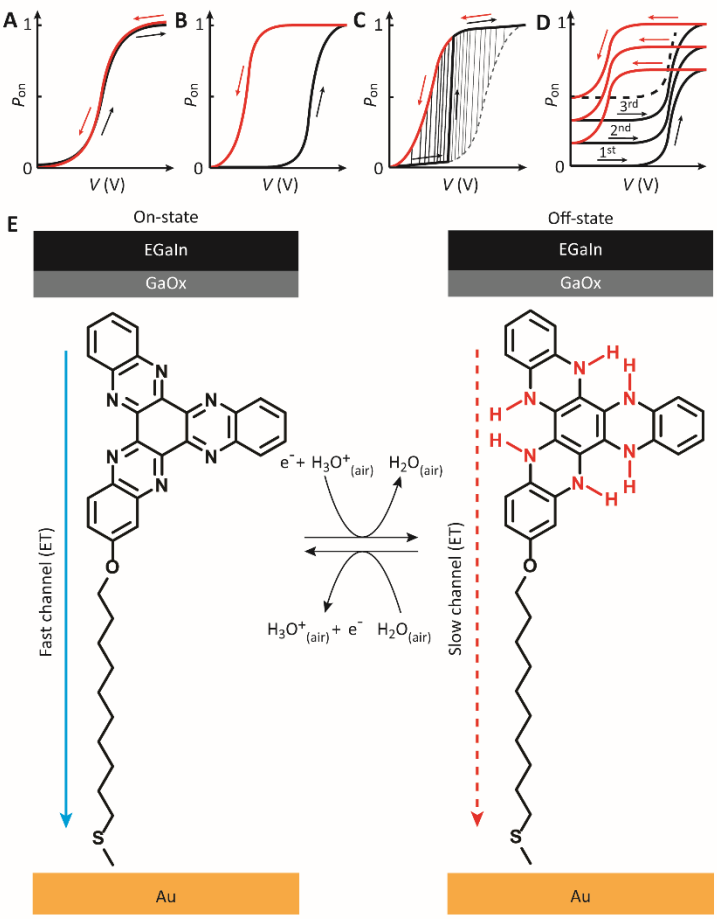


**Figure 17 Panels A-D shows various types of switches. A) Shows a 'static' switch. B) a hysteretic switch C) a stochastic switch and finally D) a dynamic switch. E) Shows a molecular schematic that represents the on and off states. Reproduced from ref [153].**

## Proton-coupled charge transport and dynamic covalent bond formation

These junctions were fabricated by our collaborators in Singapore and characterized using previously reported techniques better described in ref [153]. Figure 18E) shows our proposed mechanism of four consecutive redox steps which is supported by DFT calculations of reorganization energies λ, which were conducted by our collaborators based out of Scotland. MD simulations show that

the final redox state is the same supramolecular structure as the initial state. Figure 18F) describes the projected density of states for the steps described in Figure 18E). Figure 18G) shows the DFT calculated HOMO and LUMO energy levels for each level described by Figure 18E). From Figure 18G) we see that the initial energy gap between HOMO and LUMO states is around 2 eV, but the first protonation introduces a midgap state at around 1.1 eV and remains until the n=4 step. This midgap allows for a lower energy tunneling channel for conduction in the 'on state' until it disappears restoring the 'off' state.

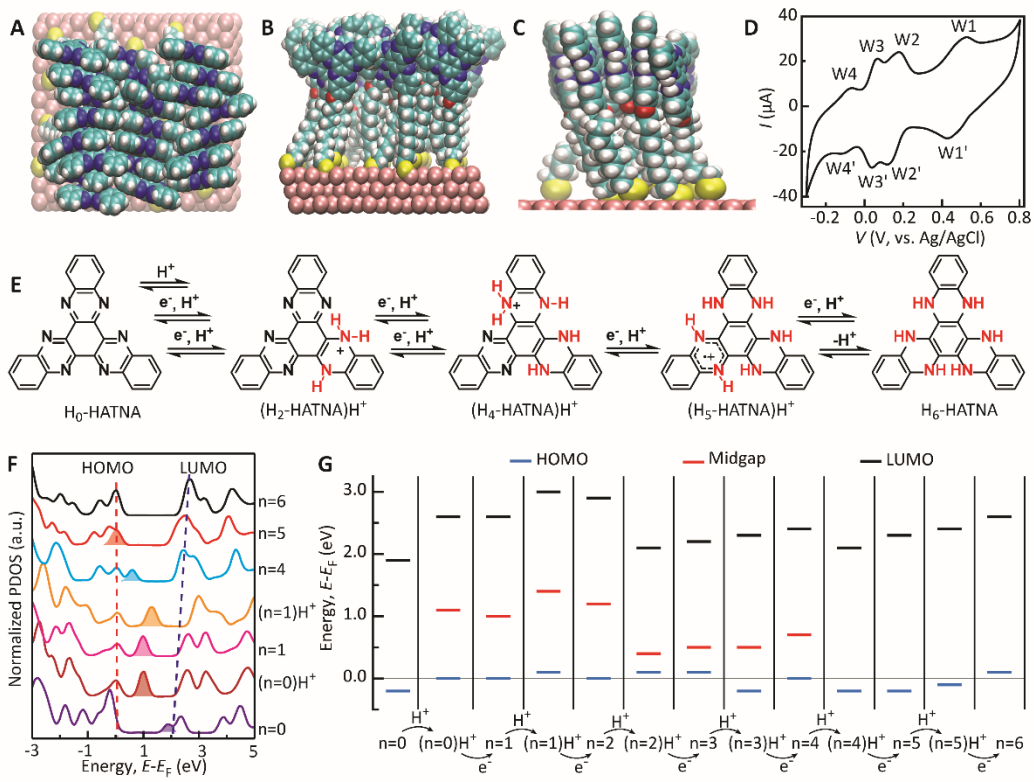


**Figure 18 A-C) Show computed simulations of the supramolecular packing in the HATNA SAMs from various perspectives including from above A) for the side B) and a 'zoomed in' side perspective C). D) Shows a cyclic voltammogram of the HATNA SAM junction. E) Shows the PCET mechanism including the multiple steps. F) Shows the DFT calculated density of states for each n-step. G) Shows the corresponding HOMO, LUMO, and midgap energies for each n-step. Reproduced from ref [153]**

## Electrically powered dynamic switches in solid-state junctions

Figure 19A) shows a heat map of J(V) curves recorded from 57 separate junctions. The black curve on top represents a gaussian log average of the 171 curves. One thing of note is the large peak shown in the graphic. Arrows 1,2,3 and 4 show the direction of the current during a voltage sweep. The voltage, starting at 0, first sweeps to positive voltages, then back again, passing through zero, and shows a large peak at negative bias. As the voltage continues to increase the current drops in magnitude and follows path 4 pack to zero as the voltage is reversed. The projected density of states data suggested that at high enough negative voltages the midgap state shown in Figure 18 disappears thereby cutting off that channel for conduction. Only at positive values is the molecule oxidized. The HATNA molecule then returns to the n=0 state and the system is reset into the 'on' state.

The J(V) curves are smooth without much fluctuation indicating that these are not stochastic switches that are plagued with excessive noise as has been seen in previous works[59, 65, 154-156]. State of the art diodes [157] report a peak to valley ratio, $R_{PtV}$ (defined in Figure 19A) that is comparable to the $R_{PtV}$ value found here of 13.7 ± 3.5. Our value for the $R_{on/off}$ ratio is 2.46 ± 1.41 x $10^2$ which is the highest value reported to our knowledge.

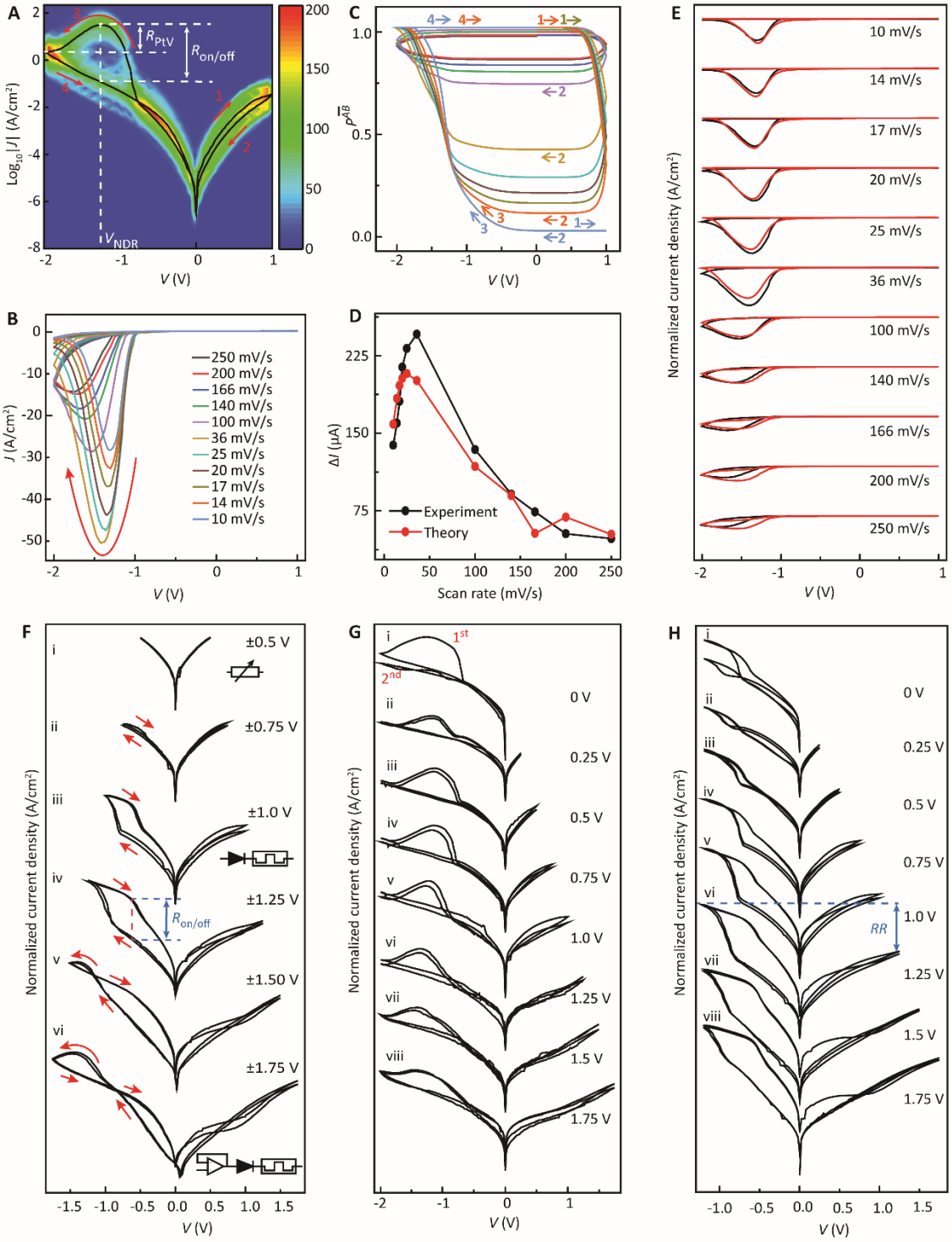
A
B
C
D
E
F
G
H
$R_{PtV}$
$R_{on/off}$
$V_{NDR}$
$\log_{10}|J|$ (A/cm²)
V (V)
250 mV/s
200 mV/s
166 mV/s
140 mV/s
100 mV/s
36 mV/s
25 mV/s
20 mV/s
17 mV/s
14 mV/s
10 mV/s
J (A/cm²)
$\rho^{AB}$
ΔI (μA)
Experiment
Theory
Scan rate (mV/s)
Normalized current density (A/cm²)
±0.5 V
±0.75 V
±1.0 V
±1.25 V
±1.50 V
±1.75 V
1st
2nd
0 V
0.25 V
0.5 V
0.75 V
1.0 V
1.25 V
1.5 V
1.75 V
RR

**Figure 19 A) Shows a heat map of 171 completed voltage sweeps from 57 separate junctions. The black line plotted on to shows the log gaussian average of these sweeps. B) Shows scan rate dependent measurements of the junction for values ranging from 10-250 mV/s. C) Represents the calculated probability of being in the 'on' state. D) Presents the change in current for the forward and backward sweeps. E) Show the scan-rate dependent sweeps (black line) and the fitted data (red line). F) Shows symmetric voltage window dependent measurements of the junction for voltage values ranging from ±0.5V to ±1.75V. G) and H) show asymmetric voltage window dependent measurements such that one voltage is kept fixed and the other is varied. For G) The negative voltage was fixed at -2.0V while the positive was varied. H) The negative voltage was kept at -1.20. Reproduced from ref [153]**

Figure 19 panels B) and E) show scan rate dependent data of the junctions. Here the scan rate was increased from 10 mV/s to 250 mV/s. The NDR peak (defined in Figure 19A) shows a steady increase in magnitude and then decreases. This is further described in Figure 19 D) which shows the difference in magnitude of the forward and backward sweeps at the $V_{NDR}$ voltage. These measurements are taken sequentially on the same junction, but the same behavior is observed when the junction is swept in reverse order. The red lines in Figure 19 panels D) and E) are theoretical fits to the data in which all parameters but the scan rate were kept constant. This indicates good agreement with the experiment. This behavior of increased then decreased NDR can be explained as follows. When the junction is in the 'on state' and begins to sweep into negative bias the NDR increases because the junction does not have time to switch to the 'off state'. The voltage does eventually switch to the 'off state'. The junction is now in the 'off state' as it crosses back into the positive voltage range, however, if the scan rate is large enough the junction doesn't have time to fully switch into the 'on state'. Therefore, a max NDR occurs in an intermediate state between these two extremes.

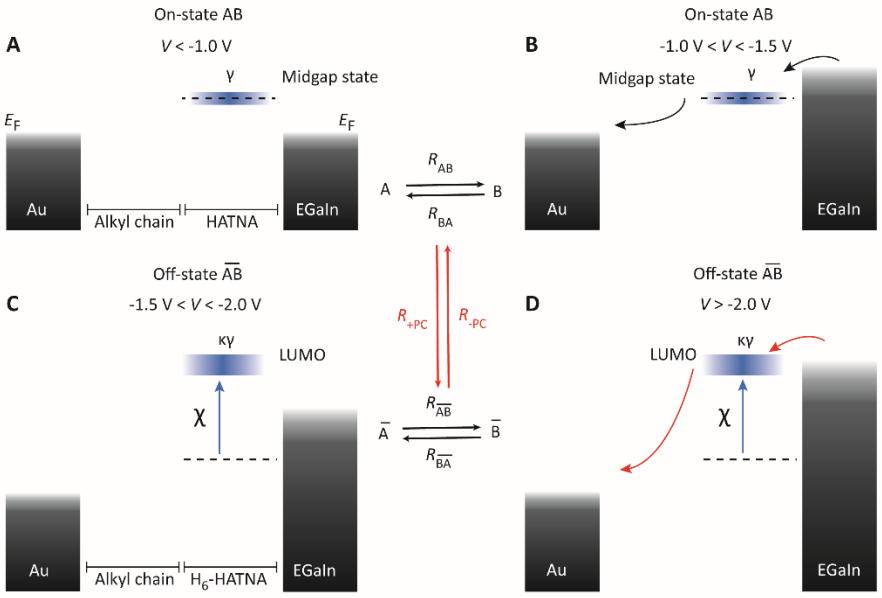


**Figure 20 Shows energy level diagrams that describe the modeling of the switch. (A, B) Describe the 'on states' and (C, D) describe the 'off states'. (A, B) utilize the mid-gap level to have higher conduction and are therefore the 'on state'. Reproduced from ref [153]**

## Mechanistic Modelling of the dynamic switches

The junctions were modeled using a framework developed by Migliore and Nitzan[154]. Note that this model was developed to describe a three-level system and here is being used to describe a molecule that is expected to make six separate transitions. Figure 20 helps to illustrate the theory developed by Migliore and Nitzan. Here the top diagram represents the junction in the 'on state' defined as the 'AB' state. Figure 20 A) shows the junction when 'off resonant' tunneling occurs. Figure 20B) shows intermediate negative voltages when the midgap energy level enters the conduction window and the 'fast' conduction transport channel is opened. This 'fast' transport channel is governed by Marcus ET rates $R_{AB}$ and $R_{BA}$. Figure 20 panels C and D represent the 'off' state. Here transport is through the reduced $H_n$-HATNA state where n = 5-6. This off state is represented by $\bar{A}\bar{B}$ where A and B are the occupied and unoccupied midgap level. Here, the midgap state is nonexistent, effectively

increasing the height of the LUMO by an amount $\chi$ and the coupling with the electrodes changes from $\Gamma$ to $\kappa\Gamma$. This change in energy causes the transition between the highly conductive 'on state' to the low conduction of the 'off state' which never enters resonance in the voltage range studied here. Here again we see that the transition rates $R_{\overline{AB}}$ and $R_{\overline{BA}}$ govern the coherent tunneling in the off state. The time scale of proton coupling $R_{+PC}$ and $R_{-PC}$ is much higher than that of electron transition. Therefore, electron rates can be modeled with Landauer formalism which describes the current through the junction. However, the slower proton coupling is described by the classical Marcus theory.

Equation (5.1) describes the total current across the junction. This is equivalent to the equation used in chapter four, Equation (4.1).

$$I(V) = P^{AB}(V)I^{AB}(V) + P^{\overline{AB}}(V)I^{\overline{AB}}(V) \tag{5.1}$$

Again, as in chapter 4, the current through the junction is governed by the percentage of molecules in the 'on' AB state or the 'off' $\overline{AB}$ state. Therefore, we have two probabilities $P^{AB}$ and $P^{\overline{AB}}$ where $P^{AB}(V) = 1 - P^{\overline{AB}}(V)$. The currents $I^{AB}$ and $I^{\overline{AB}}$ are described by the Landauer tunneling model described in chapter one, Equation (1.10). The parameters used to describe the current through $I^{AB}$ and $I^{\overline{AB}}$ are coupled through $\epsilon_{\overline{AB}} = \epsilon_{AB} + \chi$ and $\Gamma_{\overline{AB}} = \kappa\Gamma_{AB}$ where $\Gamma$ is the coupling parameter definedin chapter one. The major difference between chapter four and chapter five is the functional used for the probability. Here we use the model provided by Migliore and Nitzan[154] to provide the probability functional.

$$\frac{dP^{AB}}{dt} = (1 - P^{AB}) < R_{+PC} > \; - P^{AB} < R_{-PC} > \tag{5.2}$$

Where $< R_{+PC} >$ and $< R_{-PC} >$ are described by the Marcus transfer rates described below.

$$R_{+PC} = \frac{\gamma}{2}\sqrt{\frac{\pi k_B T}{\lambda}}\, exp\left[-\frac{(\alpha_{+PC}+\lambda)^2}{4\lambda k_B T}\right] \quad R_{-PC} = \frac{\gamma}{2}\sqrt{\frac{\pi k_B T}{\lambda}}\, exp\left[-\frac{(\alpha_{-PC}-\lambda)^2}{4\lambda k_B T}\right] \tag{5.5}$$

where $\lambda$ is the reorganization energy, $\gamma$ is the coupling parameter associated with protonation, and $\alpha_{ij} = \mu - E_{PC} + eV$. $\mu$ is the electrochemical potential of the leads and $E_{PC}$ is an energy associated with the protonation process.

Figure 19C gives the calculated probability for the scan rate junction. Since the scan rate dependent measurements were taken consecutively the final probability of the previous junction acted as the initial probability of the next junction. This is reflected in Figure 20C and shows the evolution of the probability throughout the entire set of measurements starting with $P^{\overline{AB}} = 0$ '(blue line) The system moves toward the 'off state with the $P^{\overline{AB}}$ increasing in the regime where $R_{+PC} > 0$ and $R_{-PC} \approx 0$. After the junction completely turns off and the junction shifts back to the positive bias, the rates flip with $R_{+PC} \approx 0$ and $R_{-PC} > 0$. At V=0, the scan rate increases and the junction begins another cycle. However, the $P^{\overline{AB}}$ never returns completely to 0 at positive voltages and as the scan rate increases the junction has less time to recover, therefore the probability increases after each cycle, approaching $P^{\overline{AB}} = 1$.

## Reconfigurable operation of the devices

To show the reconfigurability of these molecular devices, the applied bias window was varied. Figure 19F) shows that for small voltage ranges symmetric and reversible off resonant tunneling occurs. For intermediate voltages, the HATNA is partially reduced n=1-2 which locks the state into the 'on' state which gives a memory switch. Here the $R_{on/off}$=8.1 x$10^2$ at V = -0.63V. This shows the transition between

the variable resistor to a memory element simply by changing the bias window of the same molecule. For large values of V, an NDR region becomes accessible due to a greater reduction of HATNA.

Figure 19 G and H show asymmetric junctions in which the negative bias remained constant while the positive bias varied. This showed that the junction can only be reset at positive voltages. For the (i) data set in panel G) the first cycle shows a large NDR while the second cycle shows no NDR. Indicating that the junction stays in the 'off' state after the sweep to 0V and back. However, when the junction sweeps to +0.25 V, the NDR returns. For panel H) the negative bias was limited to -1.25 V. These junctions show a large rectification ratio of 3.1 x $10^3$ therefore, exhibiting both diode and variable resistor behavior. This is similar to the 1D-1R memory switch discussed in the previous chapter.

## Fitting of Bias Window Dependent Data

Table 5 shows all the parameters used across all junctions. Some of the parameters used were fixed for all junctions such that $T = 300$ K, $\eta^{AB} = \eta^{\overline{AB}}$ = 0.67, and $\sigma^{AB} = \sigma^{\overline{AB}} = 76$ meV, others were allowed to vary with each cycle. This is due to the complicated nature of the molecule, varying the bias window causes changes to occur.

Modeling of the asymmetric bias cycles was challenging due to the six separate oxidation states of the molecule. As the voltage range varies the oxidation states accessed by the molecule also change, causing varying couplings within the molecule. Figure 21 shows all of the fitted experimental (black) and theoretical (red) I(V) curves used for this work. The parameters in Table 5 all lie within the characteristic SAM junctions. Further, the model works remarkably well to describe the behavior of the junctions given the simplicity of the model and the complexity of the molecule. There were three main observations that the model sought to explain 1) reversible off-resonant tunneling for voltages less than -1V, 2) a

molecular memory switch with $10^3$ on/off ratio, and 3) a large NDR that is the result of the complete reduction of the HATNA molecule.

One of the parameters of particular interest is $\kappa$. $\kappa$ is a dimensionless parameter that describes the change in $\Gamma$ that occurs after protonation. Table 5 shows the values for $\kappa$ change as a function of the range of the bias window. Bias windows that end before -1.25 V tend to have a value for $\kappa$>100 while bias windows that incorporate voltages lower than -1.25V tend to have a value for $\kappa$ in the range of 40-60. Similarly, $\chi$ which Migliore and Nitzan call the exchange parameter which governs the energy shift of the orbital. However, given that $\chi$ the low conduction state ($H_n$-HATNA where n=5-6) never enters resonance the calculations are somewhat insensitive to $\chi$. We can say from the calculations that $\chi$ must be greater than 1 eV, but an upper bound for $\chi$ is not precisely known. Note that the combination of a high $\kappa$ and high $\chi$ are what give us the crossing of the high and low conduction curves seen in Figure 21 panels A-C). Every junction modeled (including the scan rate data when viewed on a log scale) in which the voltage dropped below -1.25 showed a cross over. Every other junction did not and had a lower value for $\kappa$.This occurs because the tunneling rate is higher in the 'off state' than in the 'on state', this is true because $\kappa > 1$. Therefore, the off resonant conduction is higher in the 'off state'. However, the 'on state' enters resonance sooner ($\chi > 0$). Once in resonance the conduction in the on state quickly overtakes the 'off' state.

The experimental results (black) shown in Figure 21 for the A) symmetric scans and B) asymmetric scan with variable negative voltages show similar behaviors. Further, The theory (red) accurately describes the same behavior. The junction can be seen to transit between the three regimes, variable resistor, molecular memory, and NDR. This confirms the explanation that the molecular reduction occurs at negative bias while oxidation occurs at positive bias.

Figure 21 panels C) and D) show the I(V) curves for the asymmetric bias window measurements in which the negative voltage was kept constant while the positive varied. The negative voltage was fixed at V = -2 for C) and V = -1.2 for D). Again, from Table 5 we observe the same behavior that $\kappa$ is much smaller for voltage sweeps where the minimum voltage is >-1.2V. Another thing to note is that the model nicely captures the difference between the first and second scans in panel C) (i) of Figure 21. These two cycles show conclusively that the junction is reset in the positive voltage range because the molecule stays in the reduced 'off' state when the voltage never goes larger than 0V. However, in the next cycle (ii) where the maximum bias applied increases to 0.25, then suddenly the hysteretic and NDR features return.

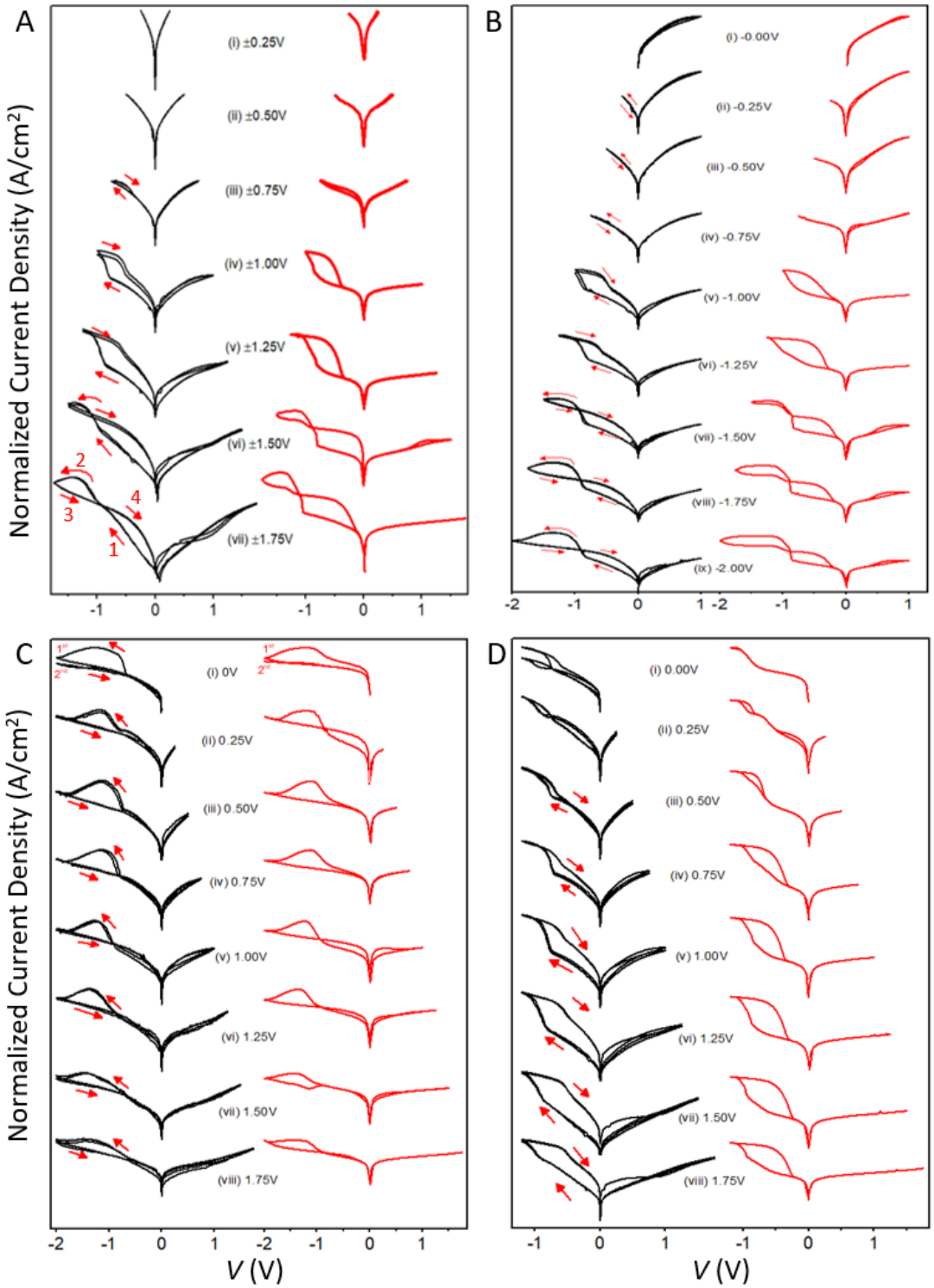


**Figure 21 A) Shows fits to the symmetric bias data (black) and fits (red for varying window widths, B) shows asymmetric positive bias window measurements. D) and C) show asymmetric negative bias window measurements. Reproduced from ref [153]**

**Table 5 Shows the fitting parameters for all junctions modeled.**

| | cycle | $\Gamma_{AB}$ (meV) | $E_{AB}$ (eV) | $E_{PC}$ (eV) | $\kappa$ | $\chi$ (eV) | $\lambda$ ($\varepsilon\varsigma$) | $\gamma$ ($\sigma^{-1}$) |
|---|---|---|---|---|---|---|---|---|
| **Scan Rate Dependence Cycles** Fixed bias voltage (-2V to +1V) Fig. 3C | all | 9 | 0.75 | -1 | 10 | 1.5 | 1.2 | 4.5 |
| **Symmetric Bias Cycles** Varying voltage Fig. 3F and Fig. SXA | i | 0.09 | 0.53 | -0.6 | 294.15 | 2.36 | 0.82 | 4.1 |
| | ii | 0.19 | 0.51 | -0.76 | 116.35 | 2.86 | 1.15 | 4.74 |
| | iii | 2.34 | 0.61 | -0.57 | 105.77 | 2.5 | 1.12 | 4.76 |
| | iv | 3.31 | 0.71 | -1.29 | 170.99 | 0.96 | 1.14 | 4.52 |
| | v | 5.55 | 0.71 | -1.29 | 171 | 0.96 | 1.14 | 4.52 |
| | vi | 13.97 | 0.81 | -0.67 | 42.2 | 3.16 | 1.29 | 13.1 |
| | vii | 14.63 | 0.78 | -0.64 | 42.21 | 3.27 | 1.3 | 12.85 |
| **Asymmetric Negative Bias Cycles** Fixed positive voltage ($V_{max}$ = +1V) Fig. Fig SXB | i | 0.01 | 0.55 | -0.91 | 192.97 | 2.88 | 1.26 | 4.5 |
| | ii | 3.88 | 0.81 | -0.55 | 197.38 | 2.55 | 1.2 | 4.5 |
| | iii | 0.13 | 0.66 | -0.64 | 199.49 | 2.7 | 1.2 | 4.5 |
| | iv | 0.03 | 0.59 | -0.55 | 25.44 | 2.67 | 1.2 | 4.5 |
| | v | 2.99 | 0.71 | -1.28 | 171.24 | 1.01 | 1.2 | 4.5 |
| | vi | 4.45 | 0.81 | -1.35 | 199.96 | 1.26 | 1.29 | 5 |
| | vii | 12.03 | 0.72 | -0.85 | 63.3 | 2.61 | 1.13 | 4.64 |
| | viii | 9.49 | 0.69 | -0.93 | 63.99 | 2.52 | 1.1 | 4.58 |
| | ix | 16.67 | 0.72 | -1.11 | 37.81 | 2.63 | 1.12 | 3.03 |
| **Asymmetric Positive Bias Cycles** Fixed negative voltage ($V_{max}$ = -2V) Fig. 3G and Fig SXC | i | 4.8 | 0.68 | -0.45 | 1.84 | 1.66 | 1.36 | 0.56 |
| | ii | 0.03 | 0.68 | -0.63 | 6.69 | 0.93 | 1.3 | 1.62 |
| | iii | 0.27 | 0.67 | -0.5 | 2.55 | 1.01 | 1.03 | 0.5 |
| | iv | 1.21 | 0.69 | -0.49 | 2.18 | 1.01 | 1.03 | 0.47 |
| | v | 2.76 | 0.77 | -0.55 | 5.56 | 1 | 1.01 | 0.43 |
| | vi | 1.71 | 0.84 | -0.67 | 6.35 | 2.44 | 1.04 | 0.44 |
| | vii | 1.2 | 0.86 | -1.21 | 1.64 | 2.3 | 0.6 | 5.46 |
| | viii | 2.2 | 0.78 | -1.12 | 2.59 | 0.59 | 1.3 | 5.5 |
| **Asymmetric Positive Bias Cycles** Fixed negative voltage ($V_{max}$ = -1.2V) Fig. 3H and Fig SXD | i | 0.06 | 0.69 | -1.29 | 61.03 | 1.11 | 0.72 | 7.55 |
| | ii | 0.01 | 0.47 | -0.97 | 181.65 | 3.2 | 0.29 | 5.31 |
| | iii | 0.14 | 0.55 | -0.89 | 181.66 | 2.78 | 0.38 | 5.11 |
| | iv | 3.31 | 0.68 | -1.31 | 170.97 | 1.17 | 1.03 | 4.97 |
| | v | 3.67 | 0.71 | -1.28 | 171 | 1.05 | 1.13 | 4.53 |
| | vi | 1.81 | 0.73 | -1.29 | 170.93 | 0.97 | 1.16 | 4.17 |
| | vii | 1.16 | 0.74 | -1.24 | 171.01 | 1.02 | 1.18 | 4.01 |
| | viii | 0.97 | 0.74 | -1.23 | 171 | 1.07 | 1.17 | 4.02 |

## Discussion and Conclusion

Reported in this chapter was a dynamic molecular switch whose functionality changes as a function of the bias window and scan rate applied. The experiment and theoretical model provided by Migliore and Nitzan[154] shows excellent agreement and can explain the data both qualitatively and quantitatively. The agreement is remarkable considering that this six step PC-ET process is effectively modeled with a one step ET process. The PCET process allows for charge locking that eliminates the stochastic behavior seen in other molecular memory devices. However, we also note the challenges that arise from modeling PCET processes[158-160]. This work utilizes the dynamic nature of this system to develop a functional molecular junction. This method of utilizing coupled rate equations with varying time constants can be applied to other molecular systems and may open up a new variety of adaptive and reconfigurable junctions for use in a variety of applications including neuromorphic computing[45, 47, 161, 162]

# CHAPTER SIX: BIAS-POLARITY DEPENDENT DIRECT INVERTED MARCUS

As mentioned in chapter one, molecular junctions are commonly described by one of two models, Landauer and Marcus. There are however multiple examples in which neither of the two models can describe the charge transport through the junction. Here we show an example in which neither model can adequately describe the junction. Instead, a combination of both models is used. For this project, a self-assembled monolayer of benzotetrathiafulvalene (BTTF) is shown to transition into the inverted, activationless Marcus region where hopping occurs for one bias polarity but not the other. These lead to a rectification ratio (R), defined by Equation (1,1), that is dependent on the temperature. A rectification of R = 124 occurs for low temperature (170K) and decreases by a factor of 30 times at (320K).

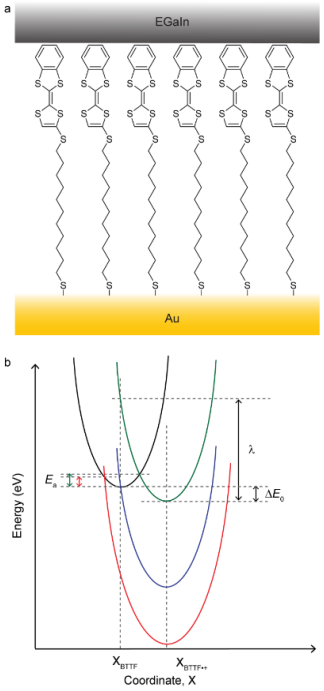


**Figure 22 A) Schematic of an Au-S$(CH_2)_{11}$S-BTTF//$GaO_x$/EGaIn. B) Show the common Marcus parabolas for the redox energies. Reproduced from ref [163].**

Figure 22B) illustrate the common Marcus Parabolas. The black parabola here depicts the potential energy of the neutral state of the molecule. The green parabola represents the charged state of the molecule. The energy difference between these two states is given as $\Delta E_0$. The activation energy is the amount of energy needed to cross from the neutral (black) state to the charged (green) state and allow for charge hopping. This is shown in Figure 22B) as the location at which the two parabolas cross. Finally, $\lambda$ is the molecular reorganization energy. The blue and red parabolas show two different scenarios in which the parabola of the charged state moves with respect to the parabola of the neutral state. This movement results in a change in the activation energy. The blue parabola gives an example in where $E_a = 0$ which results in activationless transport. The green curve represents a transition point into the inverted Marcus regime. As the red curve indicates, the activation energy should be expected to return however, the availability of electronic states in the electrodes allows the transport in this regime to remain activationless[164].

## Experimental Results

The experimental setup, characterization, and conduction measurements were conducted by our collaborators in Singapore. The SAMs of $S(CH_2)_{11}S$-BTTF on Au were prepared using procedures that have been previously reported[163]. Cyclic voltammogram measurements were conducted of the junctions which shows two pairs of redox peaks at $E_{pa}/E_{pc}$ = 0.51V/0.53V and 0.87V/0.89V. These correspond nicely to the oxidation of the BTTF unit to ($BTTF^{\bullet+}$) and ($BTTF^{2+}$). Further, photoelectron and x-ray absorption spectroscopy indicated that the energy gap between the Fermi level of the electrodes and the HOMO-1, HOMO, and LUMO molecular orbitals were 2.09 eV, 0.44 eV, and 2.17 eV respectively. This indicates that the HOMO is accessible within the applied bias window.

J(V,T) measurements were conducted in a way similar to what has been discussed in previous chapters with an EGaIn top electrode[165]. Figure 23a) shows the J(V,T) curves for both the 170K (black dots) and 320K (green dots). Fits to these data are also shown in the blue and red curves. These fits were conducted using the Landauer model from Equation (1.10). The parameters used in the fitting for the lower temperature measurements are given as $\epsilon \equiv \frac{\delta E_{HOMO}^{th}}{e} = 0.83\ V$ which is the energy of the HOMO with respect to the Fermi energy of the electrodes, n = 150, $\gamma_L = 9.92\ x\ 10^{-3}$eV, $\gamma_R = 9.88\ x\ 10^{-7}$eV, $\eta = 0.37$ and $\sigma = 0.11$. The overall tunneling rate is given by $\Gamma = \frac{\gamma_L \gamma_R}{\gamma_L + \gamma_R}$ =$9.88 \times 10^{-7} eV$ which is a very weak coupling. The 320K measurement parameters are given as $\epsilon = 0.83\ V$, n = 150, $\gamma_L = 6.20\ x\ 10^{-3}$eV, $\gamma_R = 1.90\ x\ 10^{-6}$eV, $\eta = 0.40$ and $\sigma = 0.13$. These fits show a slight asymmetry via the $\eta$ parameter. This helps to describe the rectification in the junction. Which is further described in Figure 23b) and c).

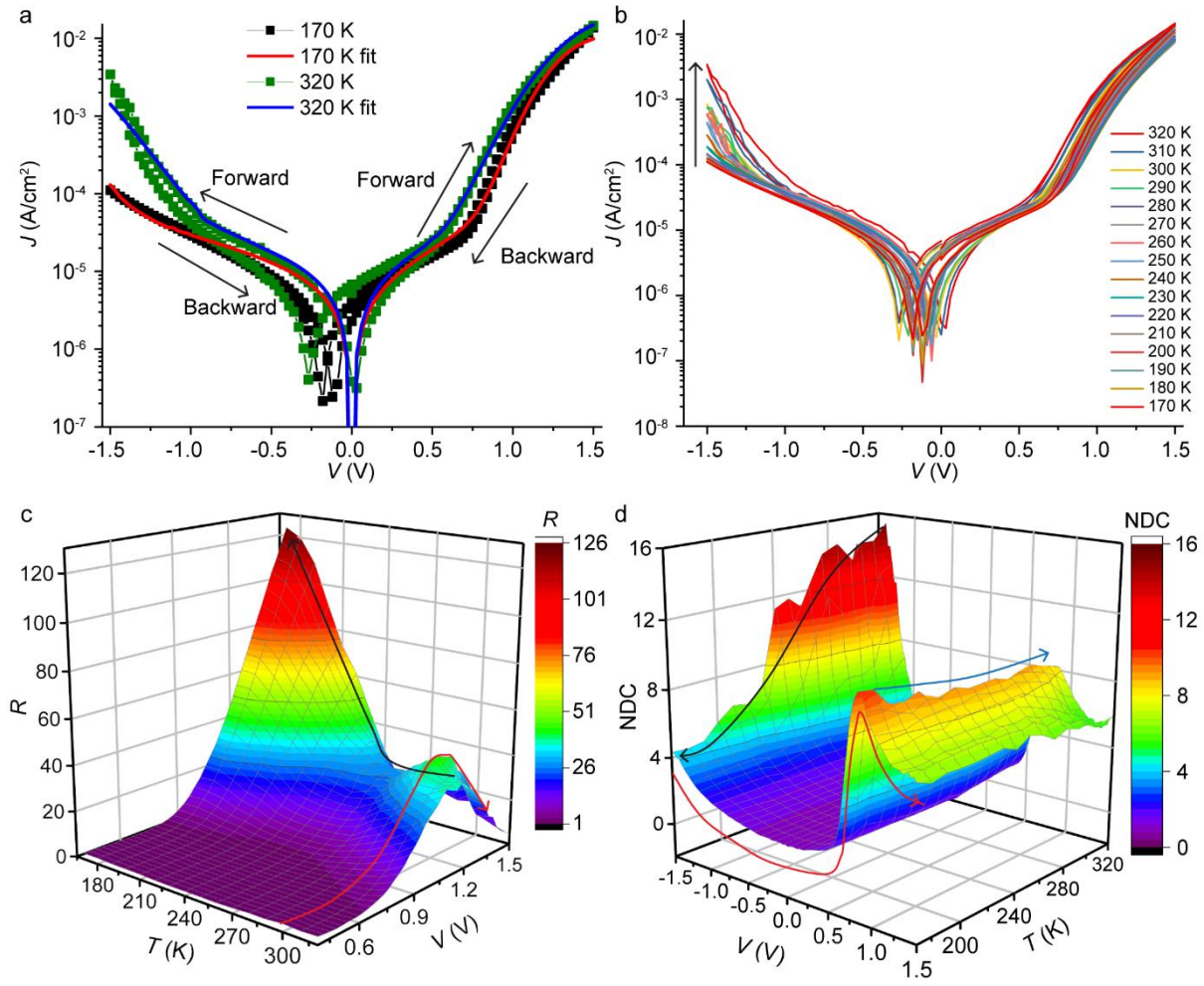


**Figure 23 A) Shows a representative J(V) curve for this junction. These were recorded at both 170K and 320K. The arrows show the direction of the scan sweep. B) Shows temperature dependent J(V) measurements. Here the current J(V) appears to increase with T. C) Surface plot of RR plotted against the temperature and voltage. D) Surface plot of NDC as a function of temperature and voltage. Reproduced from ref [163].**

Figure 23b) Shows the J(V,T) curves for the entire temperature ranged sampled (170-320K). One can see from both Figure 23a) and Figure 23b) that for higher temperatures, a sharp increase in the current occurs at negative voltages indicating that the junction has reached the conduction window. However, for low temperatures this is not present, indicating that the conduction window is no longer

accessible. For the positive voltages, the HOMO is only weakly dependent on the temperature. Figure 23c) shows the rectification ratio R as a function of voltage and temperature. The red curve shows the shape of the rectification ratio for a single temperature (300K). The curve peaks and then decreases again. This is due to the asymmetry of the molecule. The HOMO enters the conduction window more quickly in the positive regime than in the negative voltage regime. Therefore, the peak occurs when the HOMO can be seen on the positive side but is not accessible at negative voltages. The return to low rectification occurs after the HOMO is accessed at negative voltages.

To further explain the rectification and tunneling involving the HOMO, normalized differential conductance (NDC) analysis[165, 166] is shown in Figure 23d). The resonance peak at +0.90 V with an NDC = 9 shows the charge transport through the HOMO (red arrow). This large NDC value is common in diode behavior[166]. As has been discussed previously, this NDC is largely temperature independent. However, the HOMO peak at negative voltage is highly temperature dependent. The NDC peaks at around 15 for high temperatures but drops to 4.5 at 170K. This temperature dependence is further illustrated by the black curve. This indicates that incoherent tunneling dominates at large negative biases. The hopping mechanism eventually 'freezes out' thereby increasing the R-value. This behavior of having two different temperature dependent behaviors within the same junction has not been seen before.

To further explore this temperature dependence. The activation energy was determined as a function of bias voltage. Figure 24a) and b) show Arrhenius plots from which the activation energy was calculated. Figure 24c) shows the activation energy, $E_a$, as a function of the voltage, V. The activation energy peaks at around 0.87 V which is similar to the 0.90 V NDC peak. Therefore, we can explain the increase in $E_a$ by the HOMO entering the conduction window and the charge transport transitioning

from coherent off-resonant tunneling to incoherent hopping. However, after reaching a peak, $E_a$ begins decreasing again. Figure 24d) shows $E_a$ for negative biases. Here the downturn in $E_a$ isn't properly shown due to the instability of the junctions beyond -1.5V.

One interesting thing to note is that in the temperature range of 220K to 130K, a small reproducible negative $E_a$ is observed. There have been many explanations of a negative $E_a$ including phase transitions or conformational changes[167-170] or temperature dependent change in coupling with the electrodes[171].

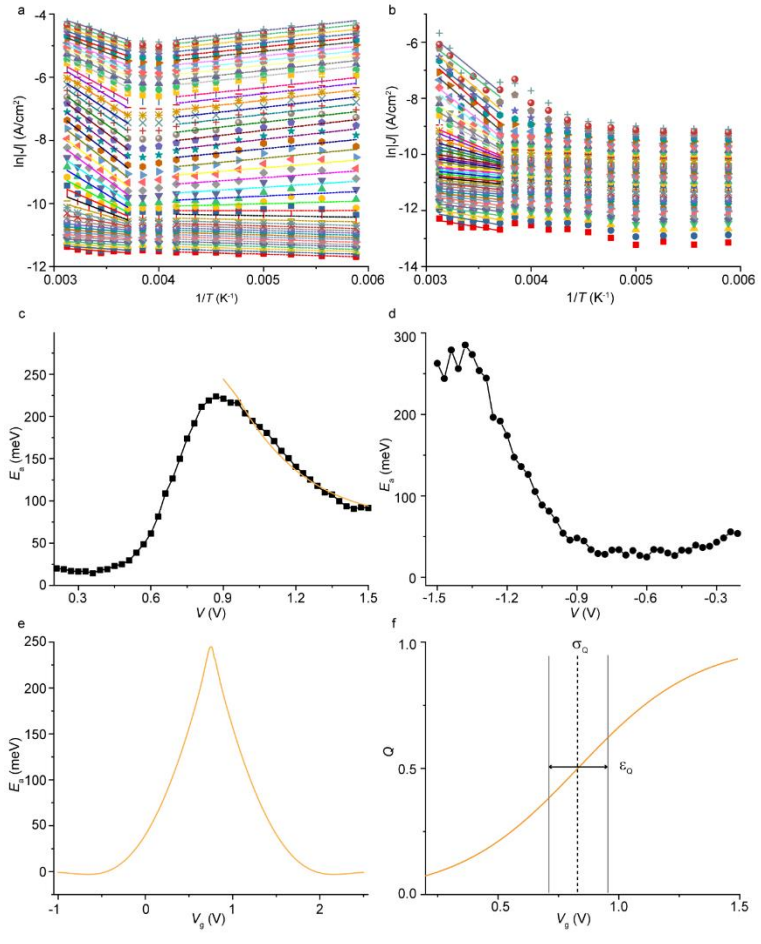


**Figure 24 A) Shows Arrhenius plots for voltages 0.21 to 1.5V. B) Shows Arrhenius plots for voltage -.21 to -1.5V. The solid lines are fits to the data using the Arrhenius Equation, Equation (6.1). C) Shows $E_a$ vs V at positive bias.**

**The solid orange line is a fit to the data using Migliori's model. D) Shows $E_a$ vs V at negative bias. E) Shows the calculated activation energy as a function of gate voltage using Migliori's model. F) Shows the charge distribution used for the fitting in panel C). Reproduced from ref [163].**

## Theoretical Modeling

Migliori, Shiff and Nitzan[164, 172] utilized Marcus theory to describe transport in solid state junctions. Here the electron is expected to fully relax on the molecule as is the case in incoherent tunneling. However, this theory combines both Marcus and Landauer formalisms to describe the transfer rates from neutral to charge states. These rate equations are reproduced in Equations (6.2) and (6.3). Comparing these to Equation (1.16) we see that two terms have been added $f(E)$ which is used in Landauer to describe the electrodes and $\Gamma(E)$ which I the tunneling rate to describe electron transfer between a single level and the electrode.

$$K_{\mathrm{BTTF}\rightarrow\mathrm{BTTF}^{\cdot+}} = \frac{1}{\sqrt{4\pi\lambda k_B T}} \int dE \Gamma(E) e^{-\frac{(\Delta E + E - \lambda)^2}{4\lambda k_B T}} f(E) \tag{6.2}$$

$$K_{\mathrm{BTTF}^{\cdot+}\rightarrow BTTF} = \frac{1}{\sqrt{4\pi\lambda k_B T}} \int dE \Gamma(E) e^{-\frac{(\Delta E + E - \lambda)^2}{4\lambda k_B T}} [1 - f(E)] \tag{6.3}$$

Here $\Gamma(E)$ is the transfer rate between the molecule and electrode, $f(E)$ is the Fermi distribution of the electrodes which as discussed in chapter one, introduces a temperature dependence of its own, $\Delta E = \Delta E_0 + \mu$, where $\Delta E_0 = \delta E^{th}_{\mathrm{BTTF}^{\cdot+}} - \delta E^{th}_{\mathrm{BTTF}}$ which gives the energy difference between the BTTF and $\mathrm{BTTF}^{\bullet+}$ states and $\mu$ is the electrochemical potential of the electrodes.

According to Migliori et al[164], a gating potential changes the energy difference between the BTTF and $\mathrm{BTTF}^{\bullet+}$ states. Conceptually speaking it moves the parabolas shown in Figure 22B) with respect

to one another and changes the activation energy. This gate dependent activation energy that can be calculated with the following:

$$\frac{E_a}{k_B T} = T\frac{\partial}{\partial T} ln(K_{BTTF \rightarrow BTTF^{\cdot+}} + K_{BTTF^{\cdot+} \rightarrow BTTF}) \quad (6.4)$$

Figure 24E) shows the calculated $E_a$ vs $V_g$ plot for the data in Figure 24C). This gating voltage comes from intramolecular gating. Therefore, the charge in the molecule determines the gating voltage which can be given by $V_g = \frac{Q(V)}{C_C^*}$ where Q is the charge in the molecule, and $C_C^*$ is the capacitive coupling between the molecule and the electrode.

Figure 24F) shows the functional used for Q(V) here where the inflection point ($\varepsilon_Q \equiv \delta E_{\mathrm{HOMO}}^{th}/e$) and width ($\sigma_Q$) of the charging curve of fitting parameters used to fit Figure 24C) and constrained by the experimental J(V) curves ($\varepsilon_Q \sim \varepsilon \equiv \delta E_{\mathrm{HOMO}}^{th}/e$ and $\sigma_Q \sim \sigma$). The model fits well using the following parameters $\lambda = 1.20\ eV$, $\Delta E_0 = 0.75\ eV$, $\varepsilon_Q = 0.83\ V (= \varepsilon)$, $\sigma_Q = 0.25\ eV (\sim \sigma)$, and $C_C^* = 1.31\ x\ 10^{-19}$ F.

This model explains and fits the decrease in activation energy and shows that the junction at large positive bias moves towards the inverted Marcus regime. However, this model only applies to the junction when the electron transport is incoherent. At low bias voltages the HOMO is not accessible as shown by Figure 25a). Figure 25e) shows the transition from BTTF to $BTTF^{\cdot+}$. The x-axis represents the reaction coordinate (rc) which shouldn't be confused with distance. The bottom row shows the activation energy as a function of gate voltage. Figure 25 b), f) and j) show the scenario in which the BTTF and $BTTF^{\cdot+}$ states enter the conduction window and the conduction method becomes incoherent hopping. Here they are in the 'normal' Marcus region and $\mu$ lies between the two states on the reaction coordinate axis. Figure 25 b), f) and j) show that with increasing applied voltage, one parabola is lowered

in energy with respect to the other. This is the effect of the gating described by the model. Eventually, the 'charged' state has been gated to such an extent that the parabola intersects at the minimum of the neutral state. At this point, the activation energy becomes 0 eV and remains at 0 eV due to the continuous availability of states within the electrodes. Beyond this point, the system is pushed into the inverted Marcus regime in which charged transport is activationless. The model helps to show the process and that the charged $BTTF^{\cdot+}$ is stabilized by the applied voltage and therefore shifts with respect to the energy of the neutral state. Further, we note that while a maximum $E_a$ is observed for all junctions, there also is an observed 'background' $E_a$ that is observed at small and large bias voltages. This could be caused by conformational changes[169, 170] or dimer formation.

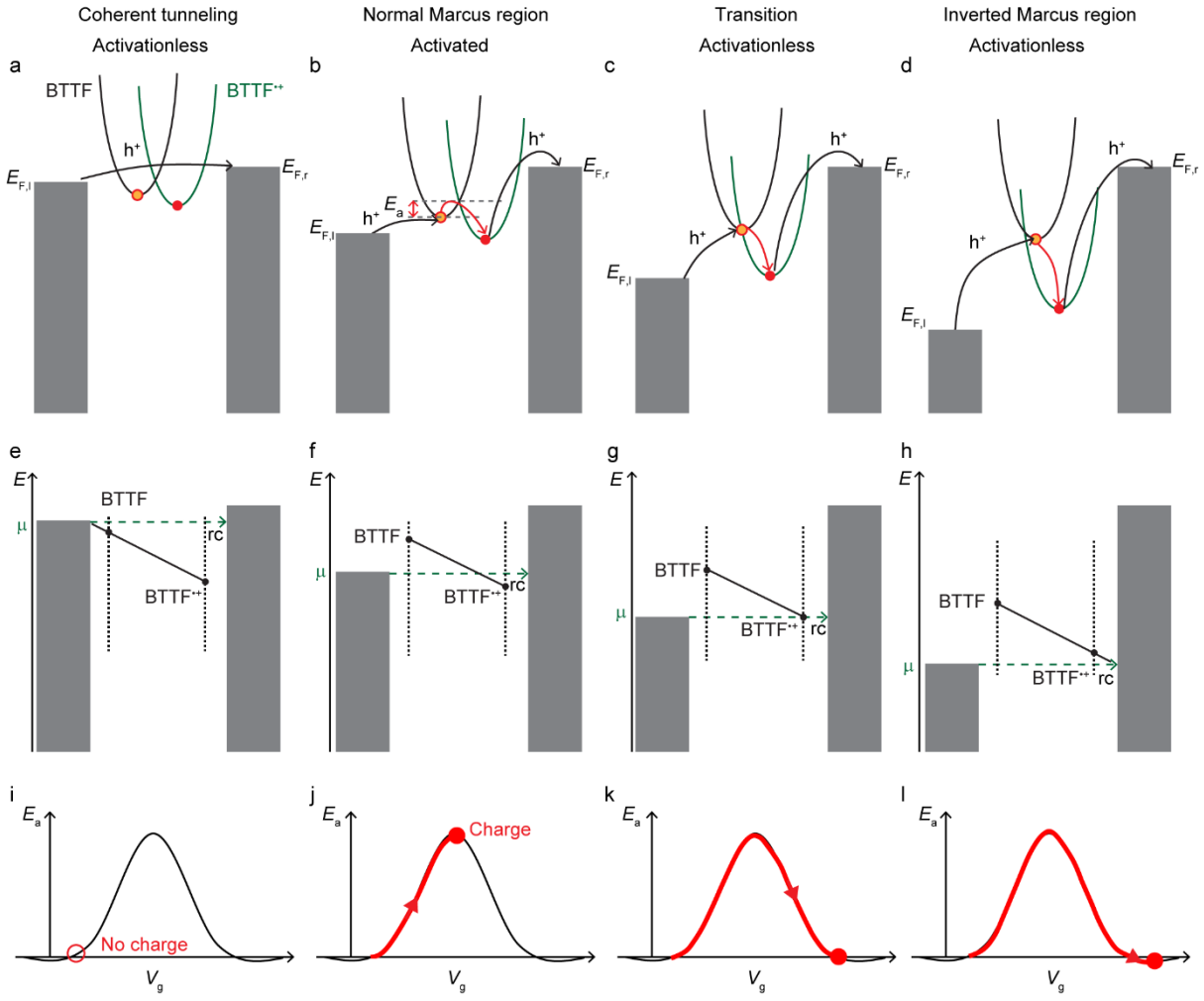


**Figure 25 a-d) shows Marcus parabolas of the BTTF->BTTF$^+$ reaction for various applied voltages. The black arrows indicate charge transport between the electrodes and the BTTF unit. The Red arrows indicate the transition between BTTF and BTTF$^+$ (e) to (h) The corresponding redox reaction depicted on a reaction coordinate (rc) with respect to $\mu$.(i) to (l) The $E_a$ *vs* $V_g$ where the red dot corresponds to the $E_a$ sketched in panels b. Reproduced from ref [163].**

Figure 26 shows the results from two additional junctions. Figure 26a) and d) show the $E_a$ vs $V_g$ plots for junctions 2 and 3 respectively. Figure 26b) and e) show the data and model fits for $E_a$ vs $V_b$ with the insets showing the charge functional. Both plots show great agreement with the model using the parameters described in Table 6.

**Table 6 Shows the parameters used for the fitting of junctions 2 and 3**

| Data Set | Data sets for Junction 2 | Data sets for Junction 3 |
|---|---|---|
| **Energy Difference ($\Delta E_0$)** | 0.89 eV | 0.459 eV |
| **Reorganization Energy ($\lambda$)** | 1.22 eV | 0.822 eV |
| **Coupling Capacitance ($C_C^*$)** | 1.45 x $10^{-19}$ F | 0.923 x $10^{-19}$ F |
| **Center of I-V Curve ($\varepsilon_Q$)** | 0.51 | 0.81 |
| **Width of I-V Curve ($\sigma_Q$)** | 0.3 | 0.266 |

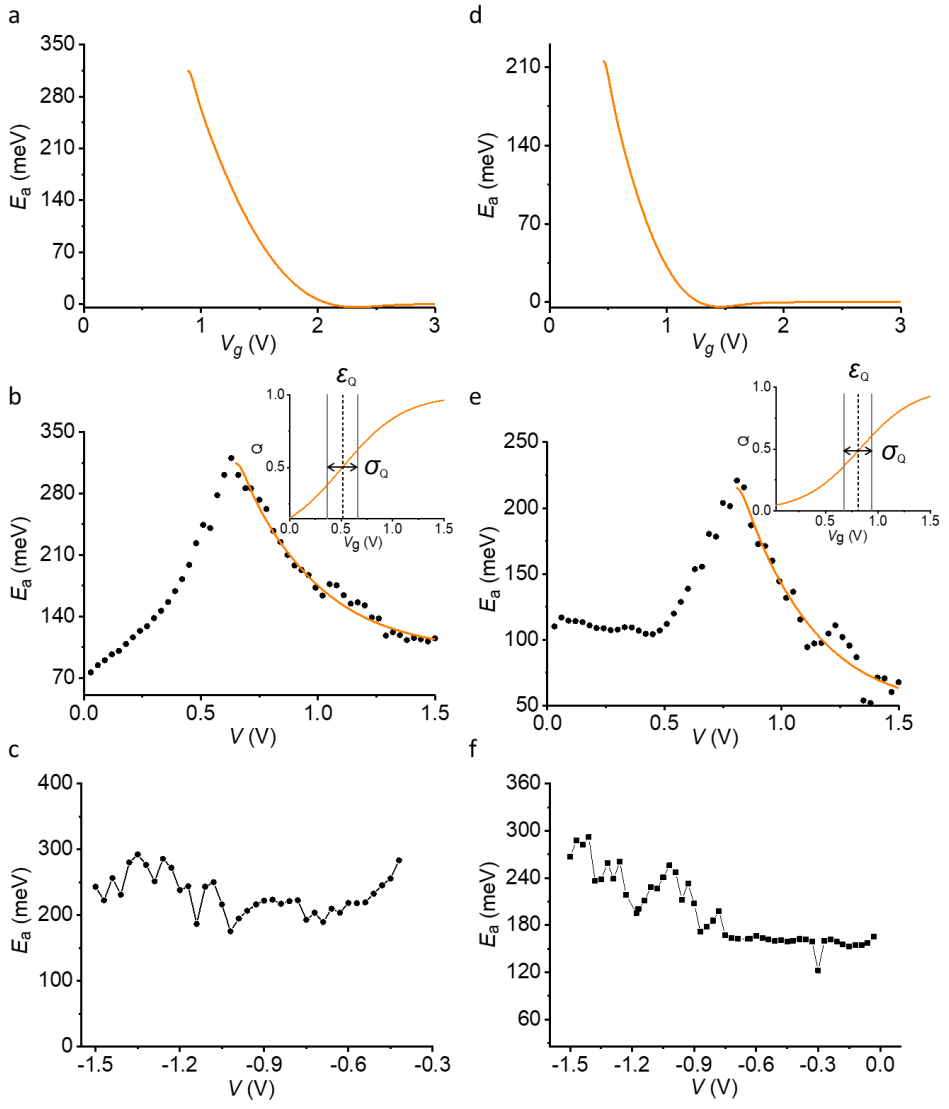


**Figure 26 a) and d) show the calculated $E_a$ vs $V_g$ for the data sets in b) and e) respectively. They were calculated using the parameters presented in Table 6. b) and e) show the experimentally obtained $E_a$ vs $V_b$ (black dots)**

**alongside the fitted model (orange line). The insets show the charge functionals used in the fit. c) and f) show the $E_a$ vs $V_b$ for the negative applied bias. Reproduced from ref [163].**

## Conclusion

Due to the charge transport rates being much larger than the diffusion rate therefore junctions were diffusion limited[107]. Molecular junctions do not have this problem therefore the complex temperature dependent behavior seen here can be observed. We show here that the inverted Marcus region is not limited to D-b-A molecules in which the HOMO and LUMO are shifted with respect to one another via intramolecular gating[102] but can be accessed via other types of redox molecules consisting only of donor units. This can be obtained by molecules with weak couplings to the electrodes which allow the charges to relax on the molecule, thereby producing the 'gating' voltages needed to push the system into the inverted Marcus region. Our junctions are operating in the weak coupling limit due to the physisorbed nature of the BTTF-EGaIn contact and the presence of the $GaO_x$ layer. Further, the $(CH_2)_{11}$ alkyl chain de couples the BTTF from the bottom Au electrode. Molecular junctions, especially single-molecule junctions, usually operate in the strong coupling regime which makes observation of the inverted Marcus region rare. These results suggest that the inverted Marcus region could be easily accessible in other junctions and could provide guidelines for future studies of complex temperature dependent phenomena.

# APPENDIX A: SUMMARY OF WORK

In each of the chapters, I did the modeling of the IV curves while leaving the experimental work and density functional theory to our collaborators. In chapter two, I focused on the modeling of the IV curves for the two bridges. This provided eta values for each of the two bridges. In chapter three, I modelled and assisted with subsequent modeling of the IV curves for each counterion used in the experimentation. This provided necessary coupling and energy level information to coordinate with the DFT calculations. In chapter four, I modeled IV curve of the junction with a combination of Landauer models and a sigmoid function to describe the switching behavior. This allowed us to accurately describe how and when the switching occurs. In chapter five, I modeled each experimental IV curve obtained. Comparing and contrasting these curves lead to interesting conclusions about when and how the complex molecules undergo numerous transitions. Finally, in chapter six, I fit IV curves for the high temperature and low temperature junctions. The results of these fits were used to fit the activation energies that were obtained experimentally.

# APPENDIX B: PYTHON SCRIPTS

## Models Used

```
# -*- coding: utf-8 -*-
"""
Created on Thu Sep 19 18:46:23 2019
Functions to be used in fitting and calculations
@author: Cameron
"""
import numpy as np
from scipy.integrate import quad
from scipy.integrate import dblquad
from numba import jit

eV = 1 #Energy
K  = 1 #Temperature Units
C  = 1 #Coulombs
s  = 1 #seconds
V  = 1 #volts

kb = 8.6173324e-5*eV/K #Boltzmann Constant
q  = 1.6e-19*C
h  = 4.1356e-15*eV*s

@jit
def linear(x,m,b):
   return b+x*m

@jit
def sigmoid(x,pos,width):
   return 1/(1+np.exp((x-pos)/width))

@jit
def fermi(E,T):
   return 1/(np.exp((E)/(kb*T))+1)

@jit
def gaussian(x,A, mu,sigma):
   return A*np.exp(-.5*((x-mu)/(sigma))**2)

@jit
def normalized_gaussian(x, mu,sigma):
   A = 1
   def gaus(ep):
      return gaussian(ep,A,mu,sigma)
```

```
    A = 1/quad(gaus,mu-3*sigma,mu+3*sigma)[0]
    return gaussian(x, A, mu, sigma)

@jit
def densityOfStates(E,ep,gamma):
    numerator = gamma
    denominator = (E-ep)**2+(gamma/2)**2
    return numerator/denominator#/(2*np.pi)

@jit
def rateRatio(gammaL,gammaR):
    return gammaL*gammaR/(gammaL+gammaR)

@jit
def single_level_tunnel_model_integrand(E,ep,c,vg,eta,vb,gammaL,gammaR,T):
    gamma = gammaL+gammaR
    return -densityOfStates(E,((ep+c*vg)+(eta-1/2)*vb),gamma)*\
        rateRatio(gammaL,gammaR)*\
        (fermi(E+vb/2,T)-fermi(E-vb/2,T))
@jit
def single_level_tunnel_model_integrand_Alt(E,ep,c,vg,eta,vb,gammaC,gammaW,T):
    return -gammaC*(fermi(E+vb/2,T)-fermi(E-vb/2,T))/\
        ((E-((ep+c*vg)+(eta-1/2)*vb))**2+(gammaW/2)**2)

def tunnelmodel_singleLevel(vb,gammaC,gammaW, deltaE1,eta,sigma,c,vg,T):

    if sigma == 0:
        limits = [-1*np.abs(vb),1*np.abs(vb)]

        def integrand (E):
            result = single_level_tunnel_model_integrand_Alt(E,deltaE1,c,vg,eta,vb,gammaC,gammaW,T)
            return result

        return q/h*quad(integrand,
                        limits[0],
                        limits[1])[0]
    else:
        A = 1
        args = (A,deltaE1,sigma)
        A = 1/quad(gaussian,deltaE1-3*sigma,deltaE1+3*sigma,args=args)[0]

        limits = [min([deltaE1-3*sigma,-1*np.abs(vb)]),\
                max([deltaE1+3*sigma,1*np.abs(vb)])]
```

```
    def integrand (E,ep):
      result = gaussian(ep,A,deltaE1,sigma)*\
      single_level_tunnel_model_integrand_Alt(E,ep,c,vg,eta,vb,gammaC,gammaW,T)
      return result

    return q/h*dblquad(integrand,
                limits[0],
                limits[1],
                lambda x: limits[0],
                lambda x: limits[1])[0]

def tunnelmodel_2level(vb,c,vg,T,
              gammaC1, gammaW1, deltaE1, eta1, sigma1,
              gammaC2, gammaW2, deltaE2, eta2, sigma2):

  args1 = (gammaC1, gammaW1, deltaE1, eta1, sigma1,c,vg,T)
  args2 = (gammaC2, gammaW2, deltaE2, eta2, sigma2,c,vg,T)

  I1 = tunnelmodel_singleLevel(vb,*args1)
  I2 = tunnelmodel_singleLevel(vb,*args2)

  return I1+I2

@jit
def averageBridgePopulation_integrand(E,ep,c,vg,eta,vb,gammaL,gammaR,T):
  gammaW = gammaL+gammaR

  return ((fermi(E+vb/2,T)*gammaL+gammaR*fermi(E-vb/2,T))/\
    ((E-((ep+c*vg)+(eta-1/2)*vb))**2+(gammaW/2)**2))

def averageBridgePopulation(vb, gammaL, gammaR, deltaE, eta, c, vg, T):
  limits = [-10,10]

  def integrand (E):
    result = averageBridgePopulation_integrand(E, deltaE, c, vg, eta, vb, gammaL, gammaR, T)
    return result

  return quad(integrand,
              limits[0],
              limits[1])[0]/(2*np.pi)

def NitzanSwitchingRate(vb, gammaL, gammaR, deltaE, eta, c, vg, T, R1, R2):
  n = averageBridgePopulation(vb, gammaL, gammaR, deltaE, eta, c, vg, T)
  return (1-n)*R1+n*R2
```

```
def nitzanmodel_fixedtemp_gatevoltage(Vg,E,l):
    T0=260
    T1=330

    def integrandOne(ep):
        num=np.exp(-((E+Vg/2)+ep-l)**2/(4*kb*T0*l))
        denom=1/(np.exp((ep-Vg/2)/(kb*T0))+1)
        return num*denom

    def integrandTwo(ep):
        num=np.exp(-((E+Vg/2)+ep+l)**2/(4*kb*T0*l))
        denom=1-1/(np.exp((ep-Vg/2)/(kb*T0))+1)
        return num*denom

    def integrandThree(ep):
        num=np.exp(-((E+Vg/2)+ep-l)**2/(4*kb*T1*l))
        denom=1/(np.exp((ep-Vg/2)/(kb*T1))+1)
        return num*denom

    def integrandFour(ep):
        num=np.exp(-((E+Vg/2)+ep+l)**2/(4*kb*T1*l))
        denom=1-1/(np.exp((ep-Vg/2)/(kb*T1))+1)
        return num*denom

    One = quad(integrandOne, -10, 10)
    Two = quad(integrandTwo, -10, 10)
    Three = quad(integrandThree, -10, 10)
    Four = quad(integrandFour, -10, 10)

    leftSide=np.log((One[0]+Two[0])*(1/(np.sqrt(4*np.pi*l*kb*T0))))
    rightSide=np.log((Three[0]+Four[0])*(1/(np.sqrt(4*np.pi*l*kb*T1))))

    FinalAns=-1000*kb*T0**2*(leftSide-rightSide)/(T1-T0)
    return FinalAns

def nitzanmodel_fixedtemp_biasvoltage(V,E,l,cap,W,A):
    Vg=cap*(1-1/(1+np.exp((V-A)/W)))
    return nitzanmodel_fixedtemp_gatevoltage(Vg,E,l)
```

# Class Sci Data

```
# -*- coding: utf-8 -*-
"""
Created on Tue Sep 17 18:21:27 2019

This file will simply be used to provide functions for manipulation of the data
files given to us via our Singapore Collaboration.

@author: Cam
"""
import csv
import matplotlib.pyplot as plt
import scipy.optimize as sco
import numpy as np
import warnings
from numpy.random import random
import math
import time

class sciData:
# %% Output Data and Plots
   def parRange(self, initpar, par, ran, size = 10, method = 'linear', plot = False):
      pars = initpar.copy()
      step = (ran[1]-ran[0])/size
      t = np.arange(ran[0],ran[1],step)

      if plot:
         plt.figure()
         plt.scatter(self.rawdat['X'],self.rawdat['Y'],color = 'black')

      output = ''
      for i in t:
         pars[par]=i
         start = time.time()
         if method == 'relative':
            Err = self.calcRelativeError(pars)
         if method == 'linear':
            Err = self.calcLinearError(pars)
         end = time.time()
         diff = np.floor(end-start)
         for name in pars.keys():
            output = output + '%e\t'%pars[name]
```

```
            output = output + '%.5e\t%.5e\t%.5e\n'%(Err, diff, np.sqrt(Err**2+diff**2))
            f= open('Test.txt',"a")
            f.write(output)
            f.close()

            print('%.3e\t%.3f\t%.3f\t%.3f'%(i,Err*100, diff, np.sqrt((Err*100)**2+diff**2)))

            if plot:
                plt.plot(self.modelDat['X'], self.modelDat['Y'], label = i, linewidth=4)
            self.modelDat=


        if plot:
            plt.legend()



# %% Tested and Reliable Functions
    def subsetData(self, xRange = []):
        X = list(self.rawdat['X'])
        Y = list(self.rawdat['Y'])

        newX=[]
        newY=[]
        for i in range(len(X)):
            if xRange[0]>X[i]:
                continue
            if xRange[1]<X[i]:
                continue

            newX+=[X[i]]
            newY+=[Y[i]]

        self.workingdat['X'] = newX
        self.workingdat['Y'] = newY

        return newX,newY

    def returnThry(self, initpar=[]):

        if self.modelDat:
            return self.modelDat['X'], self.modelDat['Y']
        else:
            return self.workingdat['X'], self.model(self.workingdat['X'], *initpar.values())
```

```
def __init__(self,fName, equation, rawdat = ):
   self.fitbool = False
   self.scaling = False
   self.multiplier = 1
   self.rawdat =
   self.parameters =
   self.errors =
   self.modelDat =
   self.fileName = fName

   if not bool(rawdat):
      self.__readData()
   else:
      self.rawdat = rawdat

   minval = min(abs(self.rawdat['Y']))
   if minval <np.sqrt(np.finfo(float).eps):
      # Due to curve_fit and machine precision limitations the data and
      # model are being scaled into the nano range. This should not
      # effect the fitting parameters
      # warnings.warn("Scaling data and equation due to floating point percision")
      self.scaling = True
      self.multiplier = 1E9
      self.rawdat['Y'] = self.rawdat['Y']*self.multiplier

   self.workingdat = self.rawdat.copy()
   self.model = np.vectorize(lambda x,*args: equation(x,*args)*\
                        self.multiplier)

def __readData(self):
   DataFileN=self.fileName

   X=[]
   Y=[]
   with open(DataFileN,newline='') as f:
      reader=csv.reader(f,delimiter='\t',quoting=csv.QUOTE_NONNUMERIC)
      for V,E in reader:
         X+=[V]
         Y+=[E]

   self.rawdat['X'] = np.float64(X)
   self.rawdat['Y'] = np.float64(Y)

   return X,Y
```

```
def __fit(self,model,parBnds,parInitial):
    p0=[]
    bnds = []
    lower = []
    upper = []
    for name in list(parInitial.keys()):
        p0 += [parInitial[name]]
        if parBnds:
            lower +=[parBnds[name][0]]
            upper +=[parBnds[name][1]]

    bnds = [lower,upper]

    X  = self.workingdat['X']
    Y  = self.workingdat['Y']

    if parBnds:
        results,covar=sco.curve_fit(model,X,Y,p0=p0,bounds=bnds)
    else:
        results,covar=sco.curve_fit(model,X,Y,p0=p0)
    return results,covar

def fit(self,parBnds, parInitial):
    self.fitbool = True

    if parBnds:
        for parm in parBnds.keys():
            if not (parInitial[parm] < parBnds[parm][1] and parInitial[parm] >parBnds[parm][0]):
                print('%s is infeasible. Choosing random number'%parm)
                parInitial[parm] = parBnds[parm][0] + (random()*(parBnds[parm][1]-parBnds[parm][0]))

    results,covar  = self.__fit(self.model,parBnds,parInitial)

    self.modelDat['X']=self.workingdat['X']
    self.modelDat['Y']=self.model(self.workingdat['X'], *results)

    cnt = 0
    for name in list(parInitial.keys()):
        self.parameters[name] = results[cnt]
        self.errors[name]  = np.sqrt(np.diag(covar))[cnt]
        cnt +=1

def customFit(self,func,parInitial):
    self.fitbool = True
```

```
    def minfunc(x):
        yThr = self.model(self.workingdat['X'],*x)
        return func(self.workingdat['Y'],yThr)

    res = sco.minimize(minfunc,x0 = list(parInitial.values()))

    self.modelDat['X']=self.workingdat['X']
    self.modelDat['Y']=self.model(self.workingdat['X'], *res.x)

    cnt = 0
    for name in list(parInitial.keys()):
        self.parameters[name] = res.x[cnt]
        self.errors[name]  = 0
        cnt +=1

def __rangeOrder(self, order):
    switchCases={
          'atto'     :   18,
          'fempto'    :   15,
          'pico'     :   12,
          'nano'      :   9,
          'micro'     :   6,
          'milli'     :   3,
          ''          :   0,
          'kilo'      :   -3,
          'mega'      :   -6,
          'giga'      :   -9,
          'tera'      :   -12,
          'peta'      :   -15,
          'exa'       :   -18
          }

    multiplier = 10**(switchCases[order])
    return multiplier

def calcLinearError(self, initpar):
    X = self.workingdat['X']
    Y = self.workingdat['Y']

    if not self.modelDat:
        self.modelDat['X'] = self.workingdat['X']
        self.modelDat['Y'] = self.model(X,*initpar.values())

    residual = np.subtract(Y,self.modelDat['Y'])
    Error = np.sqrt(np.sum(residual**2))
```

```
    return Error/len(X)

def calcRelativeError(self, initpar):
    X = self.workingdat['X']
    Y = self.workingdat['Y']

    if self.modelDat:
        Ythr = self.modelDat['Y']
    else:
        Ythr = self.model(X,*initpar.values())

    residual = np.subtract(np.log(np.abs(Y)),np.log(np.abs(Ythr)))
    Error = np.sqrt(np.sum(residual**2))
    return Error

def printFit(self,save = '', initpar =, relError = False):
    if not self.parameters:
        self.parameters = initpar.copy()
        self.errors = initpar.copy()

    if not relError:
        Err = self.calcLinearError(self.parameters)
    else:
        Err = self.calcRelativeError(self.parameters)
    output = "Fit Report:\tError:\t%.2f\n" % Err
    output = output + "\tPar:\tVal\tErr\n"

    for name in list(self.parameters.keys()):
        if initpar:
            self.errors[name] = np.inf
        output = output + "\t%s\t%e\t%e\n" %(name, self.parameters[name], self.errors[name])
    print(output)
    if save:
        output = ''
        for name in self.parameters.keys():
            output = output + '%e\t'%self.parameters[name]
        output = output + '%.5f\n'%Err
        f= open(save,"a")
        f.write(output)
        f.close()

def plot(self,pars=[],save = '',scale = ''):
    if self.scaling:
        scale = 'nano'
    mult = self.__rangeOrder(scale)
```

```
plt.figure()
plt.scatter(self.rawdat['X'],self.rawdat['Y']*mult,s=10,color='black')
plt.autoscale(False)

# If a fit has been done it will plot the model on top
if self.fitbool:
   XThr = self.workingdat['X']
   YThr = self.model(self.workingdat['X'], *self.parameters.values())*mult
   plt.plot(XThr,YThr)

if pars:
#If pars, plot will plot the data with pars given
   XThr = self.workingdat['X']
   YThr = self.model(self.workingdat['X'],*pars.values())*mult
   plt.plot(XThr,YThr)

if save:
#If the user as specified a name for the plot, then the plotwill be saved.
   plt.savefig(save)
```

```
from penguins.class_sciData import sciData
import penguins.models as models
import time

def reducedTunnelModel(vb, gammaL, gammaR, deltaE1, eta,sigma):
   T = 300
   c = 0
   vg = 0
   gammaC = gammaL*gammaR
   gammaW = gammaL+gammaR

   return models.tunnelmodel_singleLevel(vb,gammaC,gammaW, deltaE1,eta,sigma,c,vg,T)

def reducedTunnelModel_NoGauss(vb, gammaL, gammaR, deltaE1, eta):
   T = 300
   c = 0
   vg = 0
   sigma = 0
   gammaC = gammaL*gammaR
   gammaW = gammaL+gammaR

   return models.tunnelmodel_singleLevel(vb,gammaC,gammaW, deltaE1,eta,sigma,c,vg,T)

def test_2Hc2F(fName = 'tests\\2H-c-2F (amps).txt'):
   start = time.time()
   initpar = {
      'gammaL'  : 0.032248,
      'gammaR'  : 0.008489,
      'deltaE1' : 0.874857,
      'eta'     : 0.590363,
      'width'   : 0.0087
      }

   data = sciData(fName,reducedTunnelModel)
   SE=data.calcRelativeError(initpar)
   runtime = time.time()-start
   assert SE < 5 and runtime < 25

def test_2Hs2F(fName = 'tests\\2H-s-2F (amps).txt'):
   start = time.time()
   initpar = {
      'gammaL'  : 0.000060,
```

```
        'gammaR'  : 0.006331,
        'deltaE1' : 0.708984,
        'eta'     : 0.742364,
        'width'   : 0.177987
        }

    data = sciData(fName,reducedTunnelModel)
    SE=data.calcRelativeError(initpar)
    runtime = time.time()-start
    assert SE < 32 and runtime < 25

def test_2Hc2F_Nogauss(fName = 'tests\\2H-c-2F (amps).txt'):
    initpar = {
        'gammaL'  : 0.000256,
        'gammaR'  : 0.463199,
        'deltaE1' : 0.551646,
        'eta'     : 0.594323
        }

    bnds = {
        'gammaL'  : [0,1],
        'gammaR'  : [0,1],
        'deltaE1' : [0,1.5],
        'eta'     : [0,1]
        }

    par = {
        'gammaL'  : 0.000268,
        'gammaR'  : 0.464514,
        'deltaE1' : 0.574295,
        'eta'     : 0.582212
        }

    data = sciData(fName,reducedTunnelModel_NoGauss)
    data.fit(bnds,initpar)

    for key in list(par.keys()):
        assert abs((par[key]-data.parameters[key])/par[key]) < 0.05

def test_2Hs2F_Nogauss(fName = 'tests\\2H-s-2F (amps).txt'):
    initpar = {
        'gammaL'  : 0.000256,
        'gammaR'  : 0.463199,
        'deltaE1' : 0.551646,
        'eta'     : 0.594323
```

```
    }

bnds = {
    'gammaL'  : [0,1],
    'gammaR'  : [0,1],
    'deltaE1' : [0,1.5],
    'eta'     : [0,1]
    }

par = {
    'gammaL'  : 0.000042,
    'gammaR'  : 0.229306,
    'deltaE1' : 0.835175,
    'eta'     : 1.000000
    }

data = sciData(fName,reducedTunnelModel_NoGauss)
data.fit(bnds,initpar)

for key in list(par.keys()):
    assert abs((par[key]-data.parameters[key])/par[key]) < 0.05
```

# A SINGLE ATOM CHANGE TURNS

```
from class_sciData import sciData
from matplotlib import pyplot as plt
import models
import os
import numpy as np
import pandas as pd
directory = '%s'%os.getcwd()
mols = ['C14H','C14F','C14Cl','C14Br','C14I']

initpar = {



      'gammaL'   :          1.200000e-03,
          'gammaR'   :      1.000e-06,
          'deltaE1'  :      7.902064e-01,
          'eta'      :      4.7934453e-01,
          'sigma'    :      2.00060e-01
           }

bnds = {
   'gammaL'  : [0,1],
   'gammaR'  : [0,1],
   'deltaE1' : [0,1],
    'eta'    : [0,1],
   'sigma'   : [0,1]
   }

def editedModel(vb, gammaL, gammaR, deltaE, eta,sigma):
   n = 150
   I = models.tunnelmodel_1level_nogate_300K_gauss(vb, gammaL, gammaR, deltaE, eta,sigma)
   return np.log10(abs((n *I) /2.41E-06))

DataDF = pd.read_csv('Data.txt', delimiter = '\t')
DataDF = DataDF[abs(DataDF['voltage'])>0]

AllParams = pd.DataFrame()
plt.figure('All Molecules')
for mol in mols:
   print(mol)
   rawdat = {
      'X' : DataDF['voltage'],
```

```
        'Y' : DataDF[mol]
        }
    eq1 = np.vectorize(editedModel)
    data = sciData('',editedModel, rawdat = rawdat)
    data.fit(bnds,initpar)
    data.printFit()

    temp = pd.DataFrame(data.parameters,index = [0])
    temp['mol'] = mol
    AllParams = AllParams.append(temp,ignore_index = True)

    plt.plot(data.modelDat['X'], data.modelDat['Y'], label = mol)
    plt.scatter(data.rawdat['X'],   data.rawdat['Y'],   label = mol, color='black')
plt.legend()
plt.savefig('Plots\\AllMolecules.png')

plt.figure('gammaC')
plt.title('gammaC')
gammaC = AllParams['gammaL']*AllParams['gammaR']
plt.scatter(AllParams['mol'],gammaC)
plt.yscale('log')
plt.ylim(1E-9,1E-4)
plt.savefig('Plots\\par_gammaC.png')

plt.figure('gammaW')
plt.title('gammaW')
gammaW = AllParams['gammaL']+AllParams['gammaR']
plt.ylim(0,.2)
plt.scatter(AllParams['mol'],gammaW)
plt.savefig('Plots\\par_gammaW.png')

plt.figure('deltaE1')
plt.title('Delta E')
plt.ylim(0,.5)
plt.scatter(AllParams['mol'],AllParams['deltaE1'])
plt.savefig('Plots\\par_delta.png')

plt.figure('eta')
plt.title('eta')
plt.ylim(0,1)
plt.scatter(AllParams['mol'],AllParams['eta'])
plt.savefig('Plots\\par_eta.png')


plt.figure('sigma')
```

```
plt.title('sigma')
plt.ylim(0,.5)
plt.scatter(AllParams['mol'],AllParams['sigma'])
plt.savefig('Plots\\par_sigma.png')
```

## ELECTRIC FIELD DRIVEN DUAL FUNCTION

```
from penguins.class_sciData import sciData
import penguins.models as models
import time
import numpy as np

def reducedTunnelModel(vb, gammaL, gammaR, deltaE1, eta,sigma):
   T = 300
   c = 0
   vg = 0
   gammaC = gammaL*gammaR
   gammaW = gammaL+gammaR

   return models.tunnelmodel_singleLevel(vb,gammaC,gammaW, deltaE1,eta,sigma,c,vg,T)

def reducedTunnelModel_NoGauss(vb, gammaL, gammaR, deltaE1, eta):
   T = 300
   c = 0
   vg = 0
   sigma = 0
   gammaC = gammaL*gammaR
   gammaW = gammaL+gammaR

   return models.tunnelmodel_singleLevel(vb,gammaC,gammaW, deltaE1,eta,sigma,c,vg,T)

def test_memoryMolecule():
   start = time.time()
   # %% Setting the initial Parameters
   initpar = {
         'pos_L'       : -8.976e-01,
         'w_L'         :  3.300e-03 ,
         'pos_H'       : -1.677e-01,
         'w_H'         : 4.495e-02,
         'p0_H'        : -2.676e-03,
         'gammaC1'     : 2.230719e-06,
         'gammaW1'     : 5.388790e-02,
         'deltaE1'     : 3.414365e-01,
         'eta1'        : 0.78,
         'width1'      : 1.445773e-02,
         'gammaC2'     : 1.173901e-05,
         'gammaW2'     : 3.545940e-02,
         'deltaE2'     : 5.594792e-01,
```

```
    'eta2'         : 0.78,
    'width2'       : 6.554842e-03,
    'gamC_L'       : 3E-06*5.370e-03,
    'gamW_L'       : 5.370e-03+3E-06,
    'delE_L'       : 0.6,
    'eta_L'        : 5.8e-01,
    'width_L'      : 3.222e-02
    }

gamR_L = .5*(initpar['gammaW2']-np.sqrt(initpar['gammaW2']**2-4*initpar['gammaC2']))
gamR_R = initpar['gammaW2']-gamR_L

def memoryMolecule_gauss(vb, pos, width,p0,
            gammaC1_H, gammaW1_H, deltaE1_H, eta1_H,sigma1_H,
            gammaC2_H, gammaW2_H, deltaE2_H, eta2_H,sigma2_H,
            gammaL_L, gammaR_L, deltaE_L, eta_L,width_L):
  c = 0
  vg = 0
  T = 300

  args_L = (gammaL_L, gammaR_L, deltaE_L, eta_L,width_L,c,vg,T)

  P_H = models.sigmoid(vb,pos,width)+(vb-1)*p0
  P_L = 1-P_H

  I_H = models.tunnelmodel_2level(vb,c,vg,T,
                gammaC1_H,gammaW1_H,deltaE1_H,eta1_H,sigma1_H,
                gammaC2_H,gammaW2_H,deltaE2_H,eta2_H,sigma2_H)
  I_L = models.tunnelmodel_singleLevel(vb,*args_L)

  return P_H*I_H+P_L*I_L

# %% Set Up The Objects
fNameH = 'tests\\newhighEnergy.txt'
fNameL = 'tests\\newLowEnergy.txt'
highConduct = sciData(fNameH,memoryMolecule_gauss)
LowConduct = sciData(fNameL,memoryMolecule_gauss)
yexp = np.append(highConduct.workingdat['Y'],LowConduct.workingdat['Y'])

def Everything(initpar):
  #%% Permenant
  args_H = list(initpar.values())[2:]
  mod1=highConduct.model(highConduct.workingdat['X'],*args_H)

  args_L = list(initpar.values())[0:2]+list(initpar.values())[5:]
```

```
    args_L.insert(2,0)
    mod2=LowConduct.model(LowConduct.workingdat['X'],*args_L)

    #%% Setting up the Error
    return np.append(mod1,mod2)

ythr = Everything(initpar)
residual = np.subtract(np.log(np.abs(yexp)),np.log(np.abs(ythr)))
Error = np.sqrt(np.sum(residual**2))
end = time.time()
runtime = end-start
assert Error< 14 and runtime < 22
```

# Dynamic Molecular Switches

## Functions

```
import pandas as pd
import matplotlib.pyplot as plt
import penguins.models as models
from penguins.class_sciData import sciData
import time
from numpy.random import random
from numpy.random import choice
import numpy as np
import scipy.optimize as sco

eV = 1 #Energy
K  = 1 #Temperature Units
C  = 1 #Coulombs
s  = 1 #seconds
V  = 1 #volts

kb = 8.6173324e-5*eV/K #Boltzmann Constant
q  = 1.6e-19*C
h  = 4.1356e-15*eV*s

def reducedLandauer(vb,gammaL,gammaR,deltaE1,eta,sigma):
   gammaC = gammaL*gammaR
   gammaW = gammaL+gammaR

   c = 0
   vg = 0
   T = 300
   return models.tunnelmodel_singleLevel(vb,gammaC,gammaW, deltaE1,
                              eta,sigma,c,vg,T)
def reducedBridgePop(vb, gammaL, gammaR, deltaE, eta):
   c = 0
   vg = 0
   T = 300
   return models.averageBridgePopulation(vb, gammaL, gammaR, deltaE, eta, c, vg, T)

def MarcusETRates(vb, gamma, lam, E_AB):
   alpha = vb-E_AB
   T = 300*K
   S = 2*np.sqrt(np.pi*kb*T/lam)
```

```
    R_plus = (gamma/4)*S*np.exp(-(alpha+lam)**2/(4*lam*kb*T))
    R_minus = (gamma/4)*S*np.exp(-(alpha-lam)**2/(4*lam*kb*T))
    return R_plus,R_minus

def NitzFit(V, n, gammaL, gammaR, kappa, sigma, E_AB, E_AC, chi, eta, gam, lam, P, u):

    eq1 = np.vectorize(reducedLandauer)
    eq2 = np.vectorize(reducedBridgePop)
    eq3 = np.vectorize(MarcusETRates)

    I_S0 = n*eq1(V, gammaL, gammaR, E_AB, eta, sigma)
    I_S1 = n*eq1(V, kappa*gammaL, kappa*gammaR, E_AB+chi, eta,sigma)

    n_S0 = eq2(V, gammaL, gammaR, E_AB, eta)
    n_S1 = eq2(V, kappa*gammaL, kappa*gammaR, E_AB+chi, eta)

    R_AC, R_CA = eq3(V, gam, lam, E_AC)
    R_BD, R_DB = eq3(V, kappa*gam, lam, E_AC+chi)

    k_S0_S1 = (1-n_S0)*R_AC + n_S0*R_BD
    k_S1_S0 = (1-n_S1)*R_CA + n_S1*R_DB

    delt = abs(V[0]-V[1])/u
    I = []
    Parray = []
    for i in range(len(V)):
        Parray += [P]
        I += [((1-P)*I_S0[i]+P*I_S1[i])]

        dPdt = k_S0_S1[i]-P*(k_S0_S1[i]+k_S1_S0[i])
        P = P+dPdt*delt
    return V, I, Parray

def saveParams(params,err,save):
    output = ''
    for nm in params.keys():
        output = output + '%.4e\t'%params[nm]
    output = output + '%.4e\n'%err
    f= open(save,"a")
    f.write(output)
    f.close()
```

Scan Rate Dependence

```
import pandas as pd
import numpy as np
import funcs as fun
import matplotlib.pyplot as plt
import scipy.optimize as sco
import time
start = time.time()

Fixed = {
   # 'n'      : 300,
   # 'gammaL'  : 0.0142,
   # 'gammaR'  : 0.0256,
   # 'kappa'   : 10.1,
   'sigma'   : 0,
   # 'E_AB'    : 0.82,
   # 'E_AC'    :-0.301,
   # 'chi'     : 1.59,
   # 'eta'     : 0.67,
   # 'gam'     : 20,
   'lam'     : 1.2,
   'P'       : 0,
   'u'       : 10/1000
}
Fit = True

initpar = {
   'n':    500000,
            'gammaR':       4e-06,
            'gammaL':       0.00139,
            'kappa':        10.1,
            'sigma':        0,
     'E_AB':         0.81,
     'E_AC':         -1.14,
            'chi':    0.72,
            'eta':    0.67,
            'gam':  20,
            'lam':   2,
   'P'       : 0,
   'u'       : 10/1000
}
a = .75
bnds = {
       'n'      : [100,10E10],
```

```
      'gammaL'  : [1E-4,.1],
      'gammaR'  : [1E-4,.1],
      'kappa'   : [1E-6,10],
      'sigma'   : [1E-6,10],
      'E_AB'    : [0,1.5],
      'E_AC'    : [-1.5,1.5],
      'chi'     : [0,2.0],
      'eta'     : [0,1],
      'gam'     : [1E-6,200],
      'lam'     : [1E-6,2],
      'P'       : [0,1],
      'u'       : [0,300]
   }

for key in Fixed.keys():
      del bnds[key]
paramsCopy = initpar.copy()
for key in Fixed.keys():
   initpar[key] = Fixed[key]
   del paramsCopy[key]

def fitfunc(x):
   params = initpar.copy()
   for i,key in enumerate(list(paramsCopy.keys())):
      params[key] = x[i]

   #%% Setting up the voltage
   CurrDF = pd.DataFrame()
   CurrDF['Voltage'] = np.round(np.arange(-2,2,0.01),2)

   #%% Calculating the Currents
   eqI = np.vectorize(fun.reducedLandauer)

   CurrDF['I_np'] = params['n']*eqI(CurrDF['Voltage'], params['gammaL'], params['gammaR'],
params['E_AB'], params['eta'], params['sigma'])
   CurrDF['I_p'] = params['n']*eqI(CurrDF['Voltage'], params['gammaL']*params['kappa'],
params['gammaR']*params['kappa'], params['E_AB']+params['chi'], params['eta'], params['sigma'])

   # %% Calculating the Average Bridge Populations
   eqN = np.vectorize(fun.reducedBridgePop)

   CurrDF['n_np'] = eqN(CurrDF['Voltage'], params['gammaL'], params['gammaR'], params['E_AB'],
params['eta'])
   CurrDF['n_p'] = eqN(CurrDF['Voltage'], params['gammaL']*params['kappa'],
params['gammaR']*params['kappa'], params['E_AB']+params['chi'], params['eta'])
```

```
   #%% Calculating the Marcus Rates
   eqR = np.vectorize(fun.MarcusETRates)

   CurrDF['R_AC'], CurrDF['R_CA'] = eqR(CurrDF['Voltage'], params['gam'], params['lam'],
params['E_AC'])
   CurrDF['R_BD'], CurrDF['R_DB'] = eqR(CurrDF['Voltage'], params['gam']*params['kappa'],
params['lam'], params['E_AC']+params['chi'])

   #%% Calculating Ks
   CurrDF['k_S0_S1'] = (1-CurrDF['n_np'])*CurrDF['R_AC'] + CurrDF['n_np']*CurrDF['R_BD']
   CurrDF['k_S1_S0'] = (1-CurrDF['n_p'])*CurrDF['R_CA'] + CurrDF['n_p']*CurrDF['R_DB']

   #%% Plotting
   # plt.figure('Raw1')
   # plt.plot(CurrDF['Voltage'],CurrDF['k_S0_S1'])
   # plt.plot(CurrDF['Voltage'],CurrDF['k_S1_S0'])

   # %% Calcuating Probability and Current
   diff = 0
   ran = [10,14,17,20,25,36,100,140,166,200,250]
   ran = [10]
   # ran = [250,200,166,140,100,36,25,20,17,14,10]
   P = params['P']
   data = pd.read_csv('Data\\SRt_cont_Normalized.txt', delimiter = '\t')
   for colV in data.columns:
      if colV[:-2][-1] == 'C':
            continue
      if not float(colV[:-3]) in ran:
         continue

      colC = colV.replace('V','C')
      colthr = colV.replace('V','thr')
      colP   = colV.replace('V','P')

      subset = pd.DataFrame()
      subset[colV] = data[colV]
      subset[colC] = data[colC]
      subset = subset.dropna()

      val = int(colV[0:3])

      delt = abs(data[colV][2]-data[colV][3])/(val/1000)
      I = []
      Parray = []
```

```
        delArray = []
        for i,v in enumerate(subset[colV]):
            tempDf =CurrDF[CurrDF['Voltage']==np.round(v,2)].reset_index()
            calcs = dict(tempDf.iloc[0])
            Parray += [P]
            I += [((1-P)*calcs['I_np']+P*calcs['I_p'])]

            dPdt = calcs['k_S0_S1']-P*(calcs['k_S0_S1']+calcs['k_S1_S0'])
            delArray += [dPdt]
            P = P+dPdt*delt
        subset[colthr] = pd.Series(I)
        diff += np.sum(np.subtract(subset[colC],subset[colthr])**2)/(np.max(subset[colC])-
np.min(subset[colC]))
        if not Fit:
            plt.figure('Current')
            plt.plot(subset[colV],subset[colC], color = 'black')
            plt.plot(subset[colV],subset[colthr], label = colthr)
            plt.legend()

            plt.figure('Probability')
            plt.plot(subset[colV],Parray, label = colthr)
            plt.legend()
    fun.saveParams(params,np.sqrt(diff),'Params\\All\\SR_tot.txt')
    if Fit:
        print(np.log10(np.sqrt(diff)))
    return np.sqrt(diff)

if not Fit:
    print(fitfunc(list(paramsCopy.values())))
else:
    # result = sco.minimize(fitfunc,x0 = list(paramsCopy.values()), bounds = list(bnds.values()))
    result = sco.differential_evolution(fitfunc,bounds = list(bnds.values()))
    print('Total Time: %d'%(time.time()-start))

    for i,key in enumerate(list(paramsCopy.keys())):
        initpar[key] = result.x[i]
        paramsCopy[key] = result.x[i]

    # diff = result.fun
    # fun.saveParams(initpar,diff,'Params\\paramsSRReverseTot.txt')
    # fun.saveParams(initpar,diff,'Params\\All\\paramsSRReverseTot.txt')
```

Sweep Data

```
import glob
from random import choice
import pandas as pd
import time
from funcs import *
import matplotlib.pyplot as plt
import numpy as np
import scipy.optimize as sco
from scipy.stats import linregress
start = time.time()

# %% For Symmetric Normalized Data:
DataFile = 'Data\\Sym_cont_Normalized.txt'
SaveFileNote = 'SymContNormCut'
ran = [.25,.50,.75,1.00,1.25,1.50,1.75]

# %%For Asymmetric Postive Data -1.2
# DataFile = 'Data\\AsymPSh_cont_Normalized.txt'
# SaveFileNote = 'AsymPShContNorm'
# ran = [0,.25,.50,.75,1.00,1.25,1.50,1.75]

#%% Subsetting Data:
ran = [1.750]

method = 'diff'
scale = 'log'
PeakPos = 3
cut = 0

Fit = 1
Fixed ={
#           'n':        1.00e+07,
#           'gammaL':         5.26e-05,
#           'gammaR':         1.50e-05,
#           'kappa':4.14e+01,
            'sigma': 0.00e+00,
#           'E_AB':  8.65e-01,
#           'E_AC':  -1.02e+00,
#           'chi':     3.16e+00,
#           'eta':     6.70e-01,
#           'gam':   1.31e+01,
#           'lam':   1.29e+00,
            'P':        0.00e+00,
```

```
            'u':        1.00e-02
}
bnds = {
      'n'      : [0,1E10],
      'gammaL'  : [1E-11, 0.1],
      'gammaR'  : [1E-11, 0.1],
      'kappa'   : [1E-11,300],
      'sigma'   : [1E-6,.5],
      'E_AB'    : [.4,0.90],
      'E_AC'    : [-1.60, -.23],
      'chi'     : [0.1, 5],
      'eta'     : [0.50, 0.78],
      'gam'     : [0.4, 30],
      'lam'     : [.1, 1.50],
      'P'       : [0,.1],
      'u'       : [0,300]
   }
initpar ={
            'n':        1.00e+07,
            'gammaL':         5.33e-05,
            'gammaR':         6.12e-05,
            'kappa': 65,
            'sigma': 0.00e+00,
            'E_AB':  .78,
            'E_AC':  -9.75e-01,
            'chi':      3.36e+00,
            'eta':      6.82e-01,
            'gam':    1.17e+01,
            'lam':    1.16e+00,
            'P':        0.00e+00,
            'u':        1.00e-02
}
data = pd.read_csv(DataFile, delimiter = '\t')

for key in Fixed.keys():
      del bnds[key]

# %% Making sure that the params are within the bounds
for key in bnds.keys():
   if bnds[key][0] > initpar[key] or bnds[key][1] < initpar[key]:
      print(key)

def reducedLandauer(vb, n, gammaL, gammaR, deltaE1, eta, sigma):
   gammaC = gammaL*gammaR*n
   gammaW = gammaL+gammaR
```

```
    c = 0
    vg = 0
    T = 300
    return models.tunnelmodel_singleLevel(vb,gammaC,gammaW, deltaE1,
                                eta,sigma,c,vg,T)
Origin = pd.DataFrame()
totalDiff = 0
for colV in data.columns:
    # %% Making a copy of the Parameters with the 'fixed' ones removed
    paramsCopy = initpar.copy()
    for key in Fixed.keys():
        initpar[key] = Fixed[key]
        del paramsCopy[key]

    if colV[:-2][-1] == 'C':
            continue
    if not float(colV[:-3]) in ran:
        continue

    colC = colV.replace('V','C')
    colthr = colV.replace('V','thr')
    colP   = colV.replace('V','P')

    cnt = 0
    def fitfunc(x):

        global cnt
        diff = 0
        params = initpar.copy()
        for i,key in enumerate(list(paramsCopy.keys())):
            params[key] = x[i]
        if PeakPos < 2:
            params['E_AC'] = (PeakPos-params['lam'])

        subset = pd.DataFrame()
        subset[colV] = data[colV]
        subset[colC] = data[colC]
        subset = subset.dropna()

        __, subset[colthr], subset[colP] = NitzFit(subset[colV], *list(params.values()))

        subset = subset[np.abs(subset[colV])>cut]
        if scale == 'lin':
            diff =np.sqrt(np.sum(np.subtract(subset[colthr], subset[colC])**2))
```

```
    Origin[colV] = subset[colV]
    Origin[colC] = np.abs(subset[colthr])
    subset[colC]   = np.abs(subset[colC])
    subset[colthr] = np.abs(subset[colthr])

    if scale == 'log':
       # plt.figure('Curr2')
       res = np.abs(np.subtract(np.log10(subset[colthr]),np.log10(subset[colC])))
       # plt.plot(subset[colV],res, label = colthr)
       # plt.legend()
       diff =np.sum(res)

    Fixed['P'] = list(subset[colP])[-1]
    if not Fit:
       eq = np.vectorize(reducedLandauer)

       Inp = np.abs(eq(subset[colV], params['n'], params['gammaL'], params['gammaR'], params['E_AB'],
params['eta'], params['sigma']))

       Ip = np.abs(eq(subset[colV], params['n'], params['kappa']*params['gammaL'],
params['kappa']*params['gammaR'], params['E_AB']+params['chi'], params['eta'], params['sigma']))

       plt.figure('Current')
       plt.plot(subset[colV],subset[colC], color = 'black')
       plt.plot(subset[colV],subset[colthr], label = colthr)
       plt.plot(subset[colV],Inp, color = 'orange')
       plt.plot(subset[colV],Ip, color = 'gray')
       plt.legend()
       plt.yscale('log')

       plt.figure('Probability')
       plt.plot(subset[colV],subset[colP], label = colthr)
       plt.legend()

    if Fit:

       if not cnt%100:
          if scale == 'lin':
             print('%s\t%d\t\t%.2f'%(colC,cnt,np.log10(diff)))
          else:
             print('%s\t%d\t\t%.2f'%(colC,cnt,diff))
       cnt +=1
    saveParams(params,diff,'Params\\All\\par_%s_%s_%s_%s.txt'%( SaveFileNote, colV[:-
3].replace('.',''),scale,colV[-1]))
```

```
        return diff

    if not Fit:
        if scale == 'lin':
            print('%s\t%.2f'%(colC,np.log10(fitfunc(list(paramsCopy.values())))))
        else:
            print('%s\t%.2f'%(colC,fitfunc(list(paramsCopy.values()))))
    else:
        if method == 'min':
            result = sco.minimize(fitfunc,x0 = list(paramsCopy.values()), bounds = list(bnds.values()))
        if method == 'diff':
            result = sco.differential_evolution(fitfunc,bounds = list(bnds.values()))
        print('\nTotal Time: %d'%(time.time()-start))

        for i,key in enumerate(list(paramsCopy.keys())):
            initpar[key] = result.x[i]
            paramsCopy[key] = result.x[i]
        diff = result.fun
        totalDiff += diff**2
        print('Error:\t%.2f\n'%np.log10(diff))
        print(initpar['gammaL']*initpar['gammaR']/(initpar['gammaL']+initpar['gammaR'])*300*1000)
        print('initpar ={')
        for key in initpar.keys():
            if key == 'u':
                print('\t\'%s\':\t%.2e'%(key,initpar[key]))
            else:
                print('\t\'%s\':\t%.2e,'%(key,initpar[key]))
        print('}')

        # saveParams(initpar,diff,'Params\\par_%s_%03d_%s_%s.txt'%(SaveFileNote, float(colV[:-
3])*100,scale,colV[-1]))
        # saveParams(initpar,diff,'Params\\All\\par_%s_%03d_%s_%s.txt'%(SaveFileNote, float(colV[:-
3])*100,scale,colV[-1]))
```

Normalizing Data

```
import pandas as pd
import matplotlib.pyplot as plt
import numpy as np

PosDataFile = 'Data\\AsymPos_split.txt'
NegDataFile = 'Data\\AsymNeg_split.txt'
SymDataFile = 'Data\\SweepDataSet6_split.txt'
SRtDataFile = 'Data\\Air_SR.txt'
PShDataFile = 'Data\\AsymPosShort_split.txt'

PosData = pd.read_csv(PosDataFile, delimiter = '\t')
NegData = pd.read_csv(NegDataFile, delimiter = '\t')
SymData = pd.read_csv(SymDataFile, delimiter = '\t')
SRtData = pd.read_csv(SRtDataFile, delimiter = '\t')
PShData = pd.read_csv(PShDataFile, delimiter = '\t')

PosScalesFile = 'AsymPosScales.txt'
NegScalesFile = 'AsymNegScales.txt'
SymScalesFile = 'SymScales.txt'
SRtScalesFile = 'SRtScales.txt'
PShScalesFile = 'AsymPShScales.txt'

NegScales = pd.read_csv(NegScalesFile, delimiter = '\t',header = None)
NegScales = NegScales.transpose()
NegScales.columns = NegScales.iloc[0]
NegScales = NegScales[1:]

PosScales = pd.read_csv(PosScalesFile, delimiter = '\t',header = None)
PosScales = PosScales.transpose()
PosScales.columns = PosScales.iloc[0]
PosScales = PosScales[1:]

PShScales = pd.read_csv(PShScalesFile, delimiter = '\t',header = None)
PShScales = PShScales.transpose()
PShScales.columns = PShScales.iloc[0]
PShScales = PShScales[1:]

SymScales = pd.read_csv(SymScalesFile, delimiter = '\t',header = None)
SymScales = SymScales.transpose()
SymScales.columns = SymScales.iloc[0]
SymScales = SymScales[1:]

SRtScales = pd.read_csv(SRtScalesFile, delimiter = '\t',header = None)
```

```
SRtScales = SRtScales.transpose()
SRtScales.columns = SRtScales.iloc[0]
SRtScales = SRtScales[1:]

PosSecCols = []
NegSecCols = []
SymSecCols = []
PShSecCols = []

plt.figure('CurrentNegative')
for colV in NegData.columns:
   if colV[-1] == '2':
      NegSecCols += [colV]
   if colV[:-2][-1] == 'C':
      continue
   colC = colV.replace('V','C')

   plt.plot(NegData[colV],np.abs(NegData[colC]), color = 'black')
   NegData[colC] = NegData[colC]*NegScales[colV].iloc[0]
   plt.plot(NegData[colV],np.abs(NegData[colC]), color = 'red')
plt.title('Asymmetric Negative Bias Cycles\nFixed positive voltage (Vmax = +1V) Fig. Fig SXE')
plt.yscale('log')

plt.figure('CurrentPsh')
c = '0'
for colV in PShData.columns:
   if colV[-1] == '2':
      PShSecCols += [colV]
   if colV[:-2][-1] == 'C':
      continue
   colC = colV.replace('V','C')

   plt.plot(PShData[colV],np.abs(PShData[colC]), color = 'black',zorder = 50)
   PShData[colC] = PShData[colC]*PShScales[colV].iloc[0]
   if colV == c:
      plt.plot(PShData[colV],np.abs(PShData[colC]), color = 'red',zorder = 60)
   # plt.plot(PShData[colV],np.abs(PShData[colC]), color = 'red',zorder = 50)
plt.title('Asymmetric Positive Bias Cycles\nFixed negative voltage (Vmax = -2V)\nFig. 3G and Fig SXC')
plt.yscale('log')

plt.figure('CurrentPos')
c = '0'
for colV in PosData.columns:
   if colV[-1] == '2':
      PosSecCols += [colV]
```

```
    if colV[:-2][-1] == 'C':
        continue
    colC = colV.replace('V','C')

    plt.plot(PosData[colV],np.abs(PosData[colC]), color = 'black',zorder = 50)
    PosData[colC] = PosData[colC]*PosScales[colV].iloc[0]
    if colV == c:
        plt.plot(PosData[colV],np.abs(PosData[colC]), color = 'red',zorder = 60)

    plt.plot(PosData[colV],np.abs(PosData[colC]), color = 'red',zorder = 50)
plt.yscale('log')
plt.title('Asymmetric Positive Bias Cycles\nFixed negative voltage (Vmax = -2V)\nFig. 3G and Fig SXC')

plt.figure('CurrentSymmetric')
c = '0'
for colV in SymData.columns:
    if colV[-1] == '2':
        SymSecCols += [colV]
    if colV[:-2][-1] == 'C':
        continue
    colC = colV.replace('V','C')

    plt.plot(SymData[colV],np.abs(SymData[colC]), color = 'black',zorder = 10)
    SymData[colC] = SymData[colC]*SymScales[colV].iloc[0]
    if colV == c:
        plt.plot(SymData[colV],np.abs(SymData[colC]), color = 'red',zorder = 30)

    plt.plot(SymData[colV],np.abs(SymData[colC]), color = 'red',zorder = 10)
plt.title('Symmetric Bias Cycles\nVarying voltage\nFig. 3F and Fig. SXB')

plt.yscale('log')

plt.figure('ScanRate')
c = '0'
for colV in SRtData.columns:
    if colV[:-2][-1] == 'C':
        continue
    colC = colV.replace('V','C')

    plt.plot(SRtData[colV],np.abs(SRtData[colC]), color = 'black',zorder = 10)

    SRtData[colC] = SRtData[colC]*SRtScales[colV].iloc[0]
    if colV == c:
        plt.plot(SRtData[colV],np.abs(SRtData[colC]), color = 'red',zorder = 20)
```

```
    plt.plot(SRtData[colV],np.abs(SRtData[colC]),color = 'red' ,zorder = 10)
plt.title('Scan Rate Dependence Cycles\nFixed bias voltage (-1.5V to +1V)\nFig. 3C and Fig. SXA')
plt.yscale('log')

PosData = PosData.dropna(axis = 0, how = 'all')
PShData = PShData.dropna(axis = 0, how = 'all')
NegData = NegData.dropna(axis = 0, how = 'all')
SymData = SymData.dropna(axis = 0, how = 'all')
SRtData = SRtData.dropna(axis = 0, how = 'all')

PosData.to_csv('Data\\AsymPos_Split_Normalized.txt',sep = '\t',index = False)
PShData.to_csv('Data\\AsymPSh_Split_Normalized.txt',sep = '\t',index = False)
NegData.to_csv('Data\\AsymNeg_Split_Normalized.txt',sep = '\t',index = False)
SymData.to_csv('Data\\Sym_Split_Normalized.txt',sep = '\t',index = False)
SRtData.to_csv('Data\\SRt_Split_Normalized.txt',sep = '\t',index = False)

PShSecSet = PShData[PShSecCols]
PosSecSet = PosData[PosSecCols]
NegSecSet = NegData[NegSecCols]
SymSecSet = SymData[SymSecCols]

PShData = PShData.drop(PShSecCols, axis = 1)
PosData = PosData.drop(PosSecCols, axis = 1)
NegData = NegData.drop(NegSecCols,axis = 1)
SymData = SymData.drop(SymSecCols,axis = 1)

PShSecSet.columns = PShData.columns
PosSecSet.columns = PosData.columns
NegSecSet.columns = NegData.columns
SymSecSet.columns = SymData.columns

PShData = PShData.append(PShSecSet, ignore_index = 'True')
PosData = PosData.append(PosSecSet, ignore_index = 'True')
NegData = NegData.append(NegSecSet, ignore_index = 'True')
SymData = SymData.append(SymSecSet, ignore_index = 'True')

PShData.to_csv('Data\\AsymPSh_cont_Normalized.txt',sep = '\t',index = False)
PosData.to_csv('Data\\AsymPos_cont_Normalized.txt',sep = '\t',index = False)
NegData.to_csv('Data\\AsymNeg_cont_Normalized.txt',sep = '\t',index = False)
SymData.to_csv('Data\\Sym_cont_Normalized.txt',sep = '\t',index = False)
SRtData.to_csv('Data\\SRt_cont_Normalized.txt',sep = '\t',index = False)
```

# LIST OF REFERENCES


[1] A. Aviram and M. A. Ratner, "Molecular rectifiers," (in English), *Chem. Phys. Lett.,* Article vol. 29, no. 2, pp. 277-283, 1974, doi: 10.1016/0009-2614(74)85031-1.

[2] J. Bardeen and W. H. Brattain, "Physical Principles Involved in Transistor Action," *Physical Review,* vol. 75, no. 8, pp. 1208-1225, 04/15/ 1949, doi: 10.1103/PhysRev.75.1208.

[3] G. E. Moore, "Cramming More Components onto Integrated Circuits," *Electronics,* vol. 28, no. 8, pp. 114-117, 1965.

[4] Soloviev, II, N. V. Klenov, S. V. Bakurskiy, M. Y. Kupriyanov, A. L. Gudkov, and A. S. Sidorenko, "Beyond Moore's technologies: operation principles of a superconductor alternative," (in English), *Beilstein J. Nanotechnol.,* Review vol. 8, pp. 2689-2710, Dec 2017, doi: 10.3762/bjnano.8.269.

[5] A. Aviram, "MOLECULES FOR MEMORY, LOGIC, AND AMPLIFICATION," (in English), *J. Am. Chem. Soc.,* Article vol. 110, no. 17, pp. 5687-5692, Aug 1988, doi: 10.1021/ja00225a017.

[6] G. J. Ashwell, J. R. Sambles, A. S. Martin, W. G. Parker, and M. Szablewski, "RECTIFYING CHARACTERISTICS OF MG/(C16H33-Q3CNQ LB FILM)/PT STRUCTURES," (in English), *J. Chem. Soc.-Chem. Commun.,* Article no. 19, pp. 1374-1376, Oct 1990, doi: 10.1039/c39900001374.

[7] A. S. Martin, J. R. Sambles, and G. J. Ashwell, "MOLECULAR RECTIFIER," (in English), *Phys. Rev. Lett.,* Article vol. 70, no. 2, pp. 218-221, Jan 1993, doi: 10.1103/PhysRevLett.70.218.

[8] R. M. Metzger *et al.*, "Unimolecular electrical rectification in hexadecylquinolinium tricyanoquinodimethanide," (in English), *J. Am. Chem. Soc.,* Article vol. 119, no. 43, pp. 10455-10466, Oct 1997, doi: 10.1021/ja971811e.

[9] B. Chen and R. M. Metzger, "Rectification between 370 and 105 K in Hexadecylquinolinium Tricyanoquinodimethanide," *The Journal of Physical Chemistry B,* vol. 103, no. 21, pp. 4447-4451, 1999/05/01 1999, doi: 10.1021/jp990006e.

[10] T. Xu, I. R. Peterson, M. V. Lakshmikantham, and R. M. Metzger, "Rectification by a Monolayer of Hexadecylquinolinium Tricyanoquinodimethanide between Gold Electrodes," *Angewandte Chemie International Edition,* vol. 40, no. 9, pp. 1749-1752, 2001, doi: 10.1002/1521-3773(20010504)40:9<1749::Aid-anie17490>3.0.Co;2-o.

[11] R. M. Metzger, T. Xu, and I. R. Peterson, "Electrical Rectification by a Monolayer of Hexadecylquinolinium Tricyanoquinodimethanide Measured between Macroscopic Gold Electrodes," *The Journal of Physical Chemistry B,* vol. 105, no. 30, pp. 7280-7290, 2001/08/01 2001, doi: 10.1021/jp011084g.

[12] R. M. Metzger, "Unimolecular electrical rectifiers," (in English), *Chem Rev,* Review vol. 103, no. 9, pp. 3803-34, Sep 2003, doi: 10.1021/cr020413d.

[13] C. Krzeminski, C. Delerue, G. Allan, D. Vuillaume, and R. M. Metzger, "Theory of electrical rectification in a molecular monolayer," *Phys. Rev. B,* vol. 64, no. 8, p. 085405, 08/02/ 2001, doi: 10.1103/PhysRevB.64.085405.

[14] G. J. Ashwell, W. D. Tyrrell, and A. J. Whittam, "Molecular rectification: Self-assembled monolayers in which donor-(pi-bridge)-acceptor moieties are centrally located and symmetrically coupled to both gold electrodes," (in English), *J. Am. Chem. Soc.,* Article vol. 126, no. 22, pp. 7102-7110, Jun 2004, doi: 10.1021/ja049633u.

[15] G. J. Ashwell, A. Mohib, and J. R. Miller, "Induced rectification from self-assembled monolayers of sterically hindered pi-bridged chromophores," (in English), *J. Mater. Chem.,* Article vol. 15, no. 11, pp. 1160-1166, 2005, doi: 10.1039/b417880g.

[16] R. M. Metzger, "Unimolecular electronics," (in English), *Chem Rev,* Review vol. 115, no. 11, pp. 5056-115, Jun 10 2015, doi: 10.1021/cr500459d.

[17] I. Diez-Perez, J. Hihath, Y. Lee, L. P. Yu, L. Adamska, M. A. Kozhushner, Oleynik, II, and N. J. Tao, "Rectification and stability of a single molecular diode with controlled orientation," (in English), *Nat. Chem.,* Article vol. 1, no. 8, pp. 635-641, Nov 2009, doi: 10.1038/nchem.392.

[18] W. Y. Lo, N. Zhang, Z. X. Cai, L. W. Li, and L. P. Yu, "Beyond Molecular Wires: Design Molecular Electronic Functions Based on Dipolar Effect," (in English), *Accounts Chem. Res.,* Review vol. 49, no. 9, pp. 1852-1863, Sep 2016, doi: 10.1021/acs.accounts.6b00305.

[19] W. Schottky, "Vereinfachte und erweiterte Theorie der Randschicht-gleichrichter," *Zeitschrift für Physik,* vol. 118, no. 9, pp. 539-592, 1942/02/01 1942, doi: 10.1007/BF01329843.

[20] Y. Liu, Y. Xu, J. Wu, and D. Zhu, "Preparation of LB films of C60 doped poly(3-alkylthiophene)s and electronic properties of their Schottky diodes," *Solid State Commun.,* vol. 95, no. 10, pp. 695-699, 1995/09/01/ 1995, doi: https://doi.org/10.1016/0038-1098(95)00351-7.

[21] Y. Q. Liu, Y. Xu, and D. B. Zhu, "Synthesis and Langmuir-Blodgett film of an alkyl substituted thiophene oligomer," *Synthetic Metals,* vol. 84, no. 1, pp. 197-198, 1997/01/01/ 1997, doi: https://doi.org/10.1016/S0379-6779(97)80711-4.

[22] L. Yuan, N. Nerngchamnong, L. Cao, H. Hamoudi, E. del Barco, M. Roemer, R. K. Sriramula, D. Thompson, and C. A. Nijhuis, "Controlling the direction of rectification in a molecular diode," (in English), *Nat Commun,* Article vol. 6, p. 6324, Mar 2 2015, Art no. 6324, doi: 10.1038/ncomms7324.

[23] L. Jiang, L. Yuan, L. Cao, and C. A. Nijhuis, "Controlling Leakage Currents: The Role of the Binding Group and Purity of the Precursors for Self-Assembled Monolayers in the Performance of Molecular Diodes," (in English), *J. Am. Chem. Soc.,* Article vol. 136, no. 5, pp. 1982-1991, Feb 2014, doi: 10.1021/ja411116n.

[24] V. Mujica, M. A. Ratner, and A. Nitzan, "Molecular rectification: why is it so rare?," *Chem. Phys.,* vol. 281, no. 2, pp. 147-150, 2002/08/01/ 2002, doi: https://doi.org/10.1016/S0301-0104(02)00494-9.

[25] M. L. Chabinyc, X. Chen, R. E. Holmlin, H. Jacobs, H. Skulason, C. D. Frisbie, V. Mujica, M. A. Ratner, M. A. Rampi, and G. M. Whitesides, "Molecular Rectification in a Metal−Insulator−Metal Junction Based on Self-Assembled Monolayers," *J. Am. Chem. Soc.,* vol. 124, no. 39, pp. 11730-11736, 2002/10/01 2002, doi: 10.1021/ja020506c.

[26] L. Yuan, R. Breuer, L. Jiang, M. Schmittel, and C. A. Nijhuis, "A Molecular Diode with a Statistically Robust Rectification Ratio of Three Orders of Magnitude," (in English), *Nano Lett,* Article vol. 15, no. 8, pp. 5506-12, Aug 12 2015, doi: 10.1021/acs.nanolett.5b02014.

[27] M. L. Perrin, E. Galan, R. Eelkema, J. M. Thijssen, F. Grozema, and H. S. van der Zant, "A gate-tunable single-molecule diode," (in English), *Nanoscale,* Article vol. 8, no. 16, pp. 8919-23, Apr 28 2016, doi: 10.1039/c6nr00735j.

[28] C. A. Nijhuis, W. F. Reus, and G. M. Whitesides, "Molecular Rectification in Metal−SAM−Metal Oxide−Metal Junctions," *J. Am. Chem. Soc.,* vol. 131, no. 49, pp. 17814-17827, 2009/12/16 2009, doi: 10.1021/ja9048898.

[29] Y. Han, C. Nickle, Z. Zhang, H. Astier, T. J. Duffin, D. Qi, Z. Wang, E. Del Barco, D. Thompson, and C. A. Nijhuis, "Electric-field-driven dual-functional molecular switches in tunnel junctions," (in

English), *Nat Mater,* Article vol. 19, no. 8, pp. 843-848, Aug 2020, doi: 10.1038/s41563-020-0697-5.
[30] R. T. Tung, "Recent advances in Schottky barrier concepts," (in English), *Mater. Sci. Eng. R-Rep.,* Review vol. 35, no. 1-3, pp. 1-138, Nov 2001, doi: 10.1016/s0927-796x(01)00037-7.
[31] B. Capozzi, J. Xia, O. Adak, E. J. Dell, Z. F. Liu, J. C. Taylor, J. B. Neaton, L. M. Campos, and L. Venkataraman, "Single-molecule diodes with high rectification ratios through environmental control," (in English), *Nat Nanotechnol,* Article vol. 10, no. 6, pp. 522-7, Jun 2015, doi: 10.1038/nnano.2015.97.
[32] A. R. Garrigues, L. Yuan, L. Wang, E. R. Mucciolo, D. Thompon, E. Del Barco, and C. A. Nijhuis, "A Single-Level Tunnel Model to Account for Electrical Transport through Single Molecule- and Self-Assembled Monolayer-based Junctions," (in English), *Sci Rep,* Article vol. 6, p. 26517, May 24 2016, Art no. 26517, doi: 10.1038/srep26517.
[33] C. Van Dyck, V. Geskin, and J. Cornil, "Fermi Level Pinning and Orbital Polarization Effects in Molecular Junctions: The Role of Metal Induced Gap States," (in English), *Adv. Funct. Mater.,* Article vol. 24, no. 39, pp. 6154-6165, Oct 2014, doi: 10.1002/adfm.201400809.
[34] R. T. Tung, "Chemical bonding and Fermi level pinning at metal-semiconductor interfaces," (in English), *Phys. Rev. Lett.,* Article vol. 84, no. 26, pp. 6078-6081, Jun 2000, doi: 10.1103/PhysRevLett.84.6078.
[35] R. Breuer and M. Schmittel, "Redox-Stable SAMs in Water (pH 0-12) from 1,1 '-Biferrocenylene-Terminated Thiols on Gold," (in English), *Organometallics,* Article vol. 31, no. 18, pp. 6642-6651, Sep 2012, doi: 10.1021/om300718k.
[36] X. Chen, M. Roemer, L. Yuan, W. Du, D. Thompson, E. Del Barco, and C. A. Nijhuis, "Molecular diodes with rectification ratios exceeding 10(5) driven by electrostatic interactions," (in English), *Nat Nanotechnol,* Article vol. 12, no. 8, pp. 797-803, Aug 2017, doi: 10.1038/nnano.2017.110.
[37] D. M. Adams *et al.*, "Charge transfer on the nanoscale: Current status," (in English), *J. Phys. Chem. B,* Review vol. 107, no. 28, pp. 6668-6697, Jul 2003, doi: 10.1021/jp0268462.
[38] V. R. I. Kaila, "Long-range proton-coupled electron transfer in biological energy conversion: towards mechanistic understanding of respiratory complex I," *Journal of The Royal Society Interface,* vol. 15, no. 141, p. 20170916, 2018, doi: doi:10.1098/rsif.2017.0916.
[39] V. Coropceanu, X.-K. Chen, T. Wang, Z. Zheng, and J.-L. Brédas, "Charge-transfer electronic states in organic solar cells," *Nature Reviews Materials,* vol. 4, no. 11, pp. 689-707, 2019/11/01 2019, doi: 10.1038/s41578-019-0137-9.
[40] N. Amdursky, D. Marchak, L. Sepunaru, I. Pecht, M. Sheves, and D. Cahen, "Electronic transport via proteins," *Adv Mater,* vol. 26, no. 42, pp. 7142-61, Nov 12 2014, doi: 10.1002/adma.201402304.
[41] A. Shah, B. Adhikari, S. Martic, A. Munir, S. Shahzad, K. Ahmad, and H. B. Kraatz, "Electron transfer in peptides," (in English), *Chem Soc Rev,* Review vol. 44, no. 4, pp. 1015-27, Feb 21 2015, doi: 10.1039/c4cs00297k.
[42] A. Vilan, D. Aswal, and D. Cahen, "Large-Area, Ensemble Molecular Electronics: Motivation and Challenges," (in English), *Chem Rev,* Review vol. 117, no. 5, pp. 4248-4286, Mar 8 2017, doi: 10.1021/acs.chemrev.6b00595.
[43] J. Jortner, A. Nitzan, and M. A. Ratner, "Foundations of Molecular Electronics – Charge Transport in Molecular Conduction Junctions," in *Introducing Molecular Electronics*, G. Cuniberti, K. Richter, and G. Fagas Eds. Berlin, Heidelberg: Springer Berlin Heidelberg, 2005, pp. 13-54.

[44] C. Jia and X. Guo, "Molecule-electrode interfaces in molecular electronic devices," *Chem Soc Rev,* vol. 42, no. 13, pp. 5642-60, Jul 7 2013, doi: 10.1039/c3cs35527f.
[45] Y. van de Burgt, A. Melianas, S. T. Keene, G. Malliaras, and A. Salleo, "Organic electronics for neuromorphic computing," (in English), *Nature Electronics,* Review vol. 1, no. 7, pp. 386-397, Jul 2018, doi: 10.1038/s41928-018-0103-3.
[46] J. Zhu, T. Zhang, Y. Yang, and R. Huang, "A comprehensive review on emerging artificial neuromorphic devices," (in English), *Appl. Phys. Rev.,* Review vol. 7, no. 1, p. 107, Mar 2020, Art no. 011312, doi: 10.1063/1.5118217.
[47] N. K. Upadhyay, H. Jiang, Z. R. Wang, S. Asapu, Q. F. Xia, and J. J. Yang, "Emerging Memory Devices for Neuromorphic Computing," (in English), *Adv. Mater. Technol.,* Review vol. 4, no. 4, p. 13, Apr 2019, Art no. 1800589, doi: 10.1002/admt.201800589.
[48] T. Chen, J. van Gelder, B. van de Ven, S. V. Amitonov, B. de Wilde, H. C. R. Euler, H. Broersma, P. A. Bobbert, F. A. Zwanenburg, and W. G. van der Wiel, "Classification with a disordered dopantatom network in silicon," (in English), *Nature,* Article vol. 577, no. 7790, pp. 341-+, Jan 2020, doi: 10.1038/s41586-019-1901-0.
[49] S. T. Keene, C. Lubrano, S. Kazemzadeh, A. Melianas, Y. Tuchman, G. Polino, P. Scognamiglio, L. Cina, A. Salleo, Y. van de Burgt, and F. Santoro, "A biohybrid synapse with neurotransmitter-mediated plasticity," (in English), *Nat Mater,* Article; Early Access vol. 19, no. 9, pp. 969-973, Sep 2020, doi: 10.1038/s41563-020-0703-y.
[50] Q. Z. Wan, M. T. Sharbati, J. R. Erickson, Y. H. Du, and F. Xiong, "Emerging Artificial Synaptic Devices for Neuromorphic Computing," (in English), *Adv. Mater. Technol.,* Review vol. 4, no. 4, p. 34, Apr 2019, Art no. 1900037, doi: 10.1002/admt.201900037.
[51] I. Ratera and J. Veciana, "Playing with organic radicals as building blocks for functional molecular materials," (in English), *Chem Soc Rev,* Review vol. 41, no. 1, pp. 303-49, Jan 7 2012, doi: 10.1039/c1cs15165g.
[52] R. Klajn, "Spiropyran-based dynamic materials," (in English), *Chem Soc Rev,* Review vol. 43, no. 1, pp. 148-84, Jan 7 2014, doi: 10.1039/c3cs60181a.
[53] D. Bleger and S. Hecht, "Visible-Light-Activated Molecular Switches," (in English), *Angew. Chem.-Int. Edit.,* Review vol. 54, no. 39, pp. 11338-11349, Sep 2015, doi: 10.1002/anie.201500628.
[54] H. Jeong, D. Kim, D. Xiang, and T. Lee, "High-Yield Functional Molecular Electronic Devices," (in English), *ACS Nano,* Review vol. 11, no. 7, pp. 6511-6548, Jul 25 2017, doi: 10.1021/acsnano.7b02967.
[55] N. Xin, J. Guan, C. Zhou, X. Chen, C. Gu, Y. Li, M. A. Ratner, A. Nitzan, J. F. Stoddart, and X. Guo, "Concepts in the design and engineering of single-molecule electronic devices," *Nature Reviews Physics,* vol. 1, p. 211, February 01, 2019 2019, doi: 10.1038/s42254-019-0022-x.
[56] E. J. Fuller *et al.*, "Parallel programming of an ionic floating-gate memory array for scalable neuromorphic computing," (in English), *Science,* Article vol. 364, no. 6440, pp. 570-574, May 10 2019, doi: 10.1126/science.aaw5581.
[57] J. Byun, Y. Lee, J. Yoon, B. Lee, E. Oh, S. Chung, T. Lee, K. J. Cho, J. Kim, and Y. Hong, "Electronic skins for soft, compact, reversible assembly of wirelessly activated fully soft robots," (in English), *Sci. Robot.,* Article vol. 3, no. 18, p. 11, May 2018, Art no. eaas9020, doi: 10.1126/scirobotics.aas9020.
[58] S. Kumar, M. Merelli, W. Danowski, P. Rudolf, B. L. Feringa, and R. C. Chiechi, "Chemical Locking in Molecular Tunneling Junctions Enables Nonvolatile Memory with Large On-Off Ratios," (in

English), *Adv. Mater.,* Article vol. 31, no. 15, p. 6, Apr 2019, Art no. 1807831, doi: 10.1002/adma.201807831.
[59] F. Schwarz, G. Kastlunger, F. Lissel, C. Egler-Lucas, S. N. Semenov, K. Venkatesan, H. Berke, R. Stadler, and E. Lortscher, "Field-induced conductance switching by charge-state alternation in organometallic single-molecule junctions," *Nat Nanotechnol,* vol. 11, no. 2, pp. 170-6, Feb 2016, doi: 10.1038/nnano.2015.255.
[60] E. Lortscher, J. W. Ciszek, J. Tour, and H. Riel, "Reversible and controllable switching of a single-molecule junction," *Small,* vol. 2, no. 8-9, pp. 973-7, Aug 2006, doi: 10.1002/smll.200600101.
[61] S. J. van der Molen, J. H. Liao, T. Kudernac, J. S. Agustsson, L. Bernard, M. Calame, B. J. van Wees, B. L. Feringa, and C. Schonenberger, "Light-Controlled Conductance Switching of Ordered Metal-Molecule-Metal Devices," (in English), *Nano Lett.,* Article vol. 9, no. 1, pp. 76-80, Jan 2009, doi: 10.1021/nl802487j.
[62] J. Lee, H. Chang, S. Kim, G. S. Bang, and H. Lee, "Molecular Monolayer Nonvolatile Memory with Tunable Molecules," (in English), *Angew. Chem.-Int. Edit.,* Article vol. 48, no. 45, pp. 8501-8504, 2009, doi: 10.1002/anie.200902990.
[63] A. C. Aragones, D. Aravena, J. I. Cerda, Z. Acis-Castillo, H. P. Li, J. A. Real, F. Sanz, J. Hihath, E. Ruiz, and I. Diez-Perez, "Large Conductance Switching in a Single-Molecule Device through Room Temperature Spin-Dependent Transport," (in English), *Nano Lett.,* Article vol. 16, no. 1, pp. 218-226, Jan 2016, doi: 10.1021/acs.nanolett.5b03571.
[64] L. Bogani and W. Wernsdorfer, "Molecular spintronics using single-molecule magnets," (in English), *Nat. Mater.,* Article vol. 7, no. 3, pp. 179-186, Mar 2008, doi: 10.1038/nmat2133.
[65] C. Jia *et al.*, "Covalently bonded single-molecule junctions with stable and reversible photoswitched conductivity," (in English), *Science,* Article vol. 352, no. 6292, pp. 1443-5, Jun 17 2016, doi: 10.1126/science.aaf6298.
[66] M. M. Russew and S. Hecht, "Photoswitches: From Molecules to Materials," (in English), *Adv. Mater.,* Article vol. 22, no. 31, pp. 3348-3360, Aug 2010, doi: 10.1002/adma.200904102.
[67] C. Simao, M. Mas-Torrent, N. Crivillers, V. Lloveras, J. M. Artes, P. Gorostiza, J. Veciana, and C. Rovira, "A robust molecular platform for non-volatile memory devices with optical and magnetic responses," (in English), *Nat. Chem.,* Article vol. 3, no. 5, pp. 359-364, May 2011, doi: 10.1038/nchem.1013.
[68] S. Erbas-Cakmak, D. A. Leigh, C. T. McTernan, and A. L. Nussbaumer, "Artificial Molecular Machines," (in English), *Chem Rev,* Review vol. 115, no. 18, pp. 10081-206, Sep 23 2015, doi: 10.1021/acs.chemrev.5b00146.
[69] G. de Ruiter and M. E. van der Boom, "Sequential logic and random access memory (RAM): a molecular approach," (in English), *J. Mater. Chem.,* Article vol. 21, no. 44, pp. 17575-17581, 2011, doi: 10.1039/c1jm12343b.
[70] A. Sorrenti, J. Leira-Iglesias, A. J. Markvoort, T. F. A. de Greef, and T. M. Hermans, "Non-equilibrium supramolecular polymerization," (in English), *Chem Soc Rev,* Review vol. 46, no. 18, pp. 5476-5490, Sep 18 2017, doi: 10.1039/c7cs00121e.
[71] S. A. P. van Rossum, M. Tena-Solsona, J. H. van Esch, R. Eelkema, and J. Boekhoven, "Dissipative out-of-equilibrium assembly of man-made supramolecular materials," (in English), *Chem Soc Rev,* Review vol. 46, no. 18, pp. 5519-5535, Sep 18 2017, doi: 10.1039/c7cs00246g.
[72] J. Boekhoven, W. E. Hendriksen, G. J. Koper, R. Eelkema, and J. H. van Esch, "Transient assembly of active materials fueled by a chemical reaction," (in English), *Science,* Article vol. 349, no. 6252, pp. 1075-9, Sep 4 2015, doi: 10.1126/science.aac6103.

[73] C. Y. Cheng, P. R. McGonigal, S. T. Schneebeli, H. Li, N. A. Vermeulen, C. F. Ke, and J. F. Stoddart, "An artificial molecular pump," (in English), *Nat. Nanotechnol.,* Article vol. 10, no. 6, pp. 547-553, Jun 2015, doi: 10.1038/nnano.2015.96.

[74] J. T. Foy, Q. Li, A. Goujon, J. R. Colard-Itte, G. Fuks, E. Moulin, O. Schiffmann, D. Dattler, D. P. Funeriu, and N. Giuseppone, "Dual-light control of nanomachines that integrate motor and modulator subunits," (in English), *Nat. Nanotechnol.,* Article vol. 12, no. 6, pp. 540-545, Jun 2017, doi: 10.1038/nnano.2017.28.

[75] S. Erbas-Cakmak, S. D. P. Fielden, U. Karaca, D. A. Leigh, C. T. McTernan, D. J. Tetlow, and M. R. Wilson, "Rotary and linear molecular motors driven by pulses of a chemical fuel," (in English), *Science,* Article vol. 358, no. 6361, pp. 340-343, Oct 20 2017, doi: 10.1126/science.aao1377.

[76] M. Kathan, F. Eisenreich, C. Jurissek, A. Dallmann, J. Gurke, and S. Hecht, "Light-driven molecular trap enables bidirectional manipulation of dynamic covalent systems," (in English), *Nat. Chem.,* Article vol. 10, no. 10, pp. 1031-1036, Oct 2018, doi: 10.1038/s41557-018-0106-8.

[77] D. R. Weinberg, C. J. Gagliardi, J. F. Hull, C. F. Murphy, C. A. Kent, B. C. Westlake, A. Paul, D. H. Ess, D. G. McCafferty, and T. J. Meyer, "Proton-coupled electron transfer," (in English), *Chem Rev,* Review vol. 112, no. 7, pp. 4016-93, Jul 11 2012, doi: 10.1021/cr200177j.

[78] S. Y. Sayed, J. A. Fereiro, H. J. Yan, R. L. McCreery, and A. J. Bergren, "Charge transport in molecular electronic junctions: Compression of the molecular tunnel barrier in the strong coupling regime," (in English), *Proc. Natl. Acad. Sci. U. S. A.,* Article vol. 109, no. 29, pp. 11498-11503, Jul 2012, doi: 10.1073/pnas.1201557109.

[79] M. L. Perrin, C. J. Verzijl, C. A. Martin, A. J. Shaikh, R. Eelkema, J. H. van Esch, J. M. van Ruitenbeek, J. M. Thijssen, H. S. van der Zant, and D. Dulic, "Large tunable image-charge effects in single-molecule junctions," *Nat Nanotechnol,* vol. 8, no. 4, pp. 282-7, Apr 2013, doi: 10.1038/nnano.2013.26.

[80] H. Ishii, K. Sugiyama, E. Ito, and K. Seki, "Energy level alignment and interfacial electronic structures at organic/metal and organic/organic interfaces (vol 11, pg 605, 1999)," (in English), *Adv. Mater.,* Correction vol. 11, no. 12, pp. 972-972, Aug 1999. [Online]. Available: <Go to ISI>://WOS:000082435000001.

[81] C. Franco *et al.*, "Operative Mechanism of Hole-Assisted Negative Charge Motion in Ground States of Radical-Anion Molecular Wires," *J Am Chem Soc,* vol. 139, no. 2, pp. 686-692, Jan 18 2017, doi: 10.1021/jacs.6b08649.

[82] H. M. McConnell, "Intramolecular Charge Transfer in Aromatic Free Radicals," *The Journal of Chemical Physics,* vol. 35, no. 2, pp. 508-515, 1961/08/01 1961, doi: 10.1063/1.1731961.

[83] T. Hines, I. Diez-Perez, J. Hihath, H. M. Liu, Z. S. Wang, J. W. Zhao, G. Zhou, K. Muellen, and N. J. Tao, "Transition from Tunneling to Hopping in Single Molecular Junctions by Measuring Length and Temperature Dependence," (in English), *J. Am. Chem. Soc.,* Article vol. 132, no. 33, pp. 11658-11664, Aug 2010, doi: 10.1021/ja1040946.

[84] S. Ho Choi, B. Kim, and C. D. Frisbie, "Electrical resistance of long conjugated molecular wires," (in English), *Science,* Article vol. 320, no. 5882, pp. 1482-6, Jun 13 2008, doi: 10.1126/science.1156538.

[85] X. T. Zhao, C. C. Huang, M. Gulcur, A. S. Batsanov, M. Baghernejad, W. J. Hong, M. R. Bryce, and T. Wandlowski, "Oligo(aryleneethynylene)s with Terminal Pyridyl Groups: Synthesis and Length Dependence of the Tunneling-to-Hopping Transition of Single-Molecule Conductances," (in English), *Chem. Mat.,* Article vol. 25, no. 21, pp. 4340-4347, Nov 2013, doi: 10.1021/cm4029484.

[86] M. Koch, F. Ample, C. Joachim, and L. Grill, "Voltage-dependent conductance of a single graphene nanoribbon," (in English), *Nat. Nanotechnol.,* Article vol. 7, no. 11, pp. 713-717, Nov 2012, doi: 10.1038/nnano.2012.169.

[87] K. S. Kumar, R. R. Pasula, S. Lim, and C. A. Nijhuis, "Long-Range Tunneling Processes across Ferritin-Based Junctions," (in English), *Adv. Mater.,* Article vol. 28, no. 9, pp. 1824-1830, Mar 2016, doi: 10.1002/adma.201504402.

[88] K. Moth-Poulsen and T. Bjornholm, "Molecular electronics with single molecules in solid-state devices," (in English), *Nat. Nanotechnol.,* Review vol. 4, no. 9, pp. 551-556, Sep 2009, doi: 10.1038/nnano.2009.176.

[89] A. R. Garrigues, L. Wang, E. Del Barco, and C. A. Nijhuis, "Electrostatic control over temperature-dependent tunnelling across a single-molecule junction," (in English), *Nat Commun,* Article vol. 7, p. 11595, May 23 2016, Art no. 11595, doi: 10.1038/ncomms11595.

[90] J. G. Simmons, "Conduction in thin dielectric films," *Journal of Physics D: Applied Physics,* vol. 4, no. 5, pp. 613-657, 1971/05/01 1971, doi: 10.1088/0022-3727/4/5/202.

[91] J. G. Simmons, "Electric Tunnel Effect between Dissimilar Electrodes Separated by a Thin Insulating Film," *Journal of Applied Physics,* vol. 34, no. 9, pp. 2581-2590, 1963, doi: 10.1063/1.1729774.

[92] J. G. Simmons, "Generalized Formula for the Electric Tunnel Effect between Similar Electrodes Separated by a Thin Insulating Film," *Journal of Applied Physics,* vol. 34, no. 6, pp. 1793-1803, 1963, doi: 10.1063/1.1702682.

[93] W. Y. Wang, T. Lee, and M. A. Reed, "Elastic and inelastic electron tunneling in alkane self-assembled monolayers," (in English), *J. Phys. Chem. B,* Article vol. 108, no. 48, pp. 18398-18407, Dec 2004, doi: 10.1021/jp048904k.

[94] J. M. Beebe, B. Kim, J. W. Gadzuk, C. D. Frisbie, and J. G. Kushmerick, "Transition from direct tunneling to field emission in metal-molecule-metal junctions," (in English), *Phys Rev Lett,* Article vol. 97, no. 2, p. 026801, Jul 14 2006, Art no. 026801, doi: 10.1103/PhysRevLett.97.026801.

[95] A. P. Jauho, N. S. Wingreen, and Y. Meir, "Time-dependent transport in interacting and noninteracting resonant-tunneling systems," (in English), *Phys Rev B Condens Matter,* Article vol. 50, no. 8, pp. 5528-5544, Aug 15 1994, doi: 10.1103/physrevb.50.5528.

[96] S. Datta, W. Tian, S. Hong, R. Reifenberger, J. I. Henderson, and C. P. Kubiak, "Current-Voltage Characteristics of Self-Assembled Monolayers by Scanning Tunneling Microscopy," (in English), *Phys. Rev. Lett.,* Article vol. 79, no. 13, pp. 2530-2533, Sep 1997, doi: 10.1103/PhysRevLett.79.2530.

[97] J. Heurich, J. C. Cuevas, W. Wenzel, and G. Schon, "Electrical transport through single-molecule junctions: from molecular orbitals to conduction channels," (in English), *Phys Rev Lett,* Article vol. 88, no. 25 Pt 1, p. 256803, Jun 24 2002, Art no. 256803, doi: 10.1103/PhysRevLett.88.256803.

[98] R. Landauer, "Can a length of perfect conductor have a resistance?," (in English), *Physics Letters A,* vol. 85, no. 2, pp. 91-93, 1981, doi: 10.1016/0375-9601(81)90230-9.

[99] C. Kergueris, J. P. Bourgoin, S. Palacin, D. Esteve, C. Urbina, M. Magoga, and C. Joachim, "Electron transport through a metal-molecule-metal junction," (in English), *Phys. Rev. B,* Article vol. 59, no. 19, pp. 12505-12513, May 1999, doi: 10.1103/PhysRevB.59.12505.

[100] A. R. Garrigues, L. Yuan, L. Wang, S. Singh, E. Del Barco, and C. A. Nijhuis, "Temperature dependent charge transport across tunnel junctions of single-molecules and self-assembled

monolayers: a comparative study," *Dalton Trans,* vol. 45, no. 43, pp. 17153-17159, Nov 1 2016, doi: 10.1039/c6dt03204d.
[101] M. A. Sierra, D. Sanchez, A. R. Garrigues, E. del Barco, L. J. Wang, and C. A. Nijhuis, "How to distinguish between interacting and noninteracting molecules in tunnel junctions," (in English), *Nanoscale,* Article vol. 10, no. 8, pp. 3904-3910, Feb 2018, doi: 10.1039/c7nr05739c.
[102] L. Yuan, L. J. Wang, A. R. Garrigues, L. Jiang, H. V. Annadata, M. A. Antonana, E. Barco, and C. A. Nijhuis, "Transition from direct to inverted charge transport Marcus regions in molecular junctions via molecular orbital gating," (in English), *Nat. Nanotechnol.,* Article vol. 13, no. 4, pp. 322-+, Apr 2018, doi: 10.1038/s41565-018-0068-4.
[103] R. A. Marcus, "On the Theory of Oxidation-Reduction Reactions Involving Electron Transfer. I," *The Journal of Chemical Physics,* vol. 24, no. 5, pp. 966-978, 1956, doi: 10.1063/1.1742723.
[104] R. A. Marcus and N. Sutin, "ELECTRON TRANSFERS IN CHEMISTRY AND BIOLOGY," (in English), *Biochim. Biophys. Acta,* Review vol. 811, no. 3, pp. 265-322, 1985, doi: 10.1016/0304-4173(85)90014-x.
[105] R. A. Marcus, "Electron transfer reactions in chemistry. Theory and experiment," (in English), *Rev. Mod. Phys.,* Article vol. 65, no. 3, pp. 599-610, Jul 1993, doi: 10.1103/RevModPhys.65.599.
[106] J. R. Miller, L. T. Calcaterra, and G. L. Closs, "INTRAMOLECULAR LONG-DISTANCE ELECTRON-TRANSFER IN RADICAL-ANIONS - THE EFFECTS OF FREE-ENERGY AND SOLVENT ON THE REACTION-RATES," (in English), *J. Am. Chem. Soc.,* Note vol. 106, no. 10, pp. 3047-3049, 1984, doi: 10.1021/ja00322a058.
[107] D. Rehm and A. Weller, "KINETICS OF FLUORESCENCE QUENCHING BY ELECTRON AND H-ATOM TRANSFER," (in English), *Isr. J. Chem.,* Article vol. 8, no. 2, pp. 259-&, 1970. [Online]. Available: <Go to ISI>://WOS:A1970H124500012.
[108] A. Nitzan, "Electron transmission through molecules and molecular interfaces," (in English), *Annu Rev Phys Chem,* Review vol. 52, pp. 681-750, 2001, doi: 10.1146/annurev.physchem.52.1.681.
[109] Z. Xie, I. Baldea, and C. D. Frisbie, "Determination of Energy-Level Alignment in Molecular Tunnel Junctions by Transport and Spectroscopy: Self-Consistency for the Case of Oligophenylene Thiols and Dithiols on Ag, Au, and Pt Electrodes," (in English), *J Am Chem Soc,* Article vol. 141, no. 8, pp. 3670-3681, Feb 27 2019, doi: 10.1021/jacs.8b13370.
[110] G. Sedghi *et al.*, "Long-range electron tunnelling in oligo-porphyrin molecular wires," (in English), *Nat Nanotechnol,* Article vol. 6, no. 8, pp. 517-23, Jul 31 2011, doi: 10.1038/nnano.2011.111.
[111] N. B. Zhitenev, A. Erbe, Z. A. Bao, W. R. Jiang, and E. Garfunkel, "Molecular nano-junctions formed with different metallic electrodes," (in English), *Nanotechnology,* Article vol. 16, no. 4, pp. 495-500, Apr 2005, doi: 10.1088/0957-4484/16/4/027.
[112] M. Poot, E. Osorio, K. O'Neill, J. M. Thijssen, D. Vanmaekelbergh, C. A. van Walree, L. W. Jenneskens, and H. S. J. van der Zant, "Temperature Dependence of Three-Terminal Molecular Junctions with Sulfur End-Functionalized Tercyclohexylidenes," (in English), *Nano Lett.,* Article vol. 6, no. 5, pp. 1031-1035, May 2006, doi: 10.1021/nl0604513.
[113] Xiaoping Chen, Bernhard Kretz, Francis Adoah, Cameron Nickle, Xiao Chi, Xiaojiang Yu, Enrique del Barco, Damien Thompson, David A. Egger, and C. A. Nijhuis, "Turning Insulating Saturated Wires into Molecular Conductors via a Single Atom [Unpublished Manuscript]," 2020.
[114] N. Nerngchamnong, L. Yuan, D. C. Qi, J. Li, D. Thompson, and C. A. Nijhuis, "The role of van der Waals forces in the performance of molecular diodes," *Nat Nanotechnol,* vol. 8, no. 2, pp. 113-8, Feb 2013, doi: 10.1038/nnano.2012.238.

[115] D. Wang, D. Fracasso, A. Nurbawono, H. V. Annadata, C. S. Sangeeth, L. Yuan, and C. A. Nijhuis, "Tuning the Tunneling Rate and Dielectric Response of SAM-Based Junctions via a Single Polarizable Atom," (in English), *Adv Mater,* Article vol. 27, no. 42, pp. 6689-95, Nov 2015, doi: 10.1002/adma.201502968.

[116] C. S. S. Sangeeth, A. Wan, and C. A. Nijhuis, "Equivalent Circuits of a Self-Assembled Monolayer-Based Tunnel Junction Determined by Impedance Spectroscopy," (in English), *J. Am. Chem. Soc.,* Article vol. 136, no. 31, pp. 11134-11144, Aug 2014, doi: 10.1021/ja505420c.

[117] A. E. Haj-Yahia, O. Yaffe, T. Bendikov, H. Cohen, Y. Feldman, A. Vilan, and D. Cahen, "Substituent variation drives metal/monolayer/semiconductor junctions from strongly rectifying to ohmic behavior," (in English), *Adv Mater,* Article vol. 25, no. 5, pp. 702-6, Feb 6 2013, doi: 10.1002/adma.201203028.

[118] H. J. Lee, A. C. Jamison, and T. R. Lee, "Surface Dipoles: A Growing Body of Evidence Supports Their Impact and Importance," (in English), *Accounts Chem. Res.,* Review vol. 48, no. 12, pp. 3007-3015, Dec 2015, doi: 10.1021/acs.accounts.5b00307.

[119] X. P. Chen, H. V. Annadata, B. Kretz, M. Zharnikov, X. Chi, X. J. Yu, D. A. Egger, and C. A. Nijhuis, "Interplay of Collective Electrostatic Effects and Level Alignment Dictates the Tunneling Rates across Halogenated Aromatic Monolayer Junctions," (in English), *J. Phys. Chem. Lett.,* Article vol. 10, no. 14, pp. 4142-4147, Jul 2019, doi: 10.1021/acs.jpclett.9b00387.

[120] A. Asyuda, X. L. Wan, and M. Zharnikov, "Binary aromatic self-assembled monolayers: electrostatic properties and charge tunneling rates across the molecular framework," (in English), *Phys. Chem. Chem. Phys.,* Article vol. 22, no. 19, pp. 10957-10967, May 2020, doi: 10.1039/d0cp01740j.

[121] L. Romaner, G. Heimel, C. Ambrosch-Draxl, and E. Zojer, "The Dielectric Constant of Self-Assembled Monolayers," *Adv. Funct. Mater.,* vol. 18, no. 24, pp. 3999-4006, 2008, doi: 10.1002/adfm.200800876.

[122] H. M. Heitzer, T. J. Marks, and M. A. Ratner, "First-Principles Calculation of Dielectric Response in Molecule-Based Materials," (in English), *J. Am. Chem. Soc.,* Article vol. 135, no. 26, pp. 9753-9759, Jul 2013, doi: 10.1021/ja401904d.

[123] C. Van Dyck, T. J. Marks, and M. A. Ratner, "Chain Length Dependence of the Dielectric Constant and Polarizability in Conjugated Organic Thin Films," (in English), *Acs Nano,* Article vol. 11, no. 6, pp. 5970-5981, Jun 2017, doi: 10.1021/acsnano.7b01807.

[124] A. Natan, N. Kuritz, and L. Kronik, "Polarizability, Susceptibility, and Dielectric Constant of Nanometer-Scale Molecular Films: A Microscopic View," (in English), *Adv. Funct. Mater.,* Article vol. 20, no. 13, pp. 2077-2084, Jul 2010, doi: 10.1002/adfm.200902162.

[125] A. Probst, K. Raab, K. Ulm, and K. Vonwerner, "SYNTHESIS AND CHEMISTRY OF PERFLUORO-2-IODO-2-METHYL-ALKANES," (in English), *J. Fluor. Chem.,* Article vol. 37, no. 2, pp. 223-245, Nov 1987, doi: 10.1016/s0022-1139(00)82019-9.

[126] A. Vilan, "Analyzing molecular current-voltage characteristics with the simmons tunneling model: Scaling and linearization," (in English), *J. Phys. Chem. C,* Article vol. 111, no. 11, pp. 4431-4444, Mar 2007, doi: 10.1021/jp066846s.

[127] Z. Xie, I. Bâldea, C. E. Smith, Y. Wu, and C. D. Frisbie, "Experimental and Theoretical Analysis of Nanotransport in Oligophenylene Dithiol Junctions as a Function of Molecular Length and Contact Work Function," *ACS Nano,* vol. 9, no. 8, pp. 8022-8036, 2015/08/25 2015, doi: 10.1021/acsnano.5b01629.

[128] C. S. Sangeeth, A. T. Demissie, L. Yuan, T. Wang, C. D. Frisbie, and C. A. Nijhuis, "Comparison of DC and AC Transport in 1.5-7.5 nm Oligophenylene Imine Molecular Wires across Two Junction Platforms: Eutectic Ga-In versus Conducting Probe Atomic Force Microscope Junctions," *J Am Chem Soc,* vol. 138, no. 23, pp. 7305-14, Jun 15 2016, doi: 10.1021/jacs.6b02039.

[129] Q. V. Nguyen, P. Martin, D. Frath, M. L. Della Rocca, F. Lafolet, S. Bellinck, P. Lafarge, and J. C. Lacroix, "Highly Efficient Long-Range Electron Transport in a Viologen-Based Molecular Junction," *J Am Chem Soc,* vol. 140, no. 32, pp. 10131-10134, Aug 15 2018, doi: 10.1021/jacs.8b05589.

[130] S. H. Choi, C. Risko, M. C. R. Delgado, B. Kim, J.-L. Brédas, and C. D. Frisbie, "Transition from Tunneling to Hopping Transport in Long, Conjugated Oligo-imine Wires Connected to Metals," *J. Am. Chem. Soc.,* vol. 132, no. 12, pp. 4358-4368, 2010/03/31 2010, doi: 10.1021/ja910547c.

[131] L. Sepunaru, S. Refaely-Abramson, R. Lovrinčić, Y. Gavrilov, P. Agrawal, Y. Levy, L. Kronik, I. Pecht, M. Sheves, and D. Cahen, "Electronic Transport via Homopeptides: The Role of Side Chains and Secondary Structure," *J. Am. Chem. Soc.,* vol. 137, no. 30, pp. 9617-9626, 2015/08/05 2015, doi: 10.1021/jacs.5b03933.

[132] S. Gunasekaran, D. Hernangomez-Perez, I. Davydenko, S. Marder, F. Evers, and L. Venkataraman, "Near Length-Independent Conductance in Polymethine Molecular Wires," (in English), *Nano Lett.,* Article vol. 18, no. 10, pp. 6387-6391, Oct 2018, doi: 10.1021/acs.nanolett.8b02743.

[133] E. Leary *et al.*, "Bias-Driven Conductance Increase with Length in Porphyrin Tapes," (in English), *J. Am. Chem. Soc.,* Article vol. 140, no. 40, pp. 12877-12883, Oct 2018, doi: 10.1021/jacs.8b06338.

[134] Y. X. Zhang, S. Soni, T. L. Krijger, P. Gordiichuk, X. K. Qiu, G. Ye, H. T. Jonkman, A. Herrmann, K. Zojer, E. Zojer, and R. C. Chiechi, "Tunneling Probability Increases with Distance in Junctions Comprising Self-Assembled Monolayers of Oligothiophenes," (in English), *J. Am. Chem. Soc.,* Article vol. 140, no. 44, pp. 15048-15055, Nov 2018, doi: 10.1021/jacs.8b09793.

[135] N. Algethami, H. Sadeghi, S. Sangtarash, and C. J. Lambert, "The Conductance of Porphyrin-Based Molecular Nanowires Increases with Length," (in English), *Nano Lett.,* Article vol. 18, no. 7, pp. 4482-4486, Jul 2018, doi: 10.1021/acs.nanolett.8b01621.

[136] T. Stuyver, T. Zeng, Y. Tsuji, P. Geerlings, and F. De Proft, "Diradical Character as a Guiding Principle for the Insightful Design of Molecular Nanowires with an Increasing Conductance with Length," (in English), *Nano Lett.,* Article vol. 18, no. 11, pp. 7298-7304, Nov 2018, doi: 10.1021/acs.nanolett.8b03503.

[137] Y. A. Berlin and M. A. Ratner, "Conduction of Metal-Thin Organic Film-Metal Junctions at Low Bias," (in English), *J. Phys. Chem. C,* Article vol. 122, no. 13, pp. 7557-7563, Apr 2018, doi: 10.1021/acs.jpcc.8b01571.

[138] C. A. Naleway, L. A. Curtiss, and J. R. Miller, "SUPEREXCHANGE-PATHWAY MODEL FOR LONG-DISTANCE ELECTRONIC COUPLINGS," (in English), *J. Phys. Chem.,* Letter vol. 95, no. 22, pp. 8434-8437, Oct 1991, doi: 10.1021/j100175a005.

[139] M. D. Todd, A. Nitzan, and M. A. Ratner, "Electron transfer via superexchange: a time-dependent approach," *The Journal of Physical Chemistry,* vol. 97, no. 1, pp. 29-33, 1993/01/01 1993, doi: 10.1021/j100103a008.

[140] L. Yuan, L. Jiang, D. Thompson, and C. A. Nijhuis, "On the Remarkable Role of Surface Topography of the Bottom Electrodes in Blocking Leakage Currents in Molecular Diodes," (in English), *J. Am. Chem. Soc.,* Article vol. 136, no. 18, pp. 6554-6557, May 2014, doi: 10.1021/ja5007417.

[141] Z. Xie, I. Baldea, and C. D. Frisbie, "Why one can expect large rectification in molecular junctions based on alkane monothiols and why rectification is so modest," (in English), *Chem Sci,* Article vol. 9, no. 19, pp. 4456-4467, May 21 2018, doi: 10.1039/c8sc00938d.
[142] Donglei Bu, Cameron NIckle, Chun Y. Liu, Enrique Del Barco, and C. A. Nijhuis, "Enhanced Rectification Effect by Intensified Charge Localization [Unpublished Manuscript]," 2020.
[143] B. Liu, A. Blaszczyk, M. Mayor, and T. Wandlowski, "Redox-Switching in a Viologen-type Adlayer: An Electrochemical Shell-Isolated Nanoparticle Enhanced Raman Spectroscopy Study on Au(111)-(1 x 1) Single Crystal Electrodes," (in English), *Acs Nano,* Article vol. 5, no. 7, pp. 5662-5672, Jul 2011, doi: 10.1021/nn201307g.
[144] D. W. Zhang, J. Tian, L. Chen, L. Zhang, and Z. T. Li, "Dimerization of Conjugated Radical Cations: An Emerging Non-Covalent Interaction for Self-Assembly," (in English), *Chem.-Asian J.,* Review vol. 10, no. 1, pp. 56-68, Jan 2015, doi: 10.1002/asia.201402805.
[145] B. Cho, S. Song, Y. Ji, T. W. Kim, and T. Lee, "Organic Resistive Memory Devices: Performance Enhancement, Integration, and Advanced Architectures," (in English), *Adv. Funct. Mater.,* Article vol. 21, no. 15, pp. 2806-2829, Aug 2011, doi: 10.1002/adfm.201100686.
[146] X. Y. Tang, T. W. Schneider, J. W. Walker, and D. A. Buttry, "Dimerized pi-complexes in self-assembled monolayers containing viologens: An origin of unusual wave shapes in the voltammetry of monolayers," (in English), *Langmuir,* Article vol. 12, no. 24, pp. 5921-5933, Nov 1996, doi: 10.1021/la9503764.
[147] A. J. Bergren, R. L. McCreery, S. R. Stoyanov, S. Gusarov, and A. Kovalenko, "Electronic Characteristics and Charge Transport Mechanisms for Large Area Aromatic Molecular Junctions," (in English), *J. Phys. Chem. C,* Article vol. 114, no. 37, pp. 15806-15815, Sep 2010, doi: 10.1021/jp106362q.
[148] J. S. Lindsey and D. F. Bocian, "Molecules for Charge-Based Information Storage," (in English), *Accounts Chem. Res.,* Review vol. 44, no. 8, pp. 638-650, Aug 2011, doi: 10.1021/ar200107x.
[149] R. Kumar, R. G. Pillai, N. Pekas, Y. L. Wu, and R. L. McCreery, "Spatially Resolved Raman Spectroelectrochemistry of Solid-State Polythiophene/Viologen Memory Devices," (in English), *J. Am. Chem. Soc.,* Article vol. 134, no. 36, pp. 14869-14876, Sep 2012, doi: 10.1021/ja304458s.
[150] J. Wu, K. Mobley, and R. L. McCreery, "Electronic characteristics of fluorene/TiO2 molecular heterojunctions," (in English), *J. Chem. Phys.,* Article vol. 126, no. 2, p. 11, Jan 2007, Art no. 024704, doi: 10.1063/1.2423011.
[151] J. L. Segura, R. Juarez, M. Ramos, and C. Seoane, "Hexaazatriphenylene (HAT) derivatives: from synthesis to molecular design, self-organization and device applications," (in English), *Chem Soc Rev,* Review vol. 44, no. 19, pp. 6850-85, Oct 7 2015, doi: 10.1039/c5cs00181a.
[152] R. Wang, T. Okajima, F. Kitamura, N. Matsumoto, T. Thiemann, S. Mataka, and T. Ohsaka, "Cyclic and normal pulse voltammetric studies of 2,3,6,7,10,11-hexaphenylhexazatriphenylene using a benzonitrile thin layer-coated glassy carbon electrode," (in English), *J. Phys. Chem. B,* Article vol. 107, no. 35, pp. 9452-9458, Sep 2003, doi: 10.1021/jp0305281.
[153] Yulong Wang, Qian Zhang, Cameron NIckle, Dasari Venkatakrishnarao, Ziyu Zhang, Andrea Leoncini, Dong-Chen Qi, Yingmei Han, Enrique del Barco, Damien Thompson, and C. A. Nijhuis, "Dynamic Molecular Switches Drive In-Operando Reconfigurable Electronic Devices [Unpublished Manuscript]."
[154] A. Migliore and A. Nitzan, "Irreversibility and hysteresis in redox molecular conduction junctions," (in English), *J Am Chem Soc,* Article vol. 135, no. 25, pp. 9420-32, Jun 26 2013, doi: 10.1021/ja401336u.

[155] E. D. Fung, D. Gelbwaser, J. Taylor, J. Low, J. L. Xia, I. Davydenko, L. M. Campos, S. Marder, U. Peskin, and L. Venkataraman, "Breaking Down Resonance: Nonlinear Transport and the Breakdown of Coherent Tunneling Models in Single Molecule Junctions," (in English), *Nano Lett.,* Article vol. 19, no. 4, pp. 2555-2561, Apr 2019, doi: 10.1021/acs.nanolett.9b00316.

[156] B. Q. Xu and Y. Dubi, "Negative differential conductance in molecular junctions: an overview of experiment and theory," (in English), *J. Phys.-Condes. Matter,* Review vol. 27, no. 26, p. 19, Jul 2015, Art no. 263202, doi: 10.1088/0953-8984/27/26/263202.

[157] M. L. Perrin *et al.*, "Large negative differential conductance in single-molecule break junctions," (in English), *Nat. Nanotechnol.,* Article vol. 9, no. 10, pp. 830-834, Oct 2014, doi: 10.1038/nnano.2014.177.

[158] A. Migliore, N. F. Polizzi, M. J. Therien, and D. N. Beratan, "Biochemistry and theory of proton-coupled electron transfer," *Chem Rev,* vol. 114, no. 7, pp. 3381-465, Apr 9 2014, doi: 10.1021/cr4006654.

[159] J. J. Warren, T. A. Tronic, and J. M. Mayer, "Thermochemistry of proton-coupled electron transfer reagents and its implications," (in English), *Chem Rev,* Review vol. 110, no. 12, pp. 6961-7001, Dec 8 2010, doi: 10.1021/cr100085k.

[160] J. M. Mayer, "Understanding Hydrogen Atom Transfer: From Bond Strengths to Marcus Theory," (in English), *Accounts Chem. Res.,* Review vol. 44, no. 1, pp. 36-46, Jan 2011, doi: 10.1021/ar100093z.

[161] Y. van de Burgt, E. Lubberman, E. J. Fuller, S. T. Keene, G. C. Faria, S. Agarwal, M. J. Marinella, A. A. Talin, and A. Salleo, "A non-volatile organic electrochemical device as a low-voltage artificial synapse for neuromorphic computing," (in English), *Nat. Mater.,* Article vol. 16, no. 4, pp. 414-+, Apr 2017, doi: 10.1038/nmat4856.

[162] P. Chakma and D. Konkolewicz, "Dynamic Covalent Bonds in Polymeric Materials," (in English), *Angew. Chem.-Int. Edit.,* Review vol. 58, no. 29, pp. 9682-9695, Jul 2019, doi: 10.1002/anie.201813525.

[163] Yingmei Han *et al.*, "Bias-Polarity Dependent Direct and Inverted Marcus Charge Transport Affecting Rectification in a Redox-Active Molecular Junction [Submitted for Publication]."

[164] A. Migliore, P. Schiff, and A. Nitzan, "On the relationship between molecular state and single electron pictures in simple electrochemical junctions," (in English), *Phys Chem Chem Phys,* Article vol. 14, no. 40, pp. 13746-53, Oct 28 2012, doi: 10.1039/c2cp41442b.

[165] S. K. Karuppannan, H. T. Hu, C. Troadec, A. Vilan, and C. A. Nijhuis, "Ultrasmooth and Photoresist-Free Micropore-Based EGaIn Molecular Junctions: Fabrication and How Roughness Determines Voltage Response," (in English), *Adv. Funct. Mater.,* Article vol. 29, no. 38, p. 15, Sep 2019, Art no. 1904452, doi: 10.1002/adfm.201904452.

[166] A. Vilan, "Revealing tunnelling details by normalized differential conductance analysis of transport across molecular junctions," *Phys. Chem. Chem. Phys.,* 10.1039/C7CP05536F vol. 19, no. 40, pp. 27166-27172, 2017, doi: 10.1039/C7CP05536F.

[167] H. Jeong, Y. Jang, D. Kim, W.-T. Hwang, J.-W. Kim, and T. Lee, "An In-Depth Study of Redox-Induced Conformational Changes in Charge Transport Characteristics of a Ferrocene-Alkanethiolate Molecular Electronic Junction: Temperature-Dependent Transition Voltage Spectroscopy Analysis," *The Journal of Physical Chemistry C,* vol. 120, no. 6, pp. 3564-3572, 2016/02/18 2016, doi: 10.1021/acs.jpcc.5b12440.

[168] L. Sepunaru, N. Friedman, I. Pecht, M. Sheves, and D. Cahen, "Temperature-Dependent Solid-State Electron Transport through Bacteriorhodopsin: Experimental Evidence for Multiple

Transport Paths through Proteins," *J. Am. Chem. Soc.,* vol. 134, no. 9, pp. 4169-4176, 2012/03/07 2012, doi: 10.1021/ja2097139.
[169] B. A. Scott, S. J. La Placa, J. B. Torrance, B. D. Silverman, and B. Welber, "The crystal chemistry of organic metals. Composition, structure, and stability in the tetrathiafulvalinium-halide systems," *J. Am. Chem. Soc.,* vol. 99, no. 20, pp. 6631-6639, 1977/09/01 1977, doi: 10.1021/ja00462a026.
[170] H. V. Schröder and C. A. Schalley, "Tetrathiafulvalene - a redox-switchable building block to control motion in mechanically interlocked molecules," (in eng), *Beilstein J Org Chem,* vol. 14, pp. 2163-2185, 2018, doi: 10.3762/bjoc.14.190.
[171] Z.-F. Liu and J. B. Neaton, "Voltage Dependence of Molecule–Electrode Coupling in Biased Molecular Junctions," *The Journal of Physical Chemistry C,* vol. 121, no. 39, pp. 21136-21144, 2017/10/05 2017, doi: 10.1021/acs.jpcc.7b05567.
[172] A. Migliore and A. Nitzan, "Nonlinear Charge Transport in Redox Molecular Junctions: A Marcus Perspective," (in English), *Acs Nano,* Article vol. 5, no. 8, pp. 6669-6685, Aug 2011, doi: 10.1021/nn202206e.